PHOTOELECTRONIC ANALYSIS OF IMPERFECTIONS IN

GROWN STANNIC OXIDE SINGLE CRYSTALS

By

JACK EDWARD HOUSTON

Bachelor of Science
Oklahoma State University
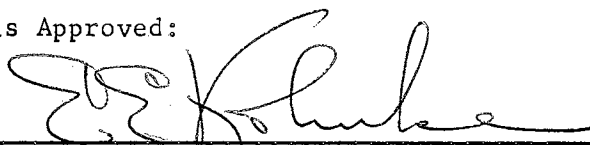Stillwater, Oklahoma
1956

Master of Science
Oklahoma State University
Stillwater, Oklahoma
1962

Submitted to the Faculty of the Graduate School of
the Oklahoma State University
in partial fulfillment of the requirements
for the degree of
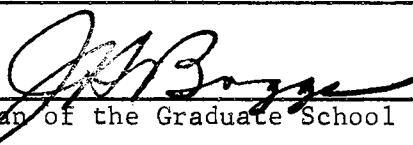DOCTOR OF PHILOSOPHY
May, 1965

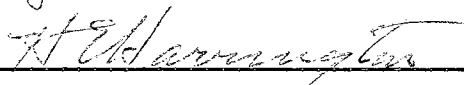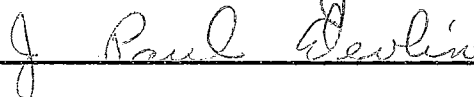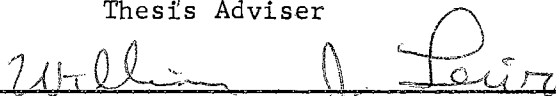PHOTOELECTRONIC ANALYSIS OF IMPERFECTIONS IN

GROWN STANNIC OXIDE SINGLE CRYSTALS

Thesis Approved:

_____
Thesis Adviser

_____

_____

_____

_____
Dean of the Graduate School

ii

ACKNOWLEDGMENT

TABLE OF CONTENTS

LIST OF TABLES

LIST OF FIGURES

CHAPTER I

INTRODUCTION

Metal Oxides

The intriguing properties of metal oxides have been known for many years and exploited in a myriad of electronic devices. Despite this history of application, a detailed understanding of the fundamental electronic processes responsible for these properties -- such as is available for germanium and silicon -- has not yet been attained. One reason for this theoretical lag has been the experimental difficulty of obtaining sample-sized single crystals of controlled purity. This is mostly attributable to the fact that many oxides have high melting points, meaning that controlled growth must be carried out at elevated temperatures. High temperatures further complicate the growth process of certain oxides which have a tendency to evaporate or partially decompose in their growth range making the composition of the final product critically dependent upon the exact growth condition. This lack of single crystals has essentially restricted the bulk of the oxide work to studies of the properties of pressed powders, sintered ceramics, poly-crystalline thin films and natural crystals. Much has been written concerning these studies and good reviews are contained in the articles by Verwey[1] and Gray[2,3].

Within recent years, a considerable body of work has been done on the properties of single crystal rutile (TiO_2). Many of the results are

1

summarized in an article by Grant[4]. A general comparison between the properties of titanium dioxide and other compounds that have the rutile crystalline structure should contribute significantly to a general understanding of the electronic processes in oxides.

One such compound is stannic oxide (SnO_2), (which also has the ditetragonal bipyrimidal rutile crystal structure). This material is again no stranger to application. Besides its commercial use as the most common ore of tin, it finds application as a ceramic material having very low temperature coefficient of capacitance[5], as a thin transparent conductive coating in de-icing equipment[6], and as a catalyst in the commercial manufacture of hydrogen and carbon monoxide from hydrocarbons[7]. As with the other oxides, however, these applications have been made despite a lack of understanding as to the fundamental properties of the material itself. Some scattered work has been done on this oxide but once again, due to the lack of single crystals, it has been generally restricted to studies of the properties of pressed powders, thin films or natural crystals.

Bauer[8] and Fisher[9] have reported, from work on thin films of stannic oxide, resistivities of the order of 10^{-2} ohm-cm, 6 cm^2/volt-sec for Hall mobility and 10^{20} cm^{-3} for electron concentration. They reported impurity activation energies from resistivity versus 1/T data of 0.02 ev near 100°K and 0.05 ev near room temperature. Ishiguro and co-workers[10] also studied thin films and have reported values of the order of 10^{-2} ohm-cm, 15-35 cm^2/volt-sec and 10^{19} to 10^{20} cm^3 for resistivity, mobility and electron concentration respectively.

Le Blanc and Sachse[11] have reported resistivities for sintered samples of around 10^8 ohm-cm at room temperature, and Guilery[12], who

studied both pressed powders and sintered samples, has reported values from 10^4 to 10^8 ohm-cm at low temperatures.

Miloslavskii[13] has studied films prepared by the pyrolytic decomposition of the tin chlorides. He found ionization energies from conductivity data, over the temperature range from 150° C to 200° C, to be approximately 0.12 ev for samples having room temperature resistivities from 10^{-2} to 10^{-3} ohm-cm and electron densities from 10^{19} to 10^{20} cm^{-3}, while optical transmission studies indicated values of approximately 0.15 ev.

Foex[14] studied pressed powders prepared by the oxidation of tin with nitric acid followed by a heat treatment in air at 1200° C. He found linear slopes in conductivity as a function of temperature data indicating activation energies of 0.77 ev and 4.0 ev over the temperature range from 20° C to 1200° C.

There has been a considerable amount of work done at Oklahoma State University on the properties of natural crystals. Northrip[15] reported resistivities of 2.4, 4.2 and 2.4 x 10^4 ohm-cm for three crystals which were rather different in appearance. Work on the transmission spectra of these crystals by Belski[16] indicated fundamental energy gap values of approximately 3.5 ev. Photoconductivity response data, again taken on these samples, by Hurt[17] also indicated an energy gap in the neighborhood of 3.5 ev.

At the time of this writing only a single report by Marley and MacAvoy[18] is known to be available on the properties of single crystal stannic oxide. They used samples grown from the vapor phase by a technique reported in an earlier article.[19] Read and co-workers[20] have also reported sample-size single crystal growth from the vapor phase

but as yet no information is known to be published on their properties.
Within the last year, sample-sized single crystals have been successfully
grown locally by Kunkle[21] from a cuprous oxide flux, and the work
presented here is the first step in an exhaustive survey of their
properties.

Photoconductivity and the Photoelectronic Analysis

Photoconductivity was observed as a phenomenon by Smith[22] as early
as 1873. And, indeed, photocells of selenium were produced by Adams
and Day[23] in 1876. The first systematic survey of the subject was made
by Gudden and Pohl[24,25] in the early 1920's. Their work contributed
to the early interpretation of photoconductivity and showed that this
process and that of luminescence often occurred concurrently in a
material. However, it was not until the close of World War II that a
consistent framework for designing photoconductivity experiments and
interpreting data was developed. Only in the literature since that
time has the process been treated in terms of the central ideas upon
which a detailed theoretical study can be based, e.g., the distinction
between traps and recombination centers, carrier lifetime, capture cross
sections and bound states for carriers.

The interest in photoconductors since World War II has been largely
responsible for the development of photoconductivity as a tool in the
research on materials. This interest has been stimulated not only by
the development of the transistor which gave a tremendous emphasis to
materials research, but also by the development of such image devices
as the Vidicon pickup tube,[26] solid state image converters[27] and elec-
trophotography by Xerography and Electrofax processes.

The general photoconductivity process involves simply an increase in the conductivity of a material by photon irradiation. In terms of the basic concepts of solid state theory, this would involve the mobilizing of carriers either by (1) creating a hole-electron pair through the excitation of a valence band electron into the conduction band or by (2) creating one free carrier through the excitation of a bound carrier into its respective free band. The nonequilibrium situation which results from these processes is relieved by recombination, i.e., by the carriers returning to their ground states (pair annihilation) and giving up their excess energy as radiation or to the lattice in the form of phonons.

Actually the photoconductivity process, in one respect, is just as simple as the above description implies. That is, it involves only the balancing of the rate of carrier mobilization by irradiation with the rate of recombination. These rates, however, are extremely complex in their relation to the physical characteristics of a given material. Consequently, a photoconductor can -- and does -- show a baffling variety of behavior depending on its impurity content and structural defects. Other than the fact that radiation usually increases the conductivity of a solid, the data does not fall into an easily understandable pattern. The photocurrent may rise as a fractional power of the radiation intensity; it may rise linearly or in some cases it may even rise at a greater power than the first with respect to the intensity. The photocurrent may increase, decrease, or it may remain fairly constant as a function of temperature. Sometimes the addition of a second source of radiation may even cause a decrease in the photocurrent. Therefore, it is not at all surprising that an understanding

of photoconductivity did not come early or in a simple form. The understanding only came with an improved knowledge of the behavior of electrons in solids and improved sources of materials.

What has actually developed, then, has been a phenomenological framework for photoconductivity which has identified the significant parameters and has acted as a guide to their quantitative exploration. These parameters characterize the bound states in the forbidden gap and generally consist of their density, position on the energy scale and their cross sections for free hole and electron capture. Ultimately, what is needed from the body of quantitative parameters which this framework is able to experimentally deduce, is their chemical or physical origin.

As the framework developed, several experimental procedures came into frequent use because of their particular utility in deducing the characteristic impurity and defect parameters. The application of this somewhat loosely defined set in obtaining the parameters for a given photoconductor has been termed in the literature a "photoelectronic analysis." While this analysis varies somewhat in its inclusions, it generally consists of several or all of the following studies:

1. Photoconductivity transients

2. Spectral response of photoconductivity

3. Thermally stimulated currrents

4. Thermal quenching

5. Optical quenching

6. Optical absorption

7. Luminescence

8. Space charge limited currents

9.   Photovoltaic effects.

Supplementary data is often obtained from a variety of other measurements

such as electrical conductivity and Hall effect as a function of temper-

ature.

Scope of the Present Study

The photoconductivity literature has become quite extensive since

Gudden and Pohl's articles in the 1920's. Writings of fundamental

importance to the development of the phenomenological framework have

been contributed by Rose[28] and Bube.[29] These articles also contain

excellent bibliographies to the general literature. Within this liter-

ature, there are several particularly pertinent examples of the appli-

cation of the photoelectronic analysis to specific materials. These

include analyses of the compounds ZnS,[30] CdS,[30,31,32] ZnSe,[30,33]

ZnTe,[30,34] CdTe,[30] GaAs doped with Cu,[35] GaSe,[36] Mn doped Ge[37] and CdSe.[38]

The primary purpose of the present work has been to make a photo-

electronic analysis of the locally grown stannic oxide single crystals.

This analysis consists of a detailed description of the theory, as

well as application techniques and results of spectral response,

thermally stimulated currents, thermal quenching and optical quenching

measurements. These measures have been supplemented by studies of dark

conductivity as a function of temperature and thermally stimulated

thermoelectric voltage. An attempt has been made to consolidate the

results obtained under the guidance of the phenomenological framework

into a consistent impurity scheme for these crystals. This scheme is

described in terms of the energy scale positions and trapping and re-

combination properties for each level found.

Another result of the present work is a detailed proposal for future studies. Given special emphasis is a series of procedures for which preliminary results have been obtained. Suggested are studies of nonequilibrium carrier lifetimes and extrinsic sensitization by intrinsic pre-illumination. Also included in these proposals are suggestions for studies which do not have the advantage of preliminary experience. The studies proposed here are chosen for their pertinence and discussed in terms of the experimental details involved. They include studies of the photo-Hall effect and relative quantum efficiency.

CHAPTER II

THEORETICAL BACKGROUND

In the present chapter a review of the general phenomenological framework will be given to establish the necessary background for the present photoelectronic analysis. This background will show the relation between the rate-balance process, as described in Chapter I, and the central ideas upon which the framework is based. However, a review of some of the fundamental electronic processes in semiconductors and insulators seems desirable before a general discussion of photoconductivity is begun.

Fundamental Processes

First, it should be recalled that electronic processes such as conductivity, optical absorption and photoconductivity involve the transition of electrons between different energy states of crystalline solids. Also, it should be noted that these states in pure semiconductors and insulators fall into two quasi-continuous bands, one filled (valence band) with electrons and the other empty (conduction band), separated by an energy region which has no electronic states (the forbidden gap).

Processes that depend on electronic mobility, such as conductivity, require the availability of quasi-continuous states into which electrons may transfer. Electronic states can, of course, exist in the forbidden gap

if they are associated with foreign atoms in the crystal (impurities) or lattice defects such as vacancies or surface discontinuities. However, electrons which reside in these levels ordinarily do not have appreciable mobilities because of the lack of quasi-continuous energy states into which they can transfer, i.e., the impurity centers are generally so widely dispersed that only negligible interactions can take place. This means that a mobility will only result when electrons reside in the unfilled conduction band or when empty states are available in the valence band (holes). In this case the conductivity will be proportional to the sum of the densities of electrons in the conduction and holes in the valence band, i.e.,

$$\sigma = e(\mu_e n + \mu_h p) \tag{1}$$

where σ is the conductivity, e the electronic charge, μ_e, μ_h are the electron and hole mobilities respectively (drift velocity per unit field strength) and n and p are their respective densities.

Therefore a semiconductor or insulator can be pictured as being made up electronically of two quasi-continuous groups of states separated by an energy gap, which may contain several more or less mono-energetic groups of states. Into this complete set of states is distributed a number of electrons and the particular occupancy distribution that they assume is specified by equilibrium thermodynamics. This distribution is mathematically embodied in the tranditional Fermi-Dirac function*

---

*The particular coefficient chosen to appear preceding the exponential term in this expression results from the occupancy model assumed and is of minor significance to the following discussion. For a discussion of this point refer to Chapter 4 of Semiconductors by R.A. Smith, Cambridge Press, Cambridge, England (1959).

$$f(E) = \frac{1}{1 + \exp[(E - E_f)/kT]} \tag{2}$$

where $f(E)$ represents the electron occupation probability of a state located at an energy E, k is the Boltzmann constant, T the absolute temperature and E_f is the Fermi energy (the chemical potential of the system described above at temperature T). It should be recalled that from this expression and a knowledge of the states density distribution function $N(E)$, a value of mobile carrier density can be obtained. This is accomplished by integrating over the mobile states, i.e.,

$$n = \int_{E_c}^{\infty} f(E)N(E)dE \tag{3}$$

where n is the conduction band electron density and E_c is the energy of the lower edge of the band. A similar expression is used for holes by integrating in terms of the lack of occupancy $[1 - f(E)]$ over the valence band states. Note that a useful simplification is obtained by assuming that $(E - E_f) \gg kT$, which is normally the case. Then Equation 2 reduces to the familiar Boltzmann equation $f(E) = \exp[-(E - E_f)/kT]$. If these integrations are carried out using the Boltzmann approximation the following expressions are obtained*

$$n = 2\left[\frac{2\pi m_e kT}{h^2}\right]^{3/2} \exp[(E_f - E_c)/kT]$$

$$p = 2\left[\frac{2\pi m_h kT}{h^2}\right]^{3/2} \exp[(E_v - E_f)/kT] \tag{4}$$

---

*A good account of this integration is given in Chapter 10 of "Introduction to Solid State Physics" by Charles Kittel, John Wiley and Sons, Inc., New York (1956).

where m_e, m_h are the effective masses for electrons and holes respectively and h is Planck's constant. Equations 4 are usually written in the literature as

$$n = N_c \exp(-E_{fn}/kT)$$

$$p = N_v \exp(-E_{fp}/kT)$$

(5)

where $E_{fn} = E_c - E_f$, $E_{fp} = E_f - E_v$ and N_c, N_v are respectively called the effective density of conduction and valence band states.

It should be realized that these equilibrium occupancies are physically established in the system outlined before by a balancing of the rates of thermal excitation from, and capture of electrons by, the individual states. And it is interesting to note that an expression can be derived for the Fermi level in terms of the parameters which characterize these rates. This derivation is presented here in order to gain familiarity with the rate-parameters, which will be useful in later discussions of nonequilibrium processes.

Assume first the simple band model of an n-type semiconductor shown in Figure 1.
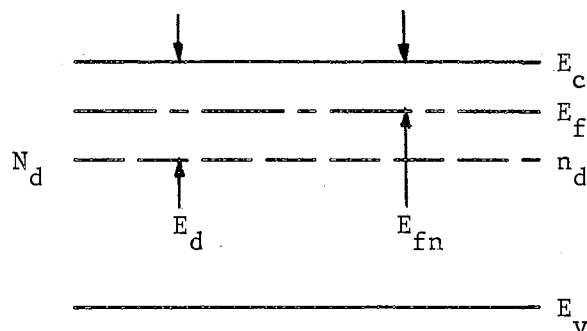
Figure 1. Simple band model of an n-type semiconductor.

In this model N_d is the density of donor states whose activation energy is E_d, n_d is their occupation density, n is the occupation density of the conduction band states, and the Fermi level is located E_{fn} below the conduction band. The n electrons in the conduction band are free to move through the crystal and thereby come into contact with the $(N_d - n_d)$ unoccupied donors. There is a finite probability that a free electron moving in the neighborhood of one of these empty states may be captured by it.

The assumption is then made that this process can be described by defining a <u>capture cross section</u> for electrons by these empty states. This concept amounts to assuming that for the capture process, the empty donor states present spherical volume elements to the migrating electrons and that the capture event will take place when one of the electrons finds itself in contact with this element. Now, of course, each electron is traveling around in the lattice with some average velocity $\bar{v}$ and it sees only the spherical cross sections of the empty donor states. Therefore the average number of free electrons which collide with a capture volume element per unit time is equal to the product of the spherical cross section, the density of free electrons, and their average thermal velocity, i.e., $S_n n \bar{v}$. Note should be made that S_n represents the capture cross section of an unoccupied donor state for a free electron and when this state becomes occupied then S_n becomes zero. Under these conditions the occupied state may have a cross section S_p for the capture of free holes. More will be said about this later. Finally, the total rate at which electrons are being captured per unit crystal volume is $n(N_d - n_d)S_n \bar{v}$.

In equilibrium the rate of electron capture is just balanced by the rate of thermal excitation. The excitation process can be thought of as the irradiation of the n_d occupied donors by a field of phonons (the quanta of lattice vibration or thermal energy). Then the total rate at which thermal transitions occur is equal to

$$n_d \nu \exp(-E_d/kT) \qquad (6)$$

where ν (sometimes called the attempt-to-escape frequency) represents the rate of phonon collisions with the occupied donor states and the exponential term gives the transition probability per collision (essentially the fraction of the phonon collisions which have sufficient energy to bring about a transition). In terms of these two rates, equilibrium exists between the donor states and the conduction band when

$$n(N_d - n_d)S_n\bar{v} = n_d \nu \exp(-E_d/kT). \qquad (7)$$

If the further assumption is made that every conduction electron came from the donor states then $n = N_d - n_d$. This means the material is completely extrinsic and implies that $E_d \ll E_c - E_v \cong E_G$. Under this assumption, Equation 7 simplifies to

$$n^2 S_n\bar{v} = (N_d - n)\nu \exp(-E_d/kT). \qquad (8)$$

Substituting the first of Equations 5 into 8 gives

$$(S_n\bar{v}/\nu)N_c \exp(-E_{fn}/kT) = [(N_d/N_c)\exp(E_{fn}/kT) - 1]\exp(-E_d/kT). \qquad (9)$$

This expression can be considered to be an equation in the two unknowns $(S_n\bar{v}/\nu)$ and E_{fn}. A useful relation can be derived by considering the

special case $n = N_d - n$, which is true when $E_{fn} = E_d$ since then the donor states are just half filled. Using this additional condition in 9 yields the relation

$$N_c S_n \bar{v} = \nu \qquad (10)$$

which states, independently of the particular model chosen, that for a given temperature the attempt-to-escape frequency is directly proportional to the capture cross section. The constant of proportionality $N_c \bar{v}$ is, of course, a function of temperature. The equilibrium expression in Equation 8 can then be given in the simplified form

$$n^2 = (N_d - n)N_c \exp(-E_d/kT). \qquad (11)$$

Equation 11 can now be used along with the first of 5 to get the desired relation between the Fermi energy and the parameters of the system, i.e.,

$$E_{fn} = E_d/2 + (kT/2)\ln(N_c/N_d) \qquad (12)$$

using the further assumption that $N_d \ll N_c$. Of course, Equation 12 is normally derived on purely thermodynamic grounds, but the above analysis has been given to provide sufficient familiarity with the rate processes to allow an immediate discussion of nonequilibrium.

In the derivation just given, it was mentioned that equilibrium between the conduction band and the donor states implied an equality between their electron exchange rates. A like "test" could be stated for nonequilibrium as the inequality in these rates. However, care must be taken in applying either of these tests to make sure that the system has been properly defined and that the exchange rates do not include external excitation rates. Thermodynamically the conditions

for equilibrium are stated in terms of maximizing the system entropy, or more appropriately for this constant P, V, T system as minimizing the free energy. Since it is convenient in these discussions to talk in terms of rate processes, a closer look at their bearing on equilibrium now seems appropriate.

First, it should be recalled that minimizing the free energy for the case represented by Figure 1 leads to an electron occupation distribution specified by the Fermi-Dirac function (Equation 2). In other words, this distribution of electrons over the available states is a result of the system being in thermodynamic equilibrium. Any other distribution, of course, would represent a nonequilibrium situation. It can also be shown from the free energy expression that the chemical potential, or in this case the Fermi level, (defined as the partial of the free energy with respect to the occupation density) for a particular set of states is solely a function of their energy and occupation density. And if two sets of states are in equilibrium then they must have the same Fermi level, which leads to a rigorous, though inconvenient, test for equilibrium between sets of states (i.e., the location of the Fermi level is not always available for each set).

It is possible in a nonequilibrium, steady-state process for some sets of states to be in equilibrium with each other but not with the rest of the system. The steady-state is here defined as that nonequilibrium for which the exchange rates are independent of time. This will become an important point in later discussions of traps and recombination centers. In order to illustrate this point, the concept of the steady-state Fermi level will first be introduced.

The Fermi level itself is only defined for equilibrium systems; however, it is helpful to define a steady-state value which gives the correct occupancy for states under these special nonequilibrium conditions. This useful device does not in itself violate any thermodynamic principles, since, as already mentioned, the Fermi level for a particular set of states is dependent only on their energy and density of electron occupation. The steady-state Fermi level for conduction band occupancy is defined by the equation

$$E_{fn}^{*} = kT\ln(N_c/n) \tag{13}$$

where E_{fn}^{*} is the steady-state Fermi energy for electrons, E the energy of the states, n is the conduction band occupation density and N_c the density of states.

It can be shown that under these nonequilibrium conditions sets of states will be in equilibrium with one another if they have a common steady-state Fermi level. As an illustration consider again the system pictured in Figure 1 and assume that by some external means, e.g., radiation, electrons and holes are being added to their respective bands at a constant rate. The steady-state is reached when the rate at which electrons recombine with holes is equal to the rate at which they are being added to the bands. This condition implies that the steady-state Fermi level for electrons has moved slightly nearer the conduction band and that for holes has moved across the gap to a location near the valence band. Obviously the conduction and the valence band are no longer in equilibrium as might be expected from the fact that energy is being continuously added to the system. However, the donor states and the conduction band may very well be in equilibrium. This again depends

on whether or not they share a common steady-state Fermi level. Or, in terms of the exchange rates, it depends on whether the rate of exchange between the donor level and the valence band is an appreciable fraction of the rate between the donors and conduction band. Therefore, states between which no net exchange of electrons takes place -- recalling again that external excitation rates are excluded from consideration -- are found to be in equilibrium under steady-state conditions.

Under these steady-state conditions, the net electron exchange rate between levels which are not in equilibrium is known as the rate of recombination. For a nonequilibrium density of free hole-electron pairs in the model of Figure 1 this can either take place by (1) a direct capture of a free electron by a free hole or by (2) an empty donor state first capturing a free electron and then a free hole. The direct process (1) is found to be highly unlikely in real materials and the bulk of the recombination normally proceeds by (2) using an impurity level as a "catalyst." As mentioned in Chapter I, this makes photoconductivity a very sensitive tool for probing impurity states.

Impurity states which only exchange electrons with one of the mobile bands (excluding direct external excitation from these states) can act as traps for the carriers of that band. To illustrate this, consider again the scheme shown in Figure 1, and assume that in equilibrium $n_d < N_d$. Then if a nonequilibrium density of electrons is established in the conduction band and negligible recombination takes place through the donor states, these states will become occupied by a nonequilibrium density of electrons, which will eventually return to the conduction band through thermal excitations. The fact that these electrons reside in the donor states for some time suggests referring to them as "trapped" carriers.

Impurity states in the forbidden gap can therefore act as either trapping or recombination centers depending on the particular process which takes prominence. By definition, a trapping center is one in which a nonequilibrium carrier has a greater probability of being thermally excited than of recombining and a recombination center is defined in a parallel fashion. A criterion which determines the characteristic of a group of states in terms of their capture parameters can now be established using these definitions. In fact, a demarcation between the trapping and recombination processes can be defined by determining the conditions for which the thermal excitation and recombination probabilities are equal.

Consider once again the system of Figure 1 and further assume that the donor states have capture cross sections S_n and S_p. Now if a non-equilibrium density of free electron-hole pairs n and p is established in the mobile bands, the demarcation between trapping and recombination is determined by equating the rates of thermal excitation and recombination from the donor states, i.e.,

$$n_d N_c S_n \bar{v} \exp(-E_d/kT) = p n_d S_p \bar{v} \qquad (14)$$

using the relation of Equation 10 and the assumption that the thermal velocities of electrons and holes are equal. A demarcation energy level E_{dn} for electrons can now be derived from Equation 14 by defining $E_{fn}^* = E_{dn}$ under the equal rate condition which leads to the general expression

$$E_{dn} = E_{fn}^* + kT\ln(S_n n/S_p p). \qquad (15)$$

Equation 15 gives the electron demarcation level of the states in terms

of the conduction band steady-state Fermi level and implies that if

$E_{dn} < E_d$ then the states act as recombination centers, but if $E_{dn} > E_d$

they act as _electron_ traps. A similar demarcation level can be derived

for holes in terms of the electron Fermi level, i.e.,

$$E_{dp} = E_{fn}^* + kT\ln(S_p/S_n) + (3kT/2)\ln(m_h/m_e) \tag{16}$$

which gives the conditions for _hole_ trapping in the donor states, a

highly unlikely situation for states lying near the conduction band.

Note that this demarcation level also gives a test for steady-state

equilibrium between the donor states and conduction band, i.e., if

E_{dn} is more than a few kT larger than E_d then the states act as trapping

centers and can be considered to be in equilibrium with the conduction

band.

The processes discussed in the last few paragraphs all depended

on the capture cross sections of the forbidden gap impurity states. The

values of these cross sections are largely determined by the fields which

they present to the free carriers. Therefore capture centers which have

attractive fields have large cross sections and those with repulsive

fields have small ones. Examples of these cases as provided for various

materials by Bube[29] are ionized donors which capture electrons with S_n

approximately 10^{-12} cm^2 and neutral centers such as un-ionized donor

states which capture free holes with S_p approximately 10^{-15} cm^2. Singly

ionized double donor states which capture holes exemplify a repulsive

case with S_p as low as 10^{-22} cm^2.

To conclude this review, a short discussion of the return to equilib-

rium seems appropriate. Consider the donor and conduction band states

as illustrated in Figure 1. Assume that by some means an initial

nonequilibrium density δn of electrons is transferred from the donor states to the conduction band. Under these conditions, there exists initially a net rate of electron flow from the conduction band equal to (from an extension of Equation 8)

$$d\hat{n}/dt = -(n + \delta n)^2 S_n \bar{v} + (N_d - n - \delta n)N_c S_n \bar{v} \exp(-E_d/kT) \quad (17)$$

where $\hat{n}$ is the total density of conduction band electrons, i.e., $\hat{n} = n + \delta n$. Therefore in view of 8, Equation 14 is simplified to

$$d\, \delta n/dt = -\{\delta \hat{n}^2 + \delta n[2n + n_c \exp(-E_d/kT)]\} S_n \bar{v} \quad (18)$$

which is the differential equation representing the transient decay of the δn nonequilibrium electrons back into the donor states, i.e., the transient recombination process.

The Photoconductive Process

It is time now to apply the fundamentals of nonequilibrium to a study of the details of the photoconductive process. Again photoconductivity is to be considered as the mobilizing of carriers in a solid by photon irradiation. This includes both the (1) "creation" of free hole-electron pairs by photon excitation of a valence band electron into the conduction band and (2) the "creation" of free electron and bound holes (or vice versa) by the excitation of an electron from (or into) a forbidden band state. These processes are known as intrinsic and extrinsic photoconductivity, respectively.

The differential equations governing the photoconductive process can be written as

$$\frac{dn}{dt} = \alpha(\lambda)L(\lambda) - R_n(n,P,T)$$

$$\frac{dp}{dt} = \beta(\lambda)L(\lambda) - R_p(n,p,T) \tag{19}$$

where $\alpha(\lambda)$ and $\beta(\lambda)$ are the quantum efficiencies for free electron and hole production (the number of respective free carriers produced per incident photon), $L(\lambda)$ is the incident photon intensity and R_n, R_p are the recombination rates for electrons and holes respectively. The assumption is made here that the quantum efficiencies are not functions of temperature. Intrinsic photoconductivity is defined by an equality between $\alpha(\lambda)$ and $\beta(\lambda)$, i.e., every photon interaction produces a free carrier pair. In this case, for the steady-state conditions dn/dt = dp/dt = 0, $R_n = R_p$. On the other hand for the pure extrinsic case either $\alpha(\lambda)$ or $\beta(\lambda)$ is zero since only one free carrier is produced.

Solving Equations 19 for the conductivity (n + p) as a function of L, in terms of the parameters of the system, is extremely complex even in the simplest cases. It requires the solution of a set of equations similar to 19 which express the rates R_n and R_p in terms of the impurity parameters. To these must be added a relation expressing charge neutrality. Examples of such solutions based on specific models are available in articles by Broser and Warminsky[39] and Rittner.[40] These solutions, in their complexity, are not too revealing physically; however, considerable information can be obtained from the phenomeno-logical behavior of the photoconductivity in terms of the nonequilibrium kinetics already discussed. The rest of the present chapter is dedicated to phenomenological discussions of specific photoelectronic procedures in terms of these kinetics.

Spectral Response

Spectral response refers here to the measurement of saturation or steady-state photoconductivity as a function of wavelength. This involves a phenomenological solution of Equations 19 in terms of $L(\lambda)$ for $dn/dt = dp/dt = 0$. The conductivity is therefore related to the quantum efficiency, the photon intensity, and the recombination rate for a given wavelength.

Experimentally the quantum efficiency is difficult to separate from the photoconductivity data and is usually taken, at least in the intrinsic region, to have the same general form as the optical absorption coefficient. For longer wavelengths, in the extrinsic region, absorption may involve the excitation of electrons out of or into the impurity states. In this region, however, the quantum efficiency may not follow the absorption coefficient because of non-photoconductive processes such as lattice vibration excitation. This part of the photoconductivity, as will be seen later, is an important tool in studying impurity proper-ties of solids. Of course $L(\lambda)$ is gotten, at least relatively, by common photometric techniques, i.e., from photocell, photomultiplier, or thermopile measurements.

It is commonly found that the spectral response in the intrinsic region does not follow the absorption coefficient. This implies a wavelength dependence of the recombination rate, which does not at first seem logical. However, when it is remembered that photo-carrier produc-tion is spatially dependent on wavelength through the absorption coeffi-cient, an explanation becomes apparent. As the absorption coefficient gets larger the hole-electron pairs are created nearer the irradiated

surface. The experimental results are thus due to a spatial dependence of the recombination rate.

DeVore[41] has developed an analysis of these effects which shows how the maximum in the spectral response can be related to the absorption coefficient of the light involved and to the material's surface recombination rate. Subashiev[42] has made a similar analysis and claims its successful application to germanium and silicon in determining surface recombination rates. Several other authors have also done work along this same line.[43,44,45] However, no attempt has been made in the present work to obtain quantitative information by applying such analyses to intrinsic spectral response data. These data have only been used here to gain a qualitative picture of environmental effects on the surface recombination.

As has already been mentioned, the extrinsic spectral response can be used in probing impurity states. This process depends upon the existence of a finite quantum efficiency for photon excitation of (1) bound electrons into the conduction band or (2) valence band electrons into empty impurity states. The extent of the forbidden gap which can be probed by this technique has practical limitations since the extrinsic quantum efficiencies are normally many orders of magnitude smaller than the intrinsic values. Thus a certain region of the short wavelength extrinsic photoconductivity may be overshadowed by the long wavelength tail of the intrinsic photoconductivity. In the present case, it is felt that roughly half of the 4 ev forbidden gap is adequately probed by the technique. Another effect of the small extrinsic quantum efficiencies is that the measurements must be done at temperatures low enough that the dark conductivity does not mask the photoconductivity.

25

Thermally Stimulated Currents

An electron trapping center was earlier defined as a state for which the thermal rate of excitation to the conduction band greatly exceeded the hole capture rate (similarly for a hole trapping center). Thus the existence of electron trapping centers depends on both the availability of empty states for electrons and the electron demarcation level for these states. Of course, hole traps must be electronically occupied and their action as traps rather than recombination centers depends upon the hole demarcation level.

To illustrate these points consider the equilibrium model of Figure 2.
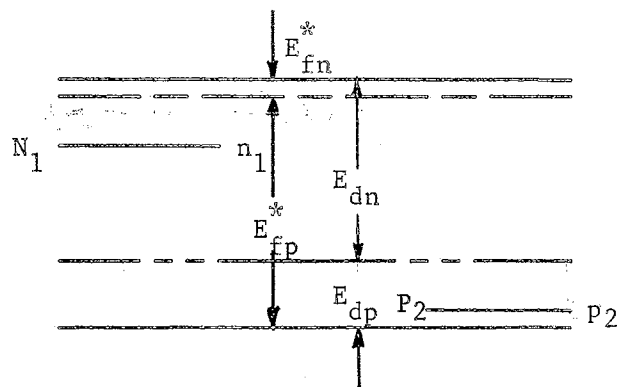
Figure 2. Simple band scheme illustrating demarcation levels.

Assume that $n_1 < N_1$ and $P_2 = 0$, p_2 being the occupancy of level P_2 by holes. This means that there are $(N_1 - n_1)$ available states for electrons and n_1 states for holes in N_1, and P_2 empty hole states available in the acceptor level. The maximum number of carriers that can actually be trapped in these levels under illumination depends on the relative positions of the Fermi and demarcation levels for the particular states involved. Equation 16 and its electronic counterpart show that although

the possibility exists for N_1 to trap holes, it would require an extremely large ratio $(S_p/S_n)_1$. As for electrons in N_1 and holes in P_2, the maximum trapping density will depend respectively upon the position of the electron and hole steady-state Fermi levels when the demarcation level lies at the energy of the states. At this point, of course, the states change into recombination centers upon an increase in illumination. Therefore if under this condition the demarcation level for the N_1 states lies far above the electron Fermi level, virtually no trapping could take place. On the other hand, if it were far below, then the trapping density could approach $(N_1 - n_1)$. Similar conditions are true for holes in P_2 in terms of the hole demarcation and steady-state Fermi levels.

Reiterating, calculation of trapping density magnitudes would require a knowledge of (1) the steady-state Fermi levels of both holes and electrons and (2) the demarcation level for the carrier being considered. Again a closed-form solution for the trapping density in terms of a specific model is extremely complex. However, the qualitative conditions expressed above are of great value and exemplify the application of the phenomenological technique.

The over-all effect of trapping states on the photoconductive process is to reduce the density of free carriers produced by the excitation. This may greatly affect both the rise and decay times of the transient process and the magnitude of the steady-state photocurrent. There are several techniques in present use which are particularly valuable in probing trapping properties. These include:[*]

---

[*]For a brief discription of these techniques refer to Chapter 9 of Bube's book.[29]

1. Rise and decay of luminescence emission and photoconductivity

2. Optically and thermally stimulated trap emptying

3. Space charge limited currents

4. Photodielectric effect

5. Paramagnetic susceptibility and paramagnetic resonance.

The technique employed in the present work is that of thermally
stimulated currents (TSC), which utilizes the temperature dependence of
the rate at which the trapping density is relieved. To illustrate this,
consider again the model of Figure 2. After the illumination is removed,
free electrons recombine with holes residing in mid-band recombination
centers; however, carriers which have been trapped during the illumin-
ation must be first thermally excited into their respective free bands
before they have a chance to recombine. As pointed out earlier, these
rates of thermal excitation depend exponentially on the reciprocal
temperature, i.e., in the case of trapped electrons

$$\frac{dn_t}{dt} = n_t N_c S_n \bar{v} \exp(-E_t/kT) \tag{20}$$

where n_t is the density of trapped electrons and E_t is their activation
energy. Therefore after the excess photoconductivity has decayed,
there remains a current whose magnitude depends upon the thermal excita-
tion and recombination rates. Of course, at a fixed temperature this
current depends directly on the trapped carrier densities and therefore
must eventually decay to zero as the occupancies of all the trapping
levels return to equilibrium.

The differential equation for this process is usually expressed in
terms of Equation 20 and an average lifetime for the free carriers τ,
i.e.,

$$\frac{dn}{dt} = n_t N_c S_n \overline{v} \exp(-E_t/kT) - n/\tau \tag{21}$$

where dn/dt is the rate of change of the conduction band electrons with time. Equation 21 neglects the possibility that during the time τ, retrapping of a part of the n free carriers might occur. This can be easily taken into account by adding to 21 the additional term $[-n(N_t - n_t)S_n \overline{v}]$.

In the normal TSC measurement, the trapping density is first established at a low temperature. Then after photo-decay upon cessation of illumination the temperature is increased at a constant rate. It is found that dn/dt is much smaller than the other rates for rates of temperature rise normally used. Therefore Equation 21 simplifies to

$$n(t) \doteq \tau n_t(t) N_c S_n \overline{v} \exp(-E_t/kT). \tag{22}$$

Under these conditions of temperature rise, the trapped density of electrons is obtained by solving the differential equation

$$\frac{dn_t}{dt} = -n_t(t) N_c S n \overline{v} \exp(-E_t/kT) \tag{23}$$

neglecting retrapping.

It can be seen from Equations 22 and 23 that for low temperatures the TSC is small and rises with increasing temperature. Eventually, however, this rise is balanced by a decrease in $n_t(t)$ at which time the TSC reaches a maximum. And finally, as $n_t(t)$ continues to fall, the TSC approaches zero.

Analysis of data such as obtained here was first done by Randall and Wilkins,[46] as applied to thermally stimulated luminescence. The activation energies of the trapping levels in terms of such an analysis

have been determined in a number of ways. The most widely used approach

is that of Garlick and Gibson[47] using the fact that the TSC rises

exponentially on the low temperature approach to its peak. They noted

that, since $T(t) = T_o + bt$, $dn/dt - (dn/dT)(dT/dt) = bdn/dT$, Equation 21

reduced to

$$n(T) = -b\tau\frac{dn_t}{dT} = b\tau n_t(T)N_c S_n \bar{v} \exp(-E_t/kT). \qquad (24)$$

So that as long as $n_t(T)$ remains fairly constant a plot of ln $n(T)$

versus $1/T$ has a slope equal to $(-E_t/k)$.

As pointed out by Haake,[48] the Garlick and Gibson method is usually

not possible due to the overlapping of peaks from nearby trapping levels.

However, Bube[49] has slightly modified their procedure to eliminate this

difficulty. This modification, known as decayed thermally stimulated

currents (DTSC), consists of raising the temperature after illumination

to a value somewhat below that of the desired peak. After sufficient

time has elapsed for the emptying of all lower energy trapping states,

the temperature is returned to its initial value and a normal TSC run

made. This procedure is repeated for the low temperature approach to

each peak in the TSC data and the activation energy is calculated using

the Garlick and Gibson technique.

Another widely used method for determining the trapping activation

energy, is Bube's[29] steady-state Fermi level calculation which assumes

that at the TSC peak the steady-state Fermi level coincides in energy

with the trapping states. Using this assumption and the definition of

steady-state Fermi level, the activation energy is calculated from the

equation

$$E_t = kT_m \ln[N_c e\mu/\sigma(T_m)] \qquad (25)$$

where T_m and $\sigma(T_m)$ are respectively the temperature and conductivity at the peak, e the electronic charge and μ the carrier mobility. In the present work, both the decayed modification to the Garlick and Gibson method and the Bube technique are used to calculate activation energies. A good review of other methods is contained in an article by Haering and Adams.[50]

Sensitization and Quenching

Some of the most interesting photoconductive phenomena are concerned with the switching of impurity levels from trapping to recombination centers. In terms of what has already been said, this is a result of the demarcation level for a set of states shifting its position through the states. Consider again the model of Figure 2 and remember from Equation 15 that the demarcation level differs from the steady-state Fermi level only by an amount $kT\ln(nS_n/pS_p)$. Actually there is some qualitative merit in assuming that they are equal, since kT is only 1/40 ev at room temperature and only slight variation comes from the logarithm term. Assume further that under excited conditions the demarcation level takes a position just under the N_1 states. This means that little recombination takes place through this level and that its occupation density is described by the conduction band steady-state Fermi level, i.e.,

$$n_1^* = N_1 \exp[(E_{fn}^* - E_1)/kT] \qquad (26)$$

where n_1^* is the total occupation density of N_1 under excitation and E_{fn}^* is the steady-state Fermi level.

The picture may drastically change if now the light intensity is increased (E_{fn}^{*} is decreased) sufficiently to position the demarcation level above the states. Recombination now takes place through the N_1 states and their occupation is specified by the recombination kinetics. It can easily be shown that for steady-state the electron occupancy as determined by these kinetics is given as

$$n_1^{*} = \frac{N_1}{1 + \frac{P}{n} \frac{S_p}{S_n}} \cdot \quad (27)$$

The effect of this shift on the photoconductive process may vary widely depending on existing conditions.

One would expect that adding recombination centers would decrease the steady-state photocurrent. However, one other effect must be taken into consideration. This is the effect of those electrons or holes which are displaced from the trapping states when they become recombination centers, i.e., the difference in occupation density as described by Equations 26 and 27. Effectively these carriers are transferred from the trapping states into the main recombination centers or into shallower trapping states, if any exist. These main recombination centers are normally assumed to be located near the center of the band and have large, essentially equal, cross sections for holes and electrons. This transfer of carriers can have a drastic effect on the lifetime under certain conditions.

In the case cited in Figure 2 for the partially ionized donor states, the effect would be only an increase in the total recombination rate, since the states are almost filled in equilibrium and $S_{n_1} > S_{p_1}$ would require only slightly additional filling after the shift. However,

large effects may occur due to the compensated acceptors P_2, if one assumes $S_{p_2} \gg S_{n_2}$. Now when the demarcation level passes through the P_2 states they become almost completely occupied by holes. Assuming that the densities of P_2 states and main recombination centers are large compared with the density of free carriers, the electrons that were originally in the P_2 centers are effectively transferred to the recombination centers. Therefore, the free electrons see recombination centers which have few holes for capture and their lifetime is thereby increased.

The model just presented is the one normally accepted for sensitization of an n-type insulator. And this method of increasing the sensitivity by controlled impurities of the acceptor-type described is found to be extremely effective. Data taken of saturation photocurrent versus temperature on such sensitized materials shows graphically the effects of the trap-to-recombination shift. An excellent example of such thermal quenching data is given in an article by Bube[51] on CdSe:i:Cu crystals and is presented there as his Figure 7.

The decrease in photocurrent for a particular light intensity as the temperature increases is again due to the rise in hole demarcation level. It is assumed that the break in sensitivity occurs when the hole demarcation level is at the acceptor states. Therefore from the conductivity and temperature at the break, it is possible to calculate the activation energy. This is done by noting that under these conditions Equation 16 reduces, assuming $m_e = m_h$, to

$$E_2 = kT_b \ln[N_v e\mu/\sigma(T_b)] + kT_b \ln(S_p/S_n)_2 \qquad (28)$$

where E_2 is the activation energy of the sensitizing centers and T_b,

$\sigma(T_b)$ are respectively the temperature and conductivity at the <u>break from</u> <u>high sensitivity</u>. Therefore a plot of $\ln \sigma(T_b)$ as a function of reciprocal temperature for several light intensities has a slope equal to $(-E_2/k)$. Also, the intercept at $1/T_b = 0$ yields the following relation

$$\left(\frac{S_p}{S_n}\right)_2 = \frac{\sigma(1/T_b = 0)}{N_c e \mu} \tag{29}$$

which allows one to calculate the ratio of electron and hole cross sections for the P_2 centers.

An analysis can also be made to determine the conditions for the <u>break to low sensitivity</u>. However, it is not easily presentable and therefore only the conditions themselves are to be given here.* They are represented by an equation very similar to 28, i.e.,

$$E_2 = kT_b \ln[N_c e \mu/\sigma(T_b)] + kT_b \ln(N_r/P_2) \tag{30}$$

where N_r is the density of the main recombination centers. It is therefore possible from the $1/T_b = 0$ intercept to calculate the ratio of the density of sensitizing centers to that of recombination centers.

Thermal quenching occurs when holes that fill the sensitizing centers are thermally excited into the valence band. Such an excitation can also be accomplished optically using light of energy equal to the sensitizing center's activation energy. This is known as optical or infrared quenching and, of course, only takes place at temperatures below that of the thermal process. It requires both an intrinsic and extrinsic source of radiation and because of the large difference in

---

*The complete analysis is contained in an article by Bube.[51]

absorption coefficients, the extrinsic must be much more intense than the intrinsic source. The activation energy of the sensitizing centers corresponds to the photon energy which causes maximum quenching. There may be several maxima if more than one sensitizing level exists.

To conclude this section, it is appropriate to discuss the effects of trapping centers on the steady-state photocurrent.* First, it should be remembered that these states are by definition in equilibrium with their nearest band and their occupancy is therefore determined by its steady-state Fermi level. Also, the general trapping effect is to reduce the free carrier density produced by the excitation process.

Consider the model of Figure 3 under the assumptions that (1) the density of main recombination centers N_r is large compared with the electron trapping density N_t, (2) virtually all the holes are immediately captured by the recombination states and (3) the trapping level is unoccupied under equilibrium conditions.
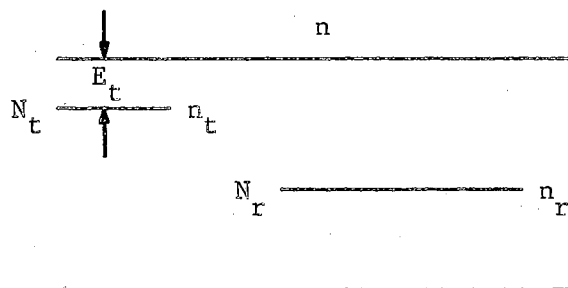
Figure 3. Simple band scheme illustrating electron trapping.

Under these assumptions the number of steady-state photo-electrons in the conduction band is given by the expression

$$n = \frac{\alpha L}{\overline{v}\, S(N_r - n_r)} \tag{31}$$

----

*A more complete survey of this material is found in an early article by Rose.[52]

where αL is the excitation rate and S the average cross section of the recombination states. For assumed conditions such that $n \ll N_t$, then $n_t \gg n$ and conservation of charge requires that $N_r - n_r = n + n_t \doteq n_t$. Therefore, the density of electrons in the conduction band is given by

$$n \doteq \frac{\alpha L}{\bar{v} \, S \, n_t} \qquad (32)$$

in the presence of trapping. This expression in the absence of trapping would contain n instead of n_t so that the over-all effect of the electron trapping states is to lower the sensitivity by the factor n/n_t. The ratio of free to trapped carriers can be shown to be proportional to $\exp(-E_t/kT)$ and therefore the sensitivity increases with increasing temperature. In such cases, this behavior allows a calculation of the trapping activation energy to be made in terms of ln n vs. 1/T data.

Carrier Lifetime

The concept of carrier lifetime has been mentioned earlier in this chapter in conjunction with the decay of thermally stimulated carriers. Defining such a constant requires the assumption that the rate of decay of nonequilibrium carriers is proportional to their density. This, of course, implies an exponential decay function. Seldom is such a simple behavior found experimentally.

To be more realistic, the differential equation describing the photoconductive process could be written as a power series in the carrier density. One normally finds regions of temperature and carrier density where all terms but one in this series effectively drop out, e.g., for high carrier densities only the second power would be present whereas in the sensitive region the power might be slightly less than one. In

other words, Equation 19 can be written quite generally in terms of the sum of carrier densities, or the conductivity, as

$$\frac{d\sigma}{dt} = A \ \alpha(\lambda)L(\lambda) - \frac{\sigma}{\tau(\sigma,T)} \tag{33}$$

where A takes into account the constants involved in changing number density to conductivity. Therefore, as far as total conductivity is concerned, a composite carrier lifetime can be obtained experimentally by noting that at saturation $d\sigma/dt = 0$, and $A\alpha(\lambda)L(\lambda) = \sigma_s/\tau(\sigma_s,T)$, and the carrier lifetime can then be calculated from the expression

$$\tau(\sigma_s,T) = \frac{\sigma_s}{(d\sigma_s/dt)_{t\approx 0}} \tag{34}$$

With sufficient data, one can map the function $\tau(\sigma_s,T)$ for all values of σ_s and T. Such data, even though it is complex, is very important in determining the density of trapped carriers in TSC measurements.

Photo-Thermoelectric Voltage

A theoretical treatment of thermoelectric effects applied to photo and thermally stimulated carriers, as far as is known, does not exist. Therefore, special difficulty is encountered in interpreting this type of data. The value of such an experimental analysis remains to be clearly established and only a preliminary, highly qualitative discussion is opened at this time.

It can be shown that the normal, one-carrier thermoelectric voltage developed across a semiconductor, over which a temperature differential exists, is related to the steady-state Fermi level by (see the Appendix for development and notation)

$$V_{\Delta T} = - \frac{1}{q} \int_{T_1}^{T_2} (\frac{E_{fq}}{T} - \frac{dE_{fq}}{dT}) \, dT \qquad (35)$$

where $V_{\Delta T}$ is the thermoelectric voltage across a sample whose ends are held at temperatures T_1 and T_2. In order to evaluate the experimental data it is necessary to know the variation of E_{fq} with temperature. Note it is possible to have conduction by one carrier type and predict the wrong sign of the thermoelectric voltage if the integral of the second term in Equation 35 should become greater than that of the first.

For the simple case of dark conductivity, the temperature dependence can be derived (see Equation 12). However, in neither the TSC or CTQ procedures is enough information available to predict the behavior of $E_{fq}(T)$ throughout the entire temperature range. In the TSC procedure, the current rises on the low temperature approach to the peak at a rate proportional to $\exp(-E_t/kT)$ which implies that the second integral term in Equation 35 is small and in this region carrier type determinations should be possible. However, on the high temperature side of the peak the Fermi level is falling fairly fast. Therefore, here the sign may be positive or negative depending upon which integral term in Equation 35 is the larger.

For the case of the CTQ procedure, the Fermi level is close to the free carrier band (E_{fq} small) and almost independent of temperature in the sensitive region. Therefore, the thermoelectric voltage is small but again identifies the carrier type. However, in the quenching region the sign may change depending again on the relative magnitude of the integrals of the terms dE_{fn}/dT and E_{fn}/T in Equation 35. Note it might be expected that the second integral term would be increased to a greater

extent than the first by placing a larger temperature gradient across the sample.

In essence it is possible to predict the behavior of the steady-state Fermi level with temperature, if it is assumed that in both the TSC and CTQ procedures only a single type carrier is involved. Under this assumption, the function $E_{fq}(T)$ can be mapped from the normal data through the use of the relation between conduction current and Fermi level (Equation 12). However, in order for this information to be of use in experiments on photo-thermoelectric voltage, the temperature differential would have to be known over the entire working temperature range.

CHAPTER III

SAMPLES, APPARATUS AND EXPERIMENTAL PROCEDURES

Samples

The samples used in this investigation were small rectangular stannic oxide single crystals* which were locally grown from a cuprous oxide flux by Kunkle.[21] Spectrographic analysis showed these crystals contained approximately 0.0021% cuprous oxide and 0.02% silicon dioxide by weight.** The flux growth generally produced a multitude of tiny needles measuring approximately one tenth millimeter on a side and several millimeters in length. However, it also produced larger crystals measuring approximately one-half millimeter on a side and two or three millimeters in length which were of sufficient size for sample use. A typical example is shown in the photograph of Figure 4a. Ordinarily the crystals are free of visible mechanical defects, however now and then one will be found containing small capillaries. These capillaries are sometimes filled with a dark red material assumed to be copper oxide. The existence of such concentrations may well be responsible for the large value of copper shown in the spectrographic analysis since it was performed on a sizable number of small crystals.

---

*Crystals perfection investigated by the Laue back-scattering X-Ray technique.

**Analysis by The Bruce Williams Laboratories, Joplin, Missouri.

Figure 4b shows a photograph of light reflected from a grown surface. Note that the surface appears to be well formed except for a slight embossed flaw pattern. The samples used were chosen for their lack of physical defects both on the surface and in the bulk.

As is the case in many pure oxides, the conductivity of these crystals is probably due to nonstoichiometry caused by oxygen vacancies. Consequently, it is extremely sensitive to past history. For example, if a crystal is heated to 700° C in air its calculated room temperature conductivity can be below 10^{-14} (ohm-cm)$^{-1}$, but if at that temperature it is heated in a vacuum $(10^{-3}$ mm Hg) the conductivity may be greater than 10^{-7} (ohm-cm)$^{-1}$. The extent of the increase due to the vacuum treatment depends, of course, on the temperature and the duration of the treatment. It is therefore somewhat misleading to quote a characteristic conductivity for each sample. This is later emphasized by the fact that several experiments were actually done as functions of the dark conductivity (varied as described above). All evidence to date points to the fact that these samples have n-type dark conductivity. Hall effect measurements showed this to be the case in the natural crystals and the sign of the thermoelectric power indicates it to be true here also. This is what would be expected when oxygen vacancies are present.

Ordinarily the grown surfaces appear to have very high resistivities making electrical contact to the bulk difficult.* However, the surface resistance is found to be extremely sensitive to abrasion, e.g., calculated sample conductivities as large as 10^{-4} (ohm-cm)$^{-1}$ may be obtained by lightly sandblasting the surfaces. This fact is utilized in making contact to the bulk by first lapping the crystal ends flat. But since

*Unpublished data by Kunkle.
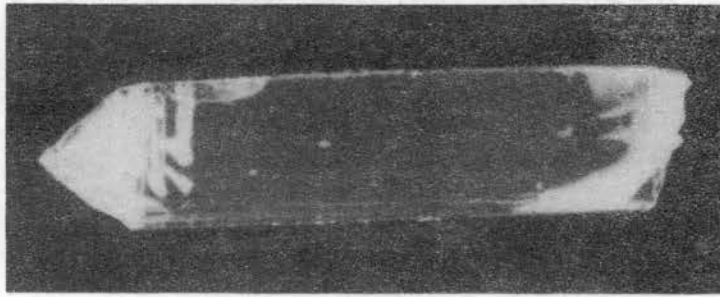
a.
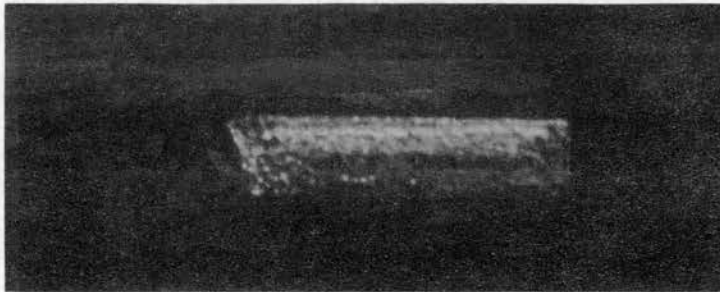
b.

Figure 4. a. Typical stannic oxide single crystal b. Light
   reflected from a single crystal surface.

the effect is not well understood, great care was taken in sample hand-
ling to insure that the grown surfaces were not damaged.

The first step in sample preparation, as mentioned before, was to
lap the ends flat. This was done by mounting the crystal in the simple
clamp shown in Figure 5 and securing it with optical wax. The crystal
end was then abraded using No. 600A Wetordry silicon carbide paper on
a hard flat surface.
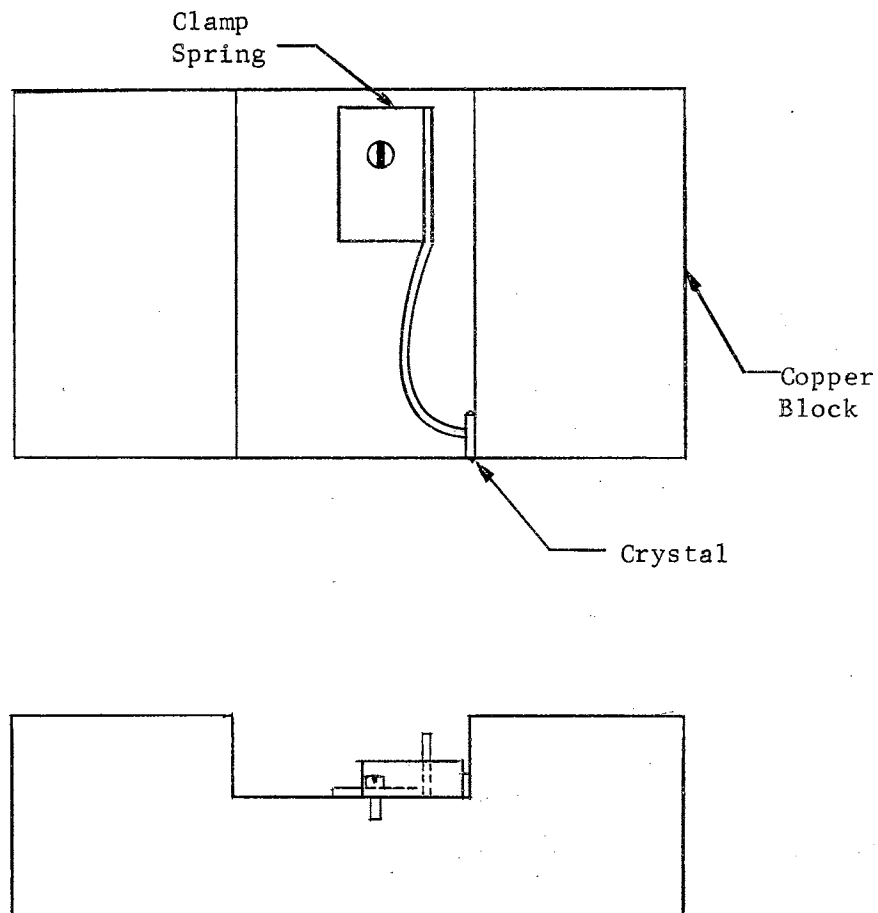
Figure 5. Holder for lapping the ends of the samples.

Because of the extraordinarily high resistance of the samples, it
was very important that they be properly cleaned before mounting. The
cleaning procedure usually started with approximately four-hour baths

in both hydrofluoric acid and aqua regia (75% HCl, 25% HNO_3). The hydro-
fluoric acid bath was generally not repeated after the first cleaning.
The acid bath was followed by short ultrasonic rinses in acetone,
distilled water and methyl alcohol.*

The final step in sample preparation was the application of electri-
cal end contacts. These consisted of pure indium applied with a small,
reostatically controlled soldering iron. It was found that for best
results the sample and iron should be separately heated to approximately
180° C. Also it was absolutely essential that the soldering tip be
properly tinned and free of oxides and flux. These techniques were found
by Houston[53] to give good contacts on natural stannic oxide. Contact
to the ends was then made through spring-loaded indium tinned copper
pressure leads.

Apparatus

All of the measurements in this study were made using the same
basic sample fixture, which consisted of a cryostat and a sample holder.
A drawing of the cryostat is shown in Figure 6. It was constructed of
glass and was capable of operation at sample temperature from 77 to 373° K.
Also, through the use of the front "O"-ring and the rear ball-joint seals,
it was made to be both easily accessible and vacuum-tight. Due to the
high system resistance requirement, the leads were brought out using
individual tungsten feed-throughs.

The heater was wound on a Housekeeper copper-to-glass seal which
was capped by silver soldering a copper disc over the open end. Nichrome

---

*The ultrasonic rinses were done in a Gulton Industries Model GT-1-10
ultrasonic cleaning unit.

Liquid Nitrogen
chamber (silvered)

Vacuum
Feed-throughs

1/4" House-
keeper copper-
glass seal

Heater

Tungsten
Pass-throughs

3/4" Housekeeper
copper-glass seal

Copper
cap

18 x 9 mm
Ball Joint

"O" Ring Flange
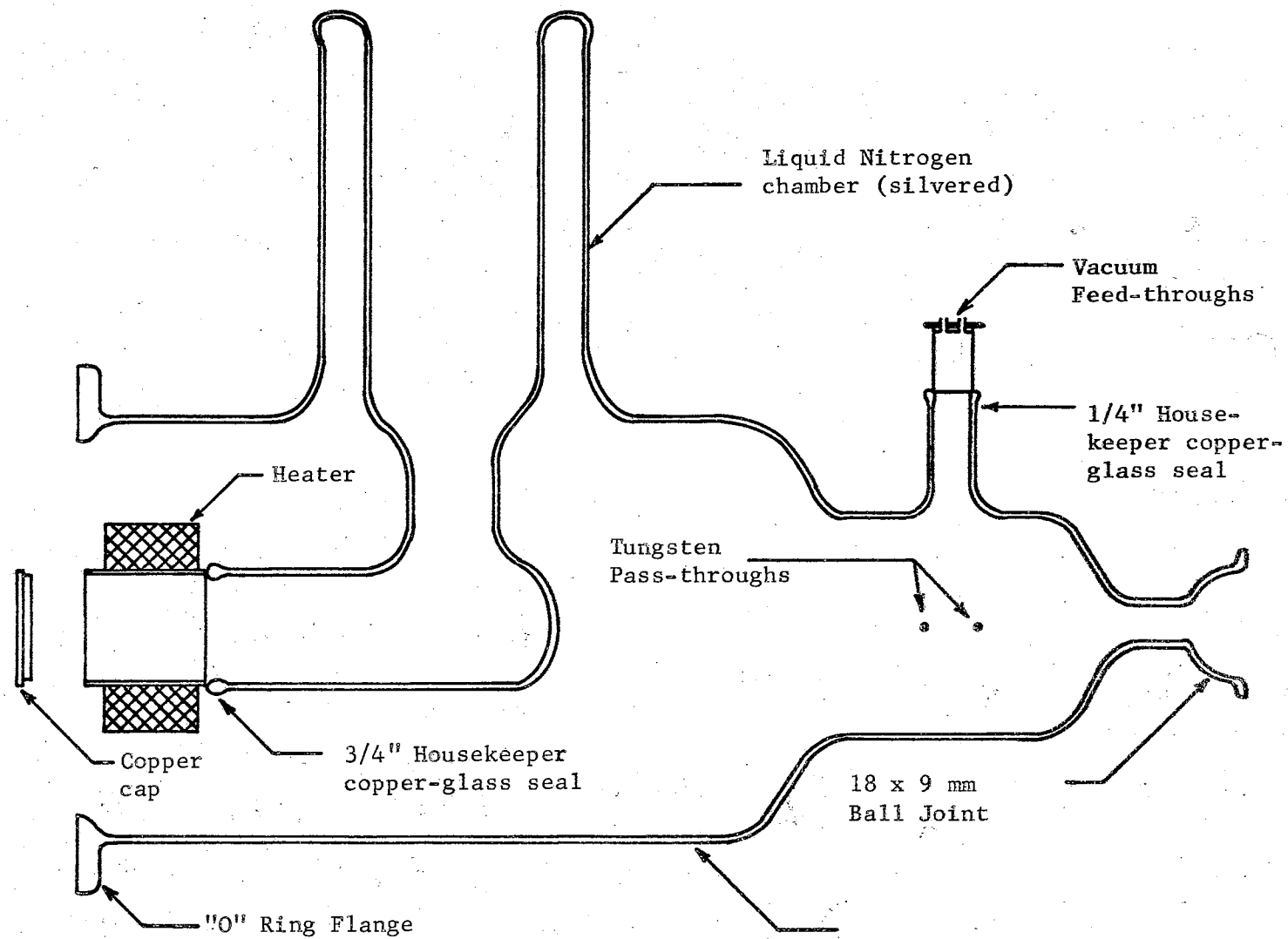
Figure 6. The sample cryostat.

44

wire was used in the windings and they were insulated from one another

by asbestos tape sealed with No. DW-30 Saureisen electrical cement.

A drawing of the sample holder is shown in Figure 7. Considerable

care was required to insure a holder design which would have very high

leakage resistance and still maintain homogeneous temperatures throughout

the sample. These requirements were well met by the symmetric quartz-

rod pressure contact arrangement shown in Figure 7. The quartz rods

used each had two capillaries through which the leads were passed. One

end of the sample was maintained at ground potential and its temperature

was monitored by a copper-constantan thermocouple. The other end was

fed directly to the current measuring electrometer and was therefore

the critical lead as far as leakage was concerned.

The sample holder was indium soldered* to the metal-to-glass cap

in the cryostat, and the entire fixture was mounted on the monochromator

as shown in Figure 8. The leakage resistance of this arrangement usually

was in excess of 10^{15} ohms. However, it should be pointed out that this

high a resistance was only attained with room humidity of less than 50%

(relative) and after careful baking of the tungsten feed-throughs.

The principal measurements in the present study required monitoring

the sample conductivity. Again, because of the low values involved, the

conductivity was measured using a standard two-probe electrometer techni-

que. The electrometers used were Keithley's Models 610B and 621. These

meters were capable of measuring full-scale currents of 10^{-14} and 10^{-11}

amperes respectively. This essentially gave resistance measuring capabil-

ities of 10^{16} and 10^{13} ohms respectively using a 90-volt series supply.

---

*The indium soldering of copper is facilitated by using Indaloy Flux #1
manufactured by The Indium Corporation of America.
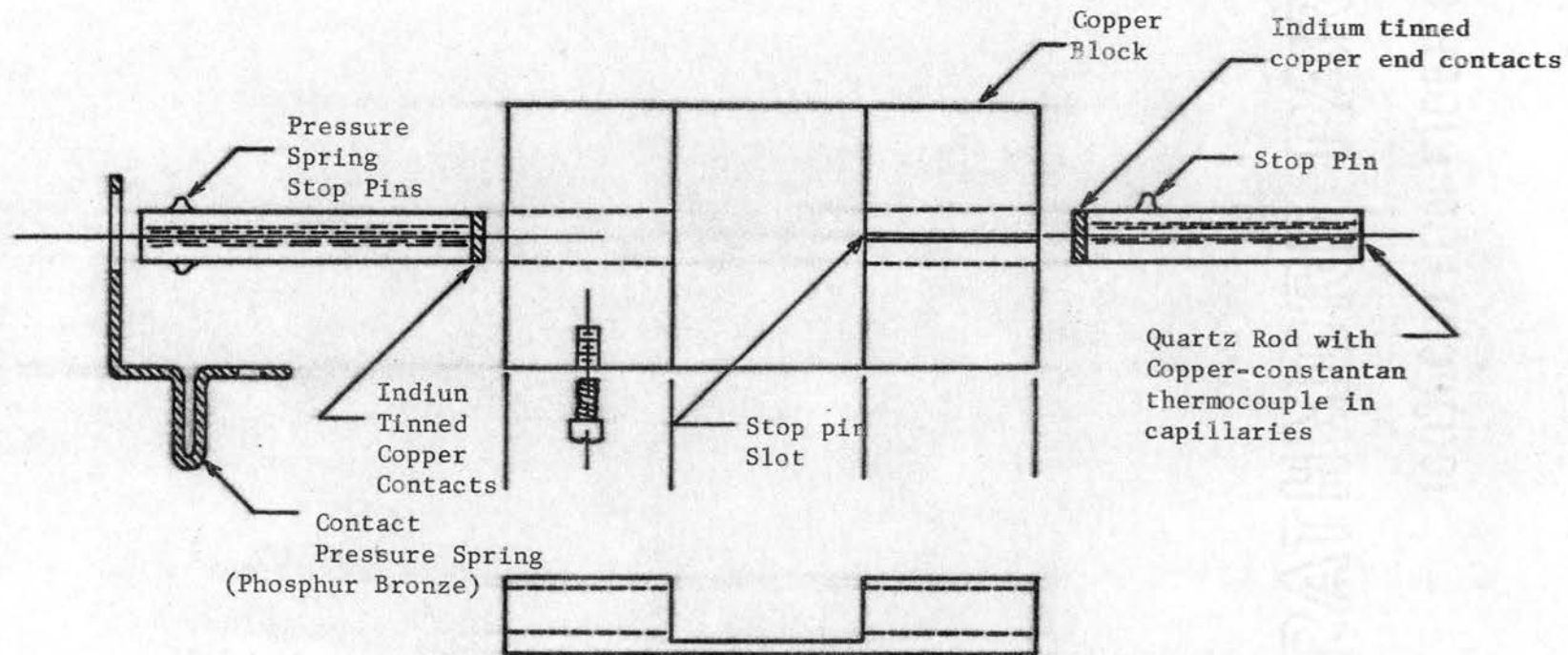
Figure 7. The sample holder.
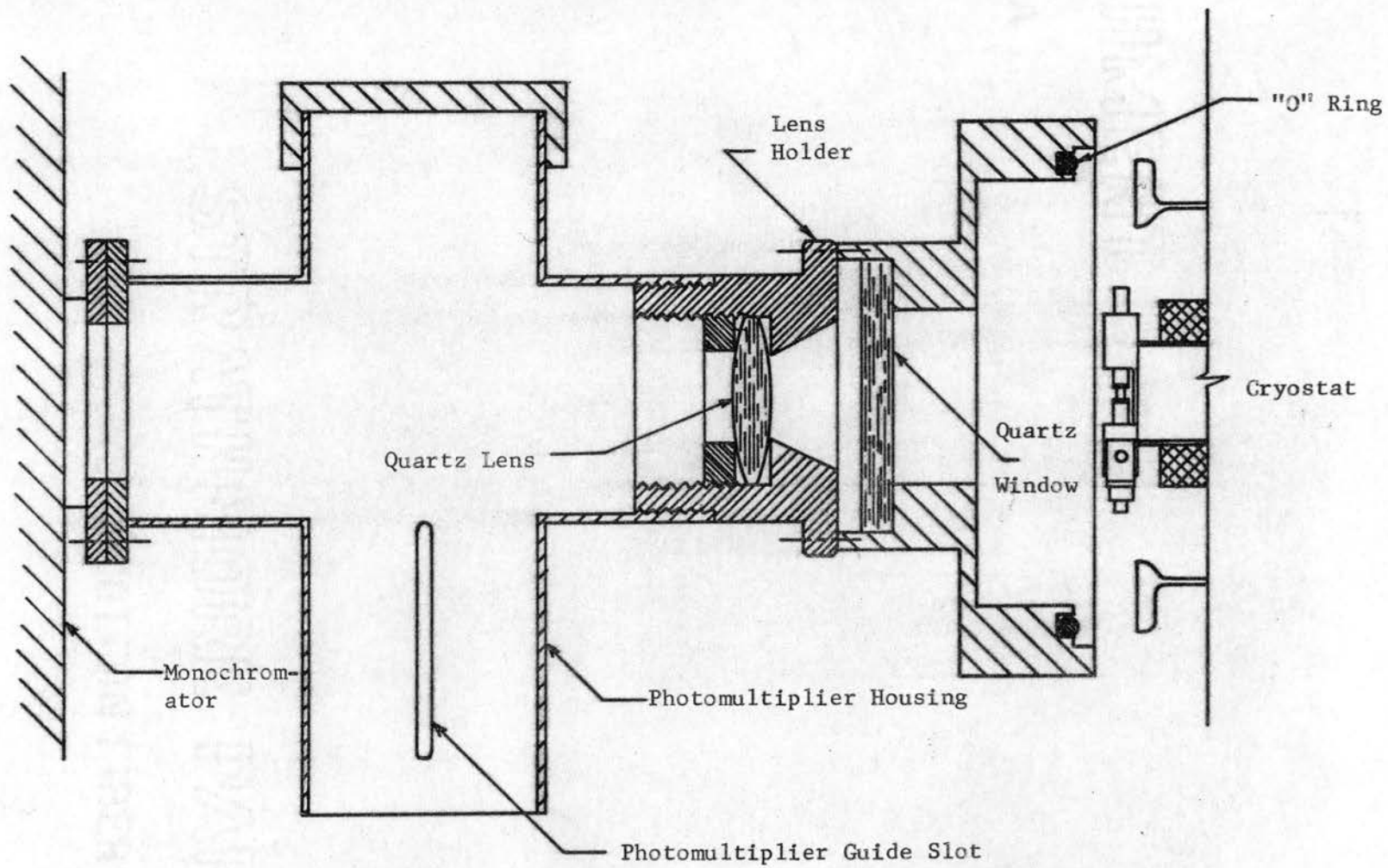
Figure 8. Mounting arrangement of cryostat flange and photomultiplier
housing to monochromator.

The ultimate value of conductivity was restricted by the system leakage
and the background noise level. In order to minimize the noise, it was
necessary to shield the entire system and common ground all neighboring
equipment.

The sizes of the samples virtually restricted conductivity measure-
ments to the two-probe technique. This, of course, raises the question
of contact effects. However, recent four-probe data indicates that this
is a negligible problem.* To additionally support this contention,
measurements were made of the saturation photocurrent as a function of
crystal voltage. A typical example of this data is shown in Figure 9.
Here it appears that the nonlinearity is so slight as to be insignificant.

Along with the conductivity, almost every measurement in this work
required a source of narrow band radiation. This was achieved by using
one of several monochromators. The one selected was determined by the
wavelength range and radiation source intensity required. A Bausch
and Lomb 500 mm grating monochromator was used most extensively. This
instrument has a wavelength range of from 200 to 700 mμ (millimicrons)
and a reciprocal linear dispersion of 3.3 mμ per mm in the first order.
It was used with either a mercury arc lamp for high intensity or with
a deuterium lamp where a continuous spectral distribution was required.**

For measurements of extrinsic photoconductivity a Beckman DK-1
quartz prism recording spectrophotometer was used. This instrument
has a wavelength range from 185 to 3500 mμ using a hydrogen (185-375 mμ)

---

*Unpublished data by Kunkle.

**The deuterium lamp was a Model D-102 distributed by The George W.
Gates Company, Inc.
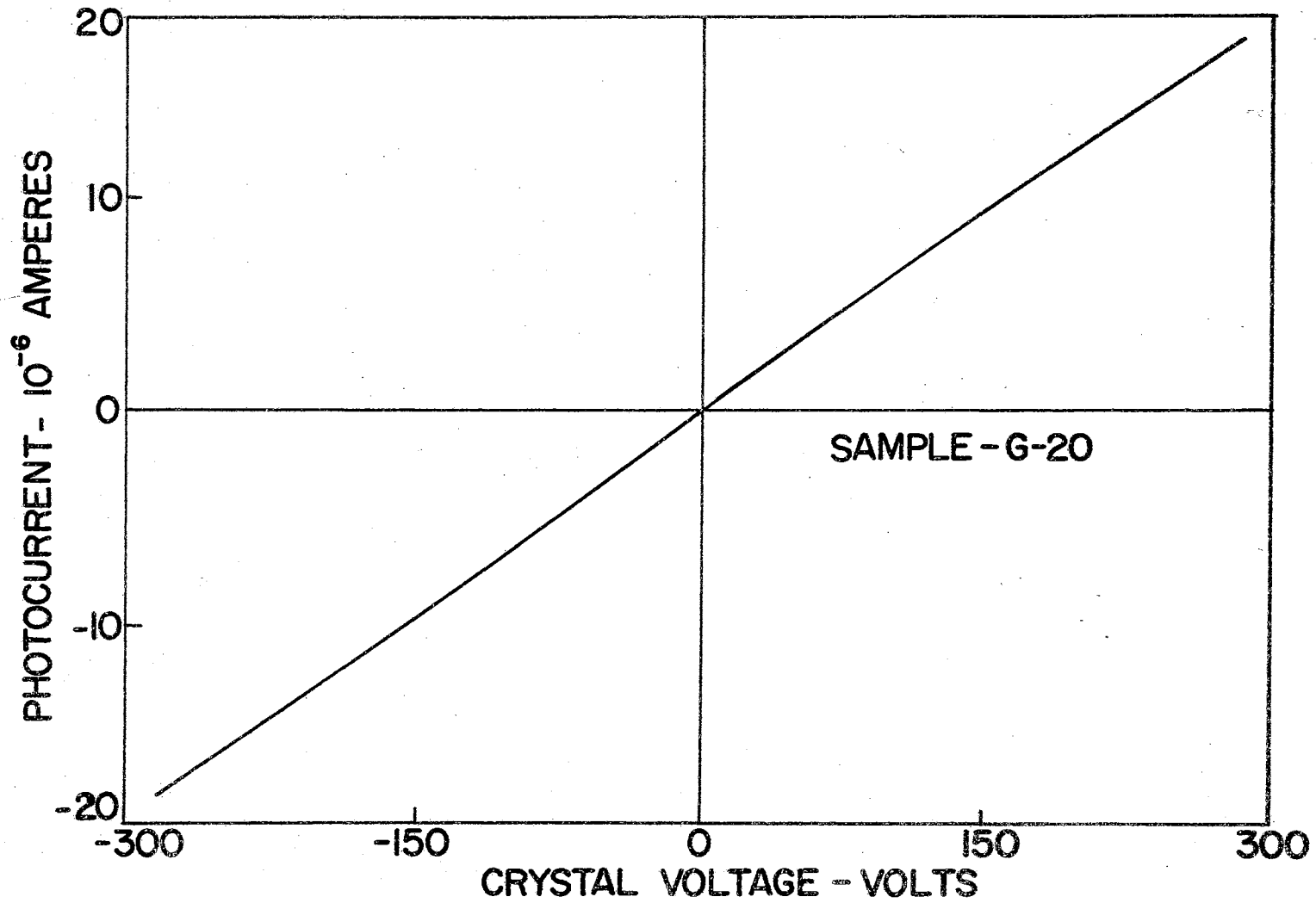
Figure 9. Typical data of saturation photocurrent as a function of crystal voltage.

and a tungsten (350-3500 mμ) lamp. When using this instrument as a
monochromator the cryostat was mounted above and to the rear of the
sample chamber. The beam was brought out of the chamber and focused
onto the sample by the arrangement shown schematically in Figure 10.
The reflectors used were aluminized front surface mirrors and the focusing
lens was quartz.

For the far infrared which was required for optical quenching data,
a Beckman IR-7 spectrophotometer was used. This instrument has a wave-
length range from 2.5 to 15.4 μ and uses a Nernst glower as a source.
The spectrophotometer had to be slightly modified in order to use it as
a monochromator. This change consisted of rearranging the last beam
mirror so that instead of falling on the thermocouple the beam was
diverted through an aperature cut for the purpose. The beam from the
aperature was then focused on the sample by a large concave aluminized
mirror. Actual focusing was accomplished visually by internally blanking
the dispersion elements with flat mirrors so that the full glower output
was brought through the aperature.

For measurements of relative spectral response it was necessary to
know the spectral distribution of intensity for each radiation source.
These sources had to be calibrated using some standard detector. In
the case of the deuterium lamp, a 1P28 photomultiplier was used assuming
the manufacturer's spectral sensitivity specifications to be correct.
The calibration was accomplished on the Bausch and Lomb monochromator
by sliding the photomultiplier into the beam as shown in Figure 8. The
actual data is shown in Figure 11. In the case of the DK-1 and its
hydrogen and tungsten sources, calibration data was available from prior

Electrostatic
Shield

Aluminized Front
Surface Mirror

Lens
Holder

Cryostat

Vacuum
Port

Mirror
Holder

Cryostat
Flange

Aluminized Front
Surface Mirror

Beckman DK-1
Spectrophotometer

Beam

DK-1
Sample
Holder
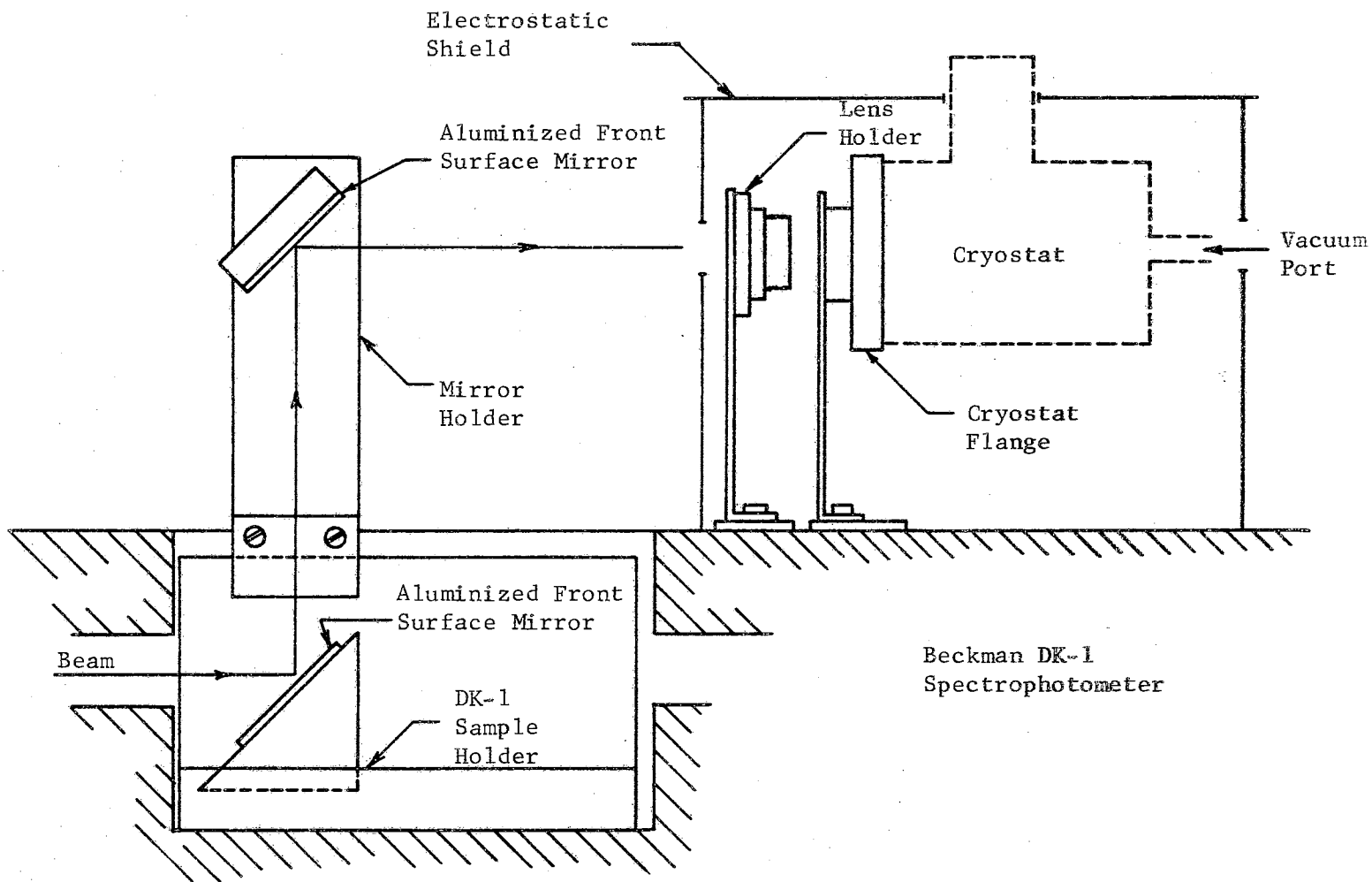
Figure 10.   Schematic of cryostat arrangement for DK-1 spectrophotometer.
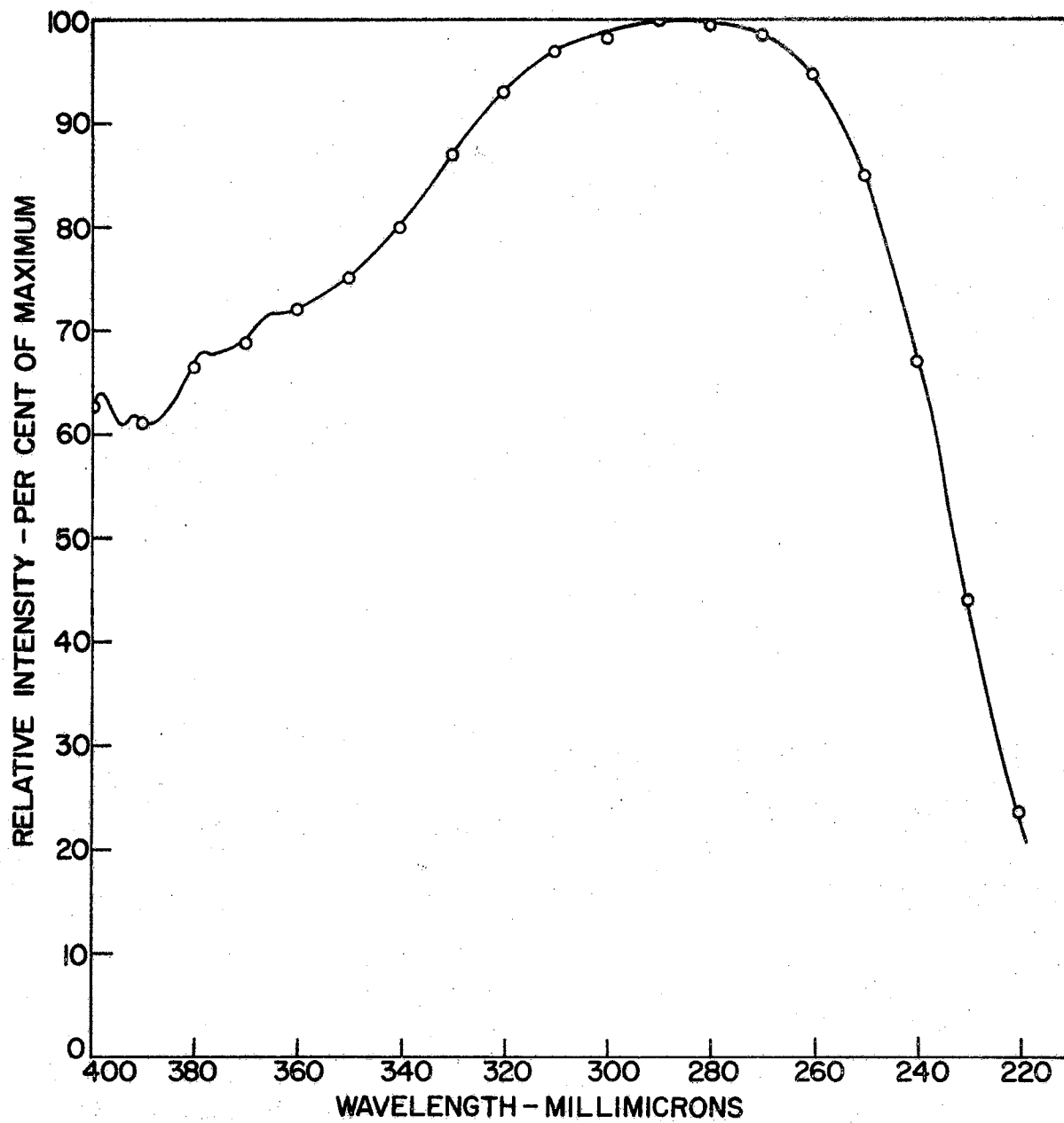
Figure 11. Output dispersion curve for the deuterium lamp.

thermopile measurements.* This data is shown in Figure 12 and 13.

Several of the experimental procedures require the continuous monitoring of the conductivity as a function of temperature. This functional relationship was taken directly by plotting the two variables on a Moseley Autograf X-Y recorder. The conductivity axis was plotted from the voltage output of the Keithley electrometer. However, the thermo-couple output had to first be amplified. This amplification was accomplished through the use of a General Electric Model 8901490G2 self-balancing potentiometer. A block schematic of the conductivity-temperature system is shown in Figure 14.

Measuring Techniques

As mentioned before, the bulk of the experimental procedures called for the system shown in Figure 14. These include measurements of normal and decayed thermally stimulated currents, continuous thermal quenching, and dark conductivity versus temperature. The techniques of taking these data differed only in application of the radiation and variation of the temperature.

The thermally stimulated current measurement (TSC) consisted of several minutes of irradiation at liquid nitrogen temperature followed, after a time sufficient for the decay of most of the resulting photo-conductivity, by a constant rate of temperature rise. This linear temperature rate was maintained manually by holding the slope of a temperature versus time plot constant and is estimated good to 5%. The plot was taken on a Texas Instruments Recti-Riter recorder and the slope control was accomplished by reostatically varying the heater current.

*Unpublished data by Northrup.
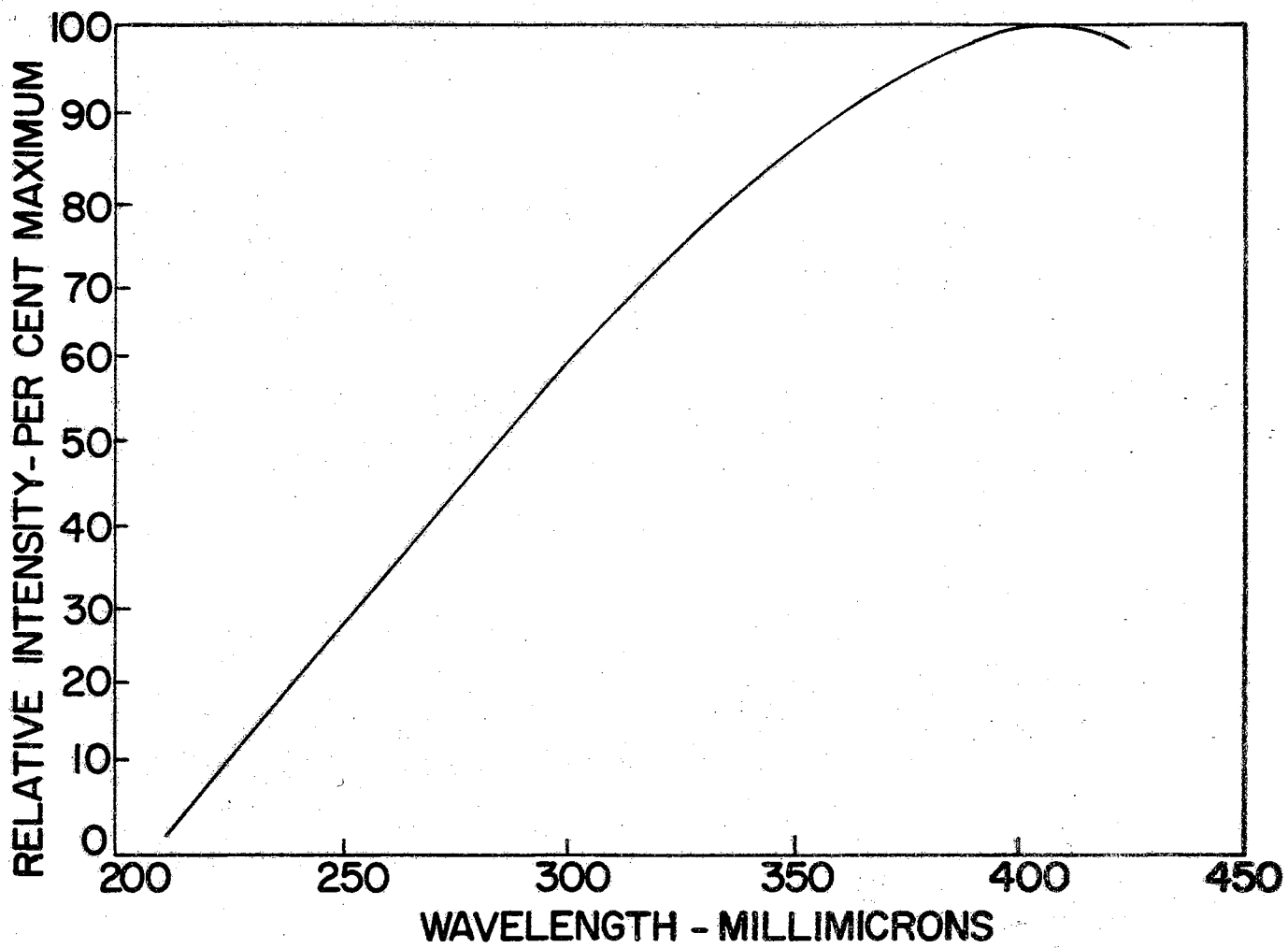
Figure 12. Output dispersion curve for the hydrogen lamp.
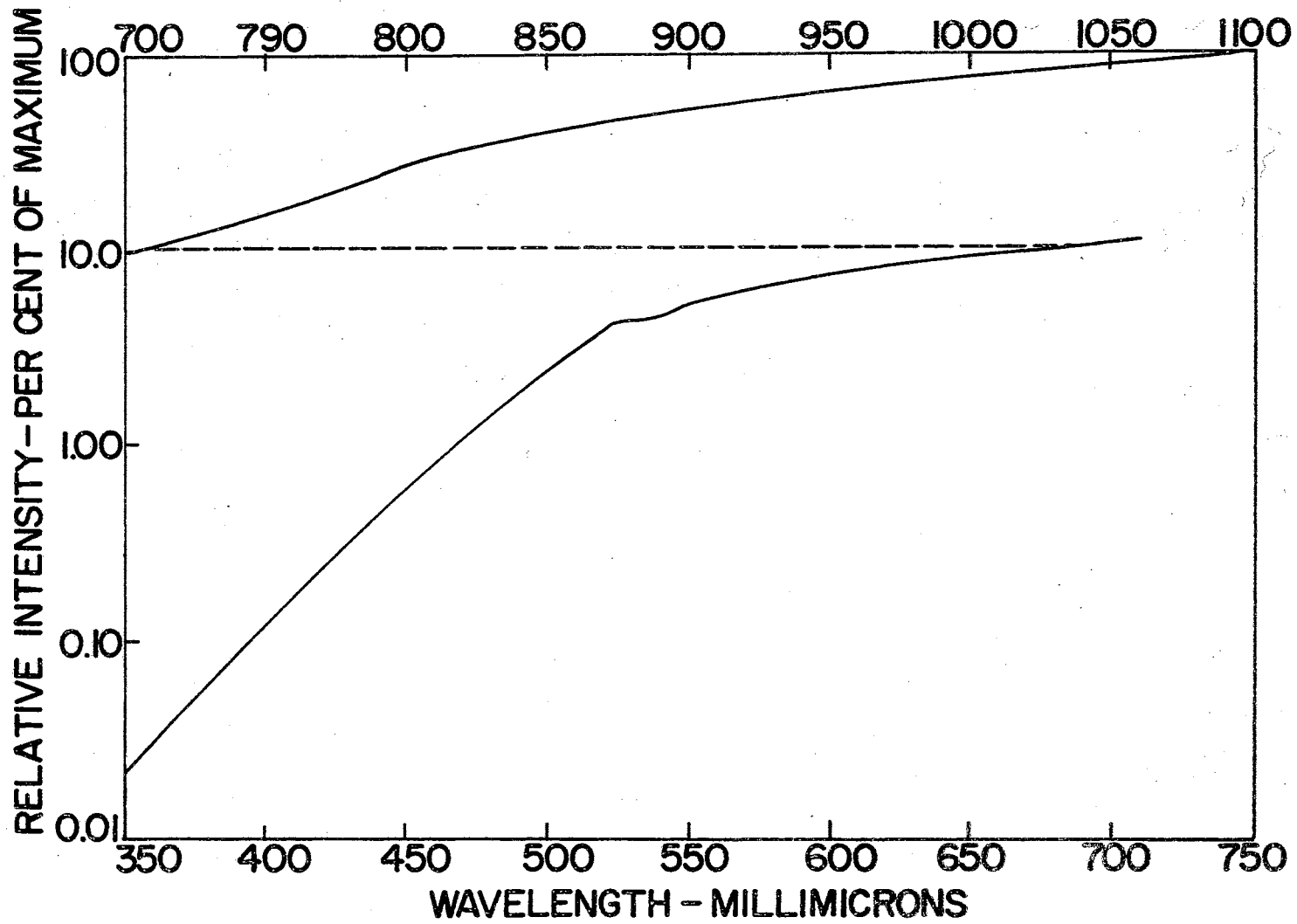
Figure 13. Output dispersion curve for the tungsten lamp.
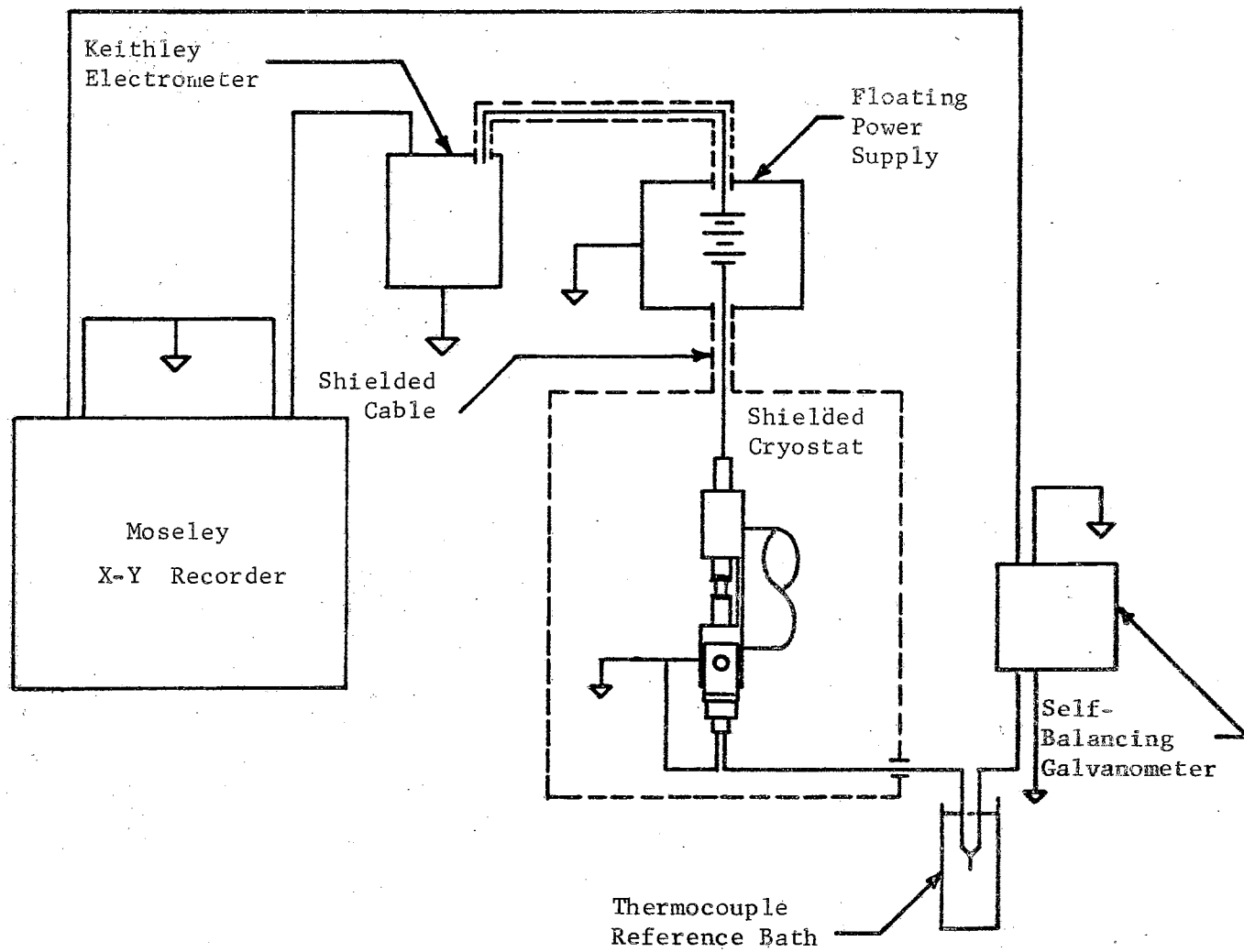
Figure 14. Block schematic of the conductivity-temperature system.

The decayed thermally stimulated currents (DTSC) technique differed from this in that the temperature was first raised after excitation to empty low lying traps before the sample was re-cooled and a normal TSC-type run was begun. This allowed the investigation of a given trapping peak by decaying away the background currents from all the lower lying levels.

In the case of continuous thermal quenching (CTQ); the sample was held at liquid nitrogen temperature until the photocurrent saturated and then its temperature was allowed to drift very slowly upward. The conductivity and temperature were again continuously plotted during the rise. This procedure was usually repeated for several radiation intensities. The relative intensities were measured by the 1P28 photomultiplier, as described earlier, and were varied using wire mesh neutral filters. Data of dark conductivity as a function of temperature was taken in exactly the same manner except that continuous excitation was omitted.

Optical quenching measurements were attempted at liquid nitrogen temperatures using the B & L monochromator as the intrinsic source and a specially adapted Beckman IR-7 recording spectrophotometer as the quenching source. No quenching effect was noted using either the IR-7 source or higher temperature black body sources. It was pointed out in the previous chapter that the quenching source would have to be several orders of magnitude more intense than the intrinsic source. It is estimated that the highest IR source intensity used here was some three orders of magnitude below that of the intrinsic source, which would account for the lack of an effect. Since more intense extrinsic sources were not readily available, this general procedure was not pursued.

Ideally, spectral response data would be taken as saturation photo-current as a function of wavelength (for a constant temperature). However, experimentally this procedure presents some practical problems. In the first place, the illumination time required to actually reach saturation was found to be excessively long. Further, the trapping properties of these crystals required that if saturation data was to be obtained the traps would have to be emptied between each measurement for accurate results. As a compromise, spectral response data in the present work was taken continuously by very slowly sweeping the wavelength range from long to short values. These procedures were repeated (after trap emptying) for several temperatures.

Some exploratory measurements of photocarrier lifetime have been made using the procedure outlined in the previous chapter. The measure-ment of initial decay rate on these high resistance crystals requires extremely wide-band electronics. The circuit used in the present study limited lifetime measurements to saturation photocurrents of greater than 0.1 μamp. And the mercury lamp intensity limited maximum photocurrents to just over 1.0 μamp.

The transient decay schematic is shown in Figure 15a. The mono-chromator was equipped with a camera shutter capable of closing in 1 msec and the oscilloscope is a Hewlett-Packard Model 122A. The shutter was arranged to trigger the oscilloscope sweep as it closed. The transient decay was recorded on film by using a Polaroid oscilloscope camera, and the saturation photocurrent was monitored with a Sensitive Research University Model microammeter.

Figure 15b shows the buffer circuit used to match impedances between the crystal and the oscilloscope. This particular cathode follower had
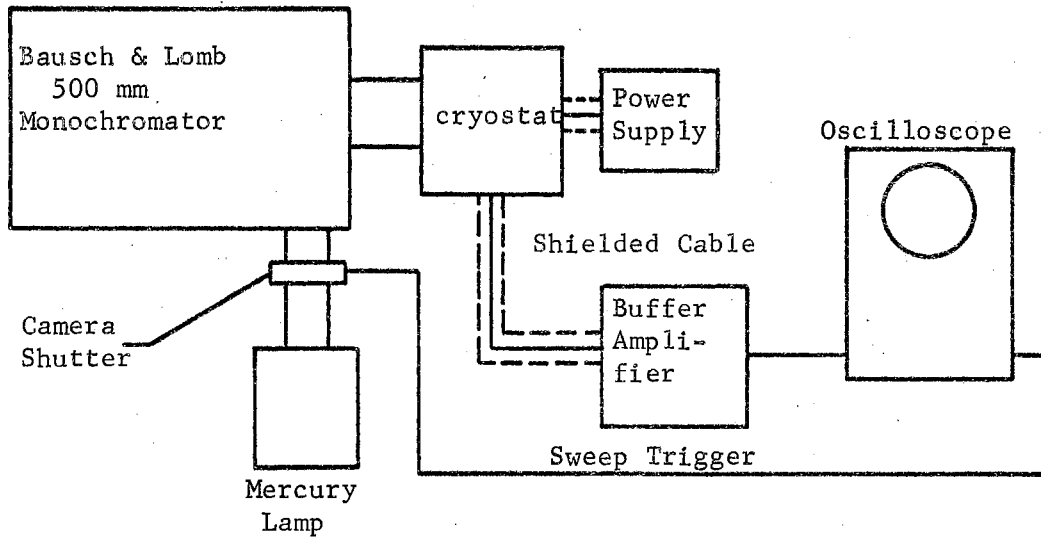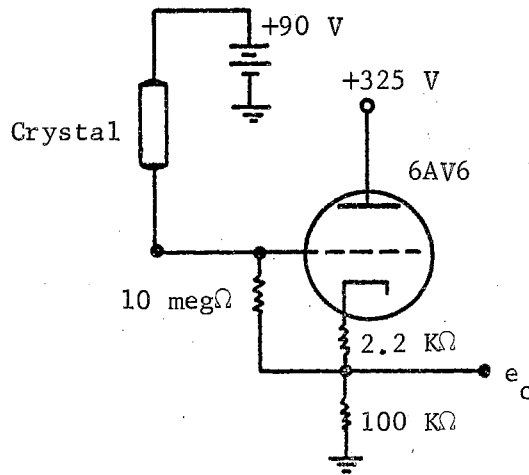
Figure 15. a. Block schematic of the transient decay data system.
b. Impedance matching buffer amplifier circuit.

an input resistance of 10^8 ohms (1 KC) and an input capacitance of 6 pfd, which gave the circuit a rise time of about 0.6 msec. The data was taken by saturating the photocurrent at a particular value, closing the shutter and recording the transient. The initial decay rate was then measured from the film recording and divided into the saturation photocurrent value to give the lifetime. This procedure was repeated over the limited range of photocurrents.

Preliminary photo-thermoelectric voltage measurements have been made using a modification of the crystal holder shown in Figure 7. The modification (Figure 16) allowed one end of the crystal to be heated and its temperature to be monitored.
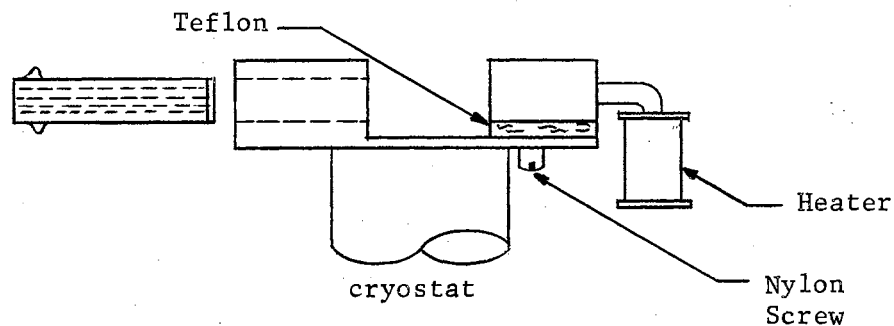
Figure 16. Sample holder for photo-thermoelectric voltage measurements.

The fact that these crystals have such high resistances made it very difficult to monitor the temperature of the cool end. However, for the qualitative information sought, a knowledge of the temperature gradient was less important than the sign of the thermoelectric voltage. This voltage itself was measured at the cool end by a Keithly Model 610B electrometer which has an input resistance of 10^{14} ohms and a maximum sensitivity of 1 millivolt full scale.

In the data taking procedure, the crystal holder was first taken to liquid nitrogen temperature and after depletion of the coolant was warmed by heating one end. This tended to maintain a moderate temperature gradient along the sample over the entire -185 to 100° C range. The same heating program was used in all three of the photoelectronic technique analogs applied, i.e., those of dark conductivity, TSC and CTQ.

CHAPTER IV

RESULTS

Introductory Remarks

The purpose of the present chapter is to systematically present the
results of the experimental procedures outlined previously. It should
be noted here that measurements taken on these single crystals under
similar conditions are found to be quite repeatable from sample to
sample. Therefore the data given while showing only one example for
each measurement is typical of that taken on several similar crystals.

The results are broken into the two broad categories of primary and
exploratory work. The primary data concerns the application of the
photoelectronic analysis to a number of stannic oxide samples. It sets
down comparative results from measurements of spectral response, normal
and decayed thermally stimulated currents, thermal quenching, photo-
current as a function of light intensity and dark conductivity as a
function of temperature. The exploratory data concerns the results of
a number of general photoelectronic techniques applied to special prob-
lems. These results not only act as aids in understanding the primary
data but also are useful as guides to worthwhile future work. Experi-
ments include measurements on carrier decay times, high temperature
oxygen effects, combination intrinsic-extrinsic excitation effects, and
photo-thermoelectric voltage measurements. Many of the suggestions given
in Chapter VI for future studies concern extensions of these particular
procedures.

62

Primary Results

As previously mentioned, the spectral response technique was used
in this work only as a qualitative guide to a general understanding.
The data is separated into intrinsic and extrinsic parts because of the
difference in experimental apparatus used. The intrinsic data covers
the wavelength region from 200-350 mμ and is presented as a qualitative
indication of the ambient effect on the photoconductive process. A
typical example of such data is shown in Figure 17. The effect of both
dry and wet air is to slightly increase the surface rate of recombina-
tion with wet air producing the greater effect. However, the results
seem to indicate only a small, short-range effect.

Extrinsic spectral response data gives a qualitative look at
impurity levels by investigating the photon mobilization of bound elec-
trons from these states. An example is shown in Figure 18, where res-
ponse extends to 750 mμ at 0° C. The vast difference between the
responses for the two temperatures, as will be discussed later, is due to
variations in the carrier lifetimes (or recombination rates) as a
function of temperature.

The character of the thermally stimulated current (TSC) data dif-
fered little from sample to sample and invariably indicated three main
trapping levels. Typical peaks are shown in Figure 19 along with their
activation energies as calculated by the Bube method (Equation 25). A
list of the Bube data for the samples used is given in Table I. Care
was taken in these experiments to insure identical conditions of satura-
tion photocurrent, wavelength, excitation and decay periods, and temper-
ature rise rates. These factors under certain conditions can have
marked effects on the TSC data.
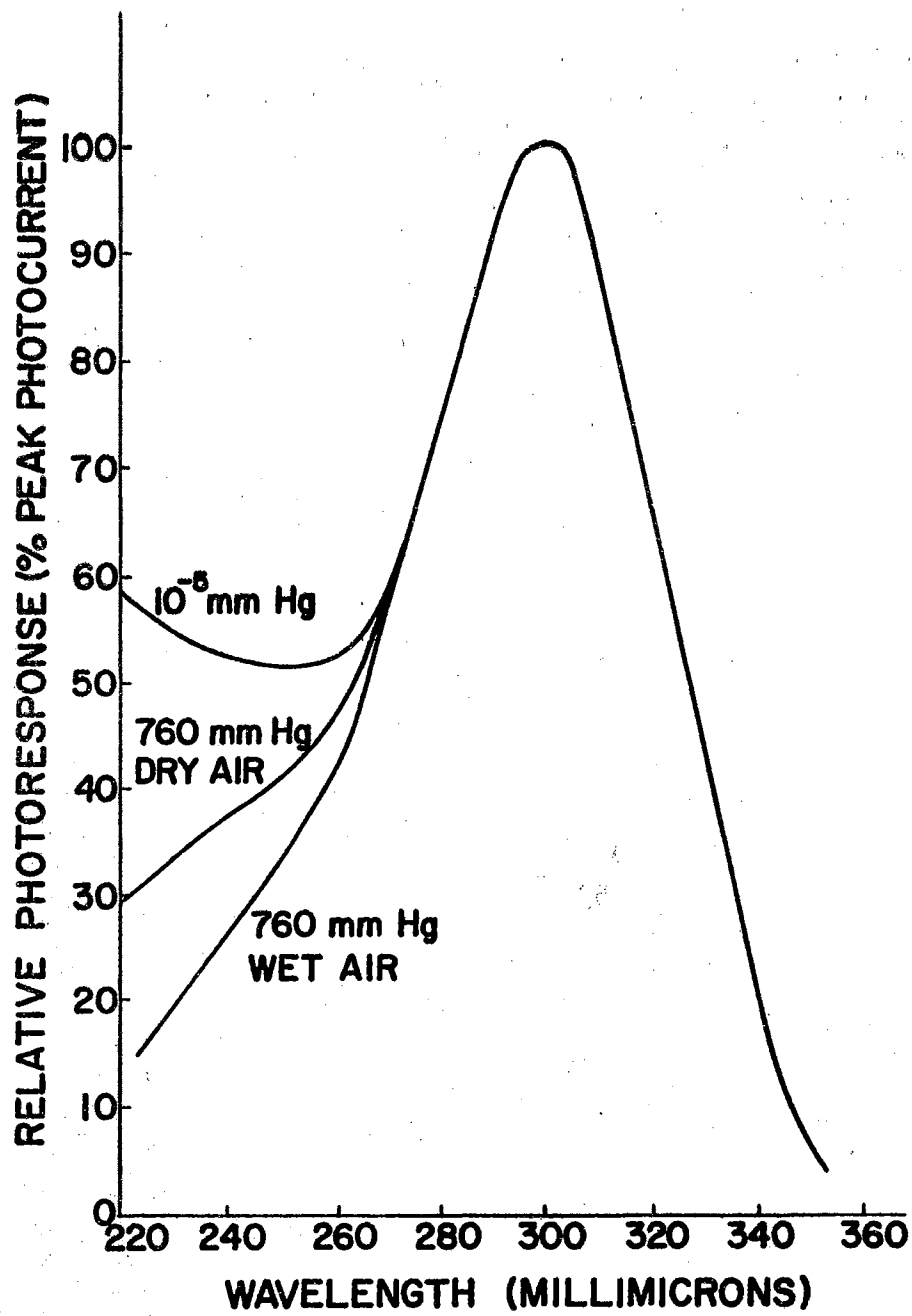
Figure 17. Relative photoconductivity as a function of
wavelength for different ambients.
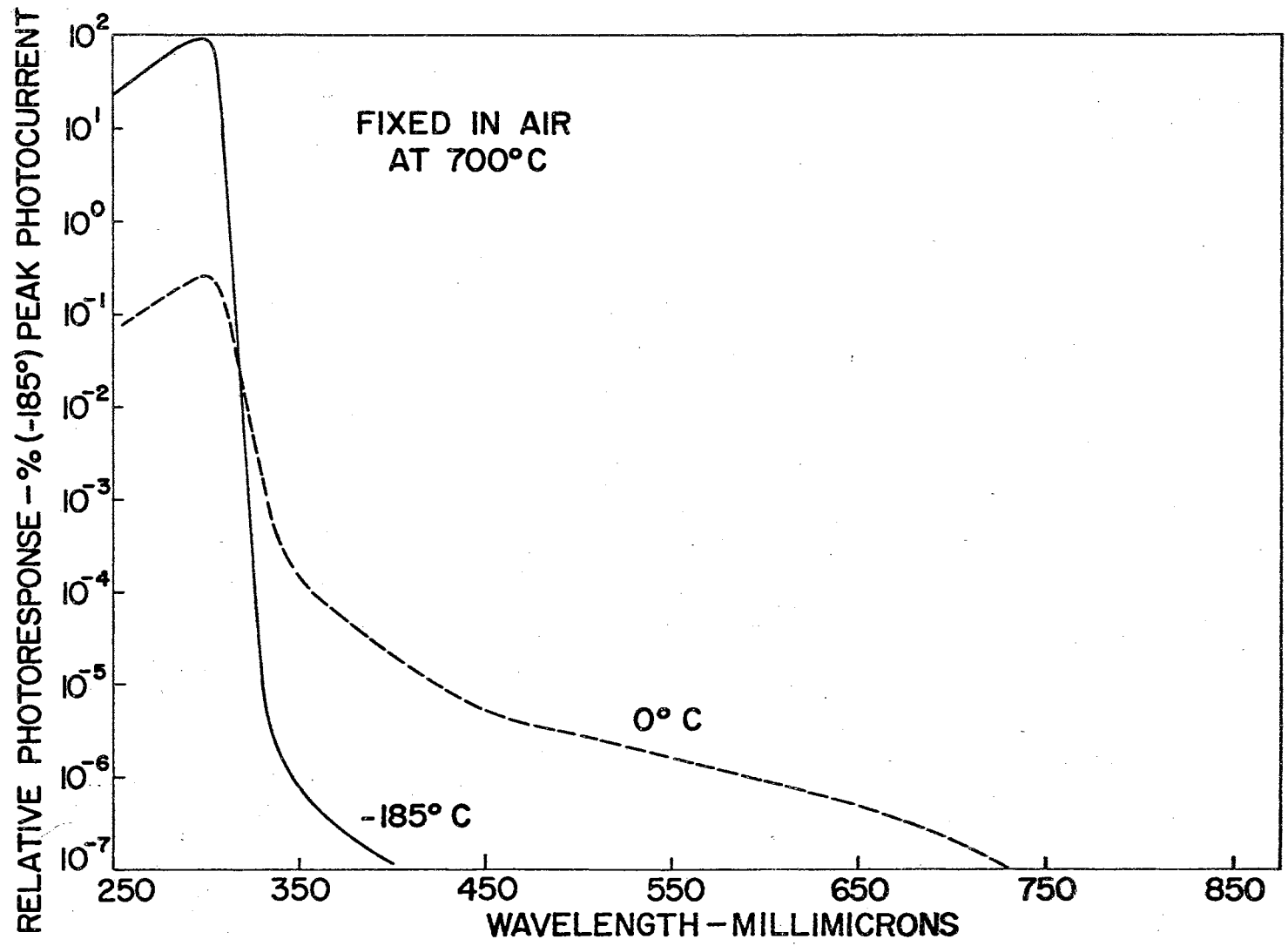
Figure 18. Extrinsic photoconductivity as a function of wavelength.
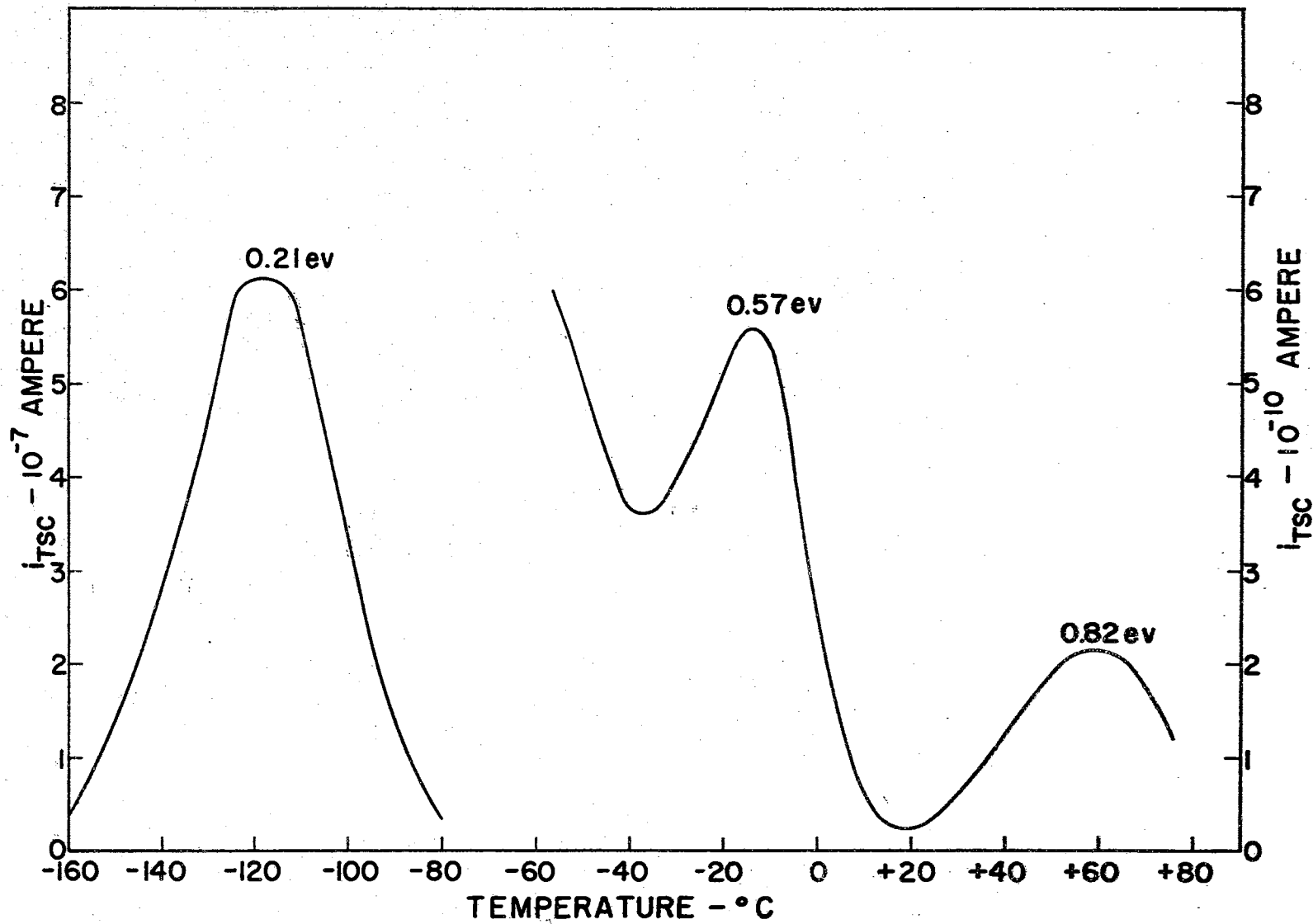
Figure 19. Thermally stimulated currents as a function of temperature.

Figure 20 shows the effect of saturation photocurrent on the appearance of the TSC data. Note that as the photocurrent is decreased, the 0.21 ev trapping peak is depressed -- finally to such an extent as to reveal several other peaks. This behavior can be understood in terms of later data on intensity-dependent thermal quenching. Figure 21 indicates the effect of excitation wavelength on the TSC and shows a general behavior to be expected for carrier mobilization restricted to regions near the surface. Lastly, Figure 22 illustrates the shift of the high temperature TSC peak and its calculated Bube activation energy with heating rate. Note that the Bube energy only varies by about 6% with an order of magnitude change in the rate.

The two high temperature peaks of Figure 19 overlap, making it impossible to investigate their activation energies by the Garlick and Gibson method. Therefore, it is necessary to use Bube's decayed thermally stimulated current method, the results of which are illustrated in Figure 23. These data as taken on several samples are comparatively shown in Table I.

Because of the difficulty of taking thermal quenching data, even continuously, it was decided only to take that which was necessary to establish a general behavior. Therefore, comparative data are not available for all the samples used in the other techniques. An example of the data continuously taken is given in Figure 24 as a function of relative light intensity (the L values). Calculations of the activation energy for the sensitizing centers can be made using Equation 28 by plotting, from this CTQ data, the logarithm of the photocurrent at the break from high sensitivity versus the reciprocal temperature at the break. The slope is then $(-E/k)$, and the $(1/T = 0)$ intercept additionally
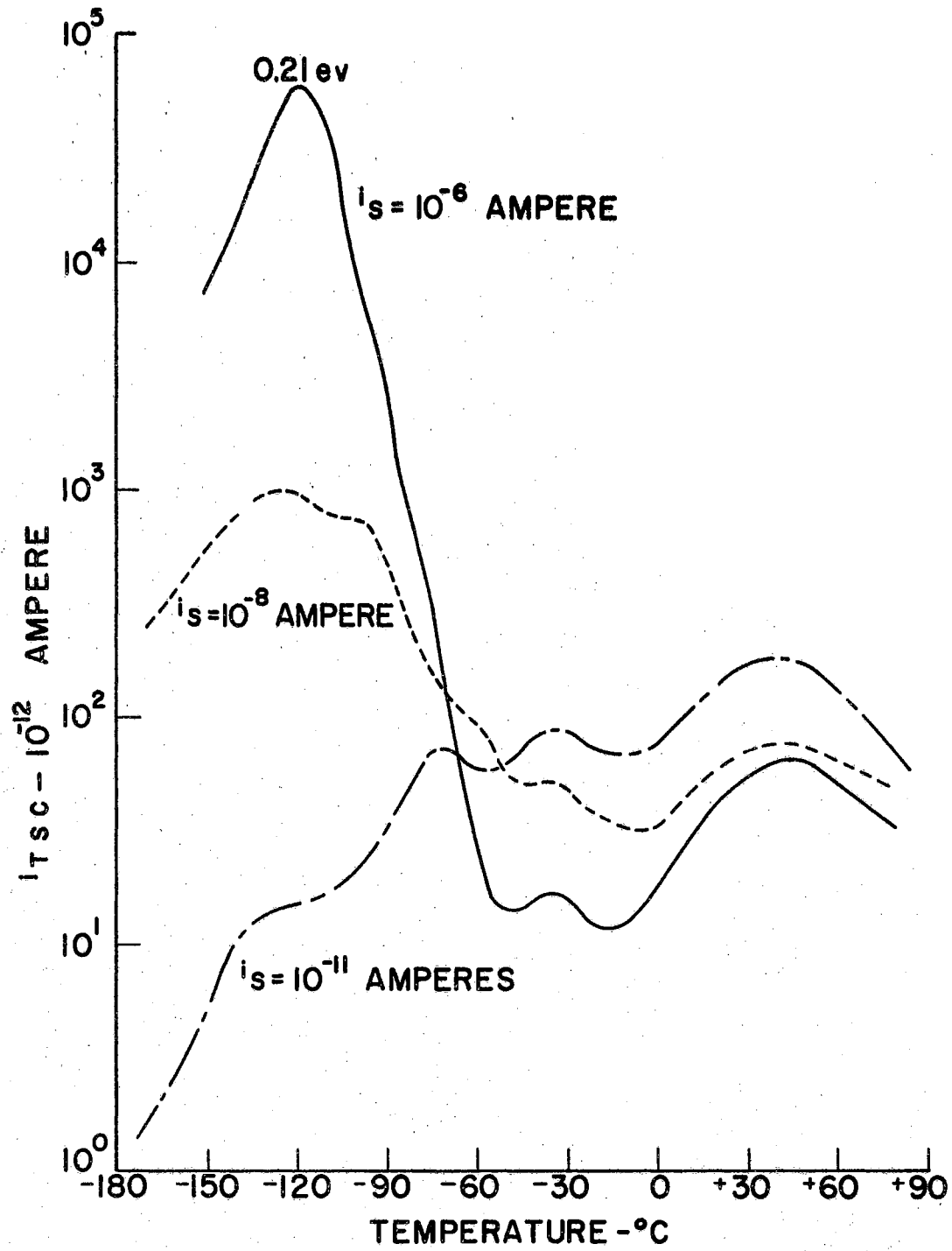
Figure 20. Thermally stimulated currents as a
function of temperature for several saturation
photocurrents.
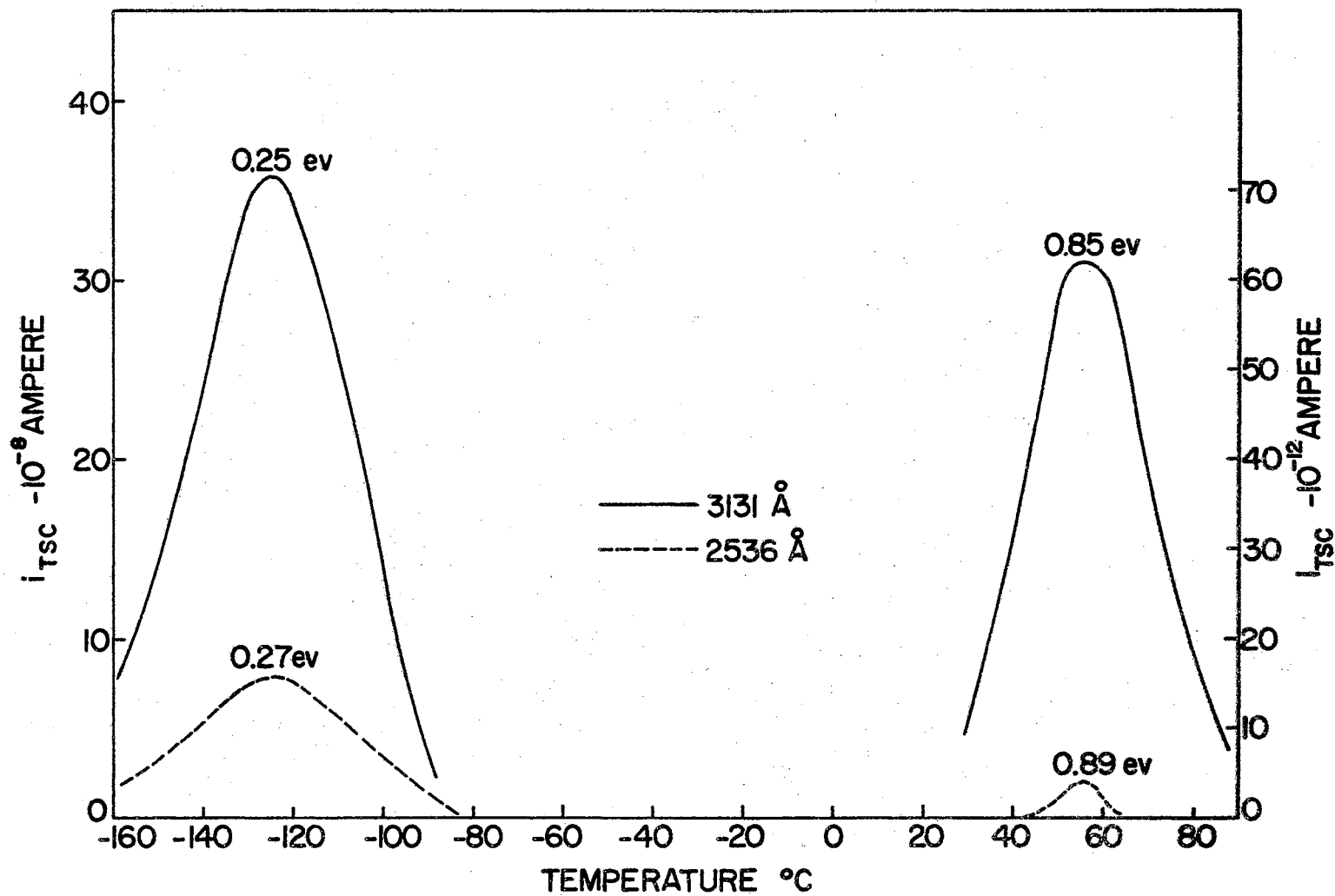
Figure 21. Thermally stimulated currents as a function of temperature for two wavelengths
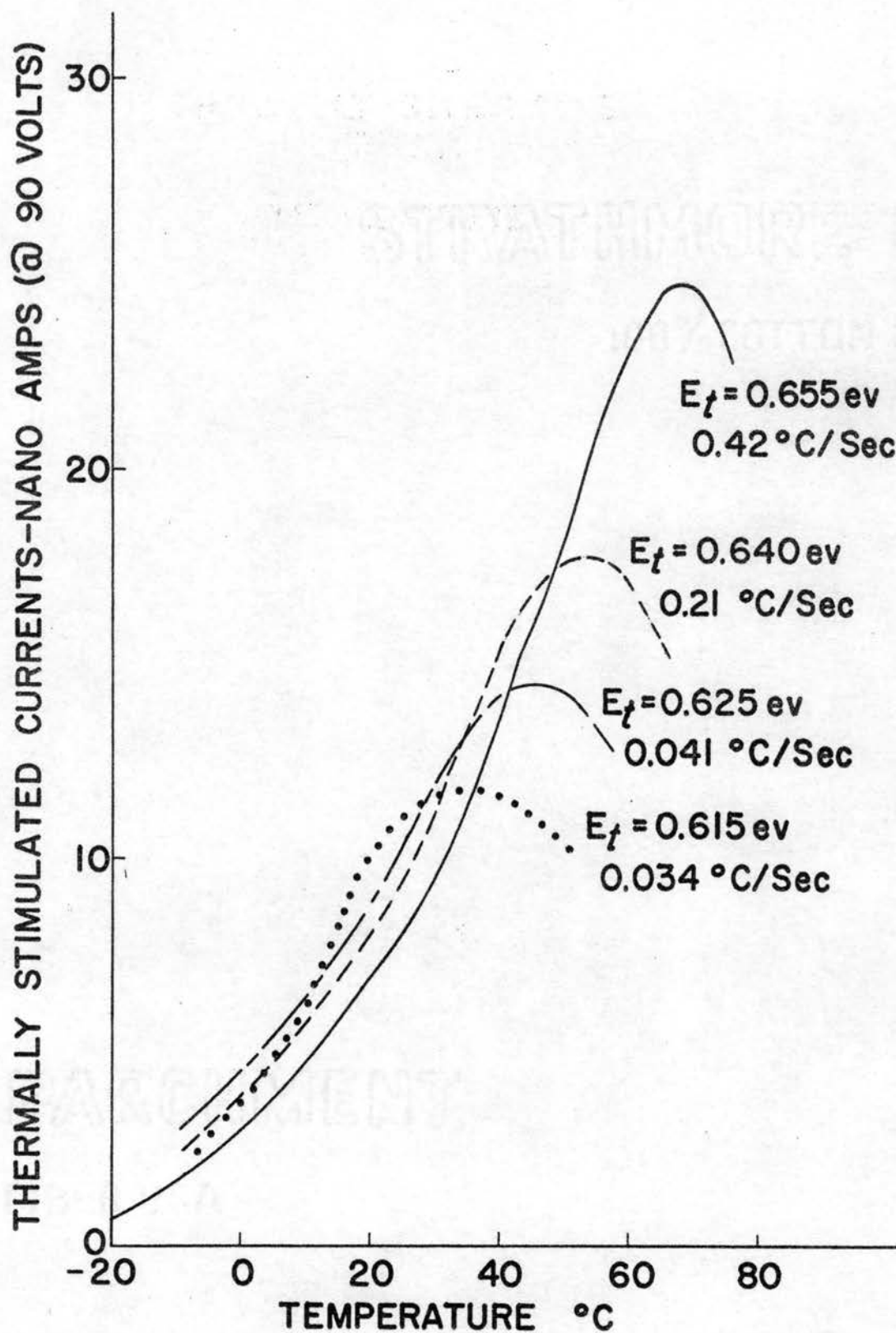
Figure 22. Thermally stimulated current for the high temperature peak taken at several heating rates.
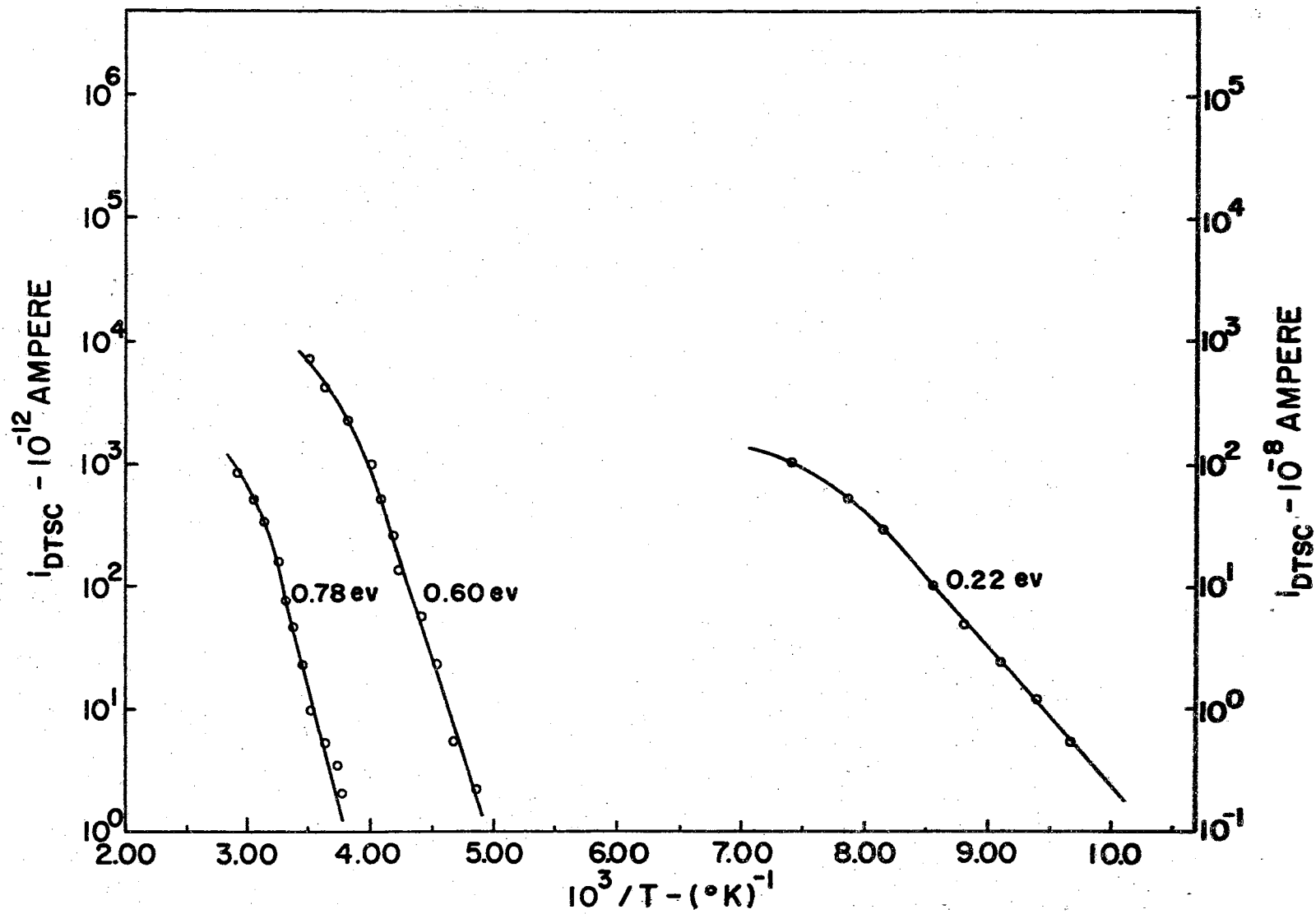
Figure 23. Decayed thermally stimulated currents.
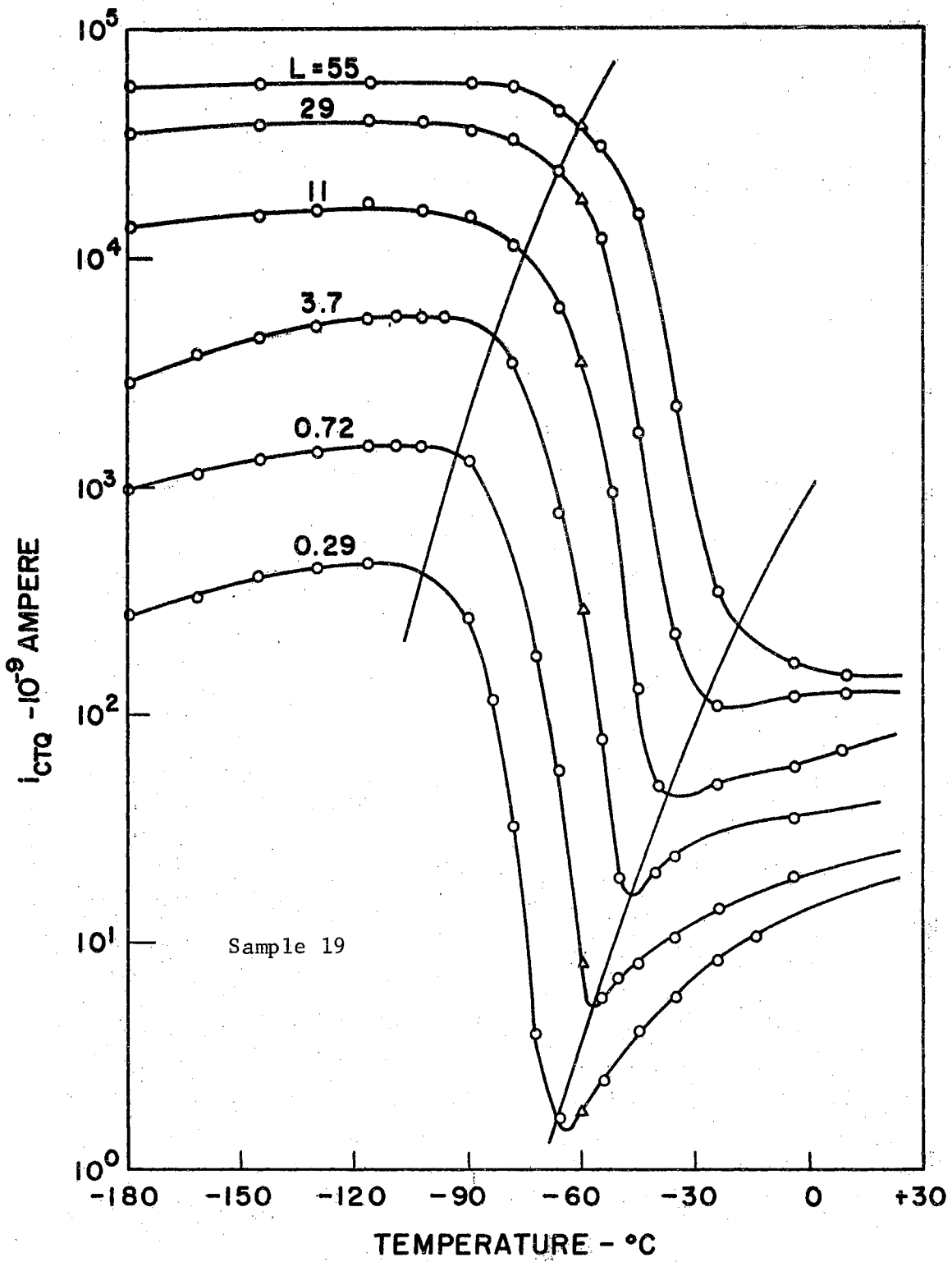
Figure 24. Continuous thermal quenching.

yields a value of the capture cross section ratio according to Equation 29. The actual data and the values calculated are shown in Figure 25, where the effective density of conduction band states has been assumed to be 10^{19} $(cm)^{-3}$ independent of temperature, and the carrier mobility has been taken as approximately 100 cm^2/volt-sec.*

Also included in Figure 25 is the plot of the photocurrent at the break to low sensitivity as a function of the reciprocal temperature at the break. From this it should be possible to calculate again the activation energy and the ratio of the density of sensitizing centers to main recombination centers (Equation 30). Note that the activation energy from this last data differs from that calculated before by about 30%. It is felt that this is due to an interaction mechanism at the higher temperatures causing a distortion of the CTQ curves. These facts are to be discussed in more detail in the next chapter. Figures 26 and 27, where very careful CTQ data was taken over only the high break region, indicate the repeatability of this type data. Note that there is good agreement between the calculated values of activation energy for the two different specimens.

Figure 28, showing a comparison of CTQ data as taken for two intrinsic wavelengths, indicates little variation. However, as will be shown later in the chapter, this data changes drastically as the wavelength is lengthened beyond the fundamental absorption edge as would be expected because of the differences in excitation and recombination mechanisms. Also, in analogy to the data of Figure 20, CTQ has been taken for a very low light level. This is illustrated in Figure 29 which shows similarity

---

*This value of mobility was taken from earlier Hall data on natural stannic oxide crystals by Tolley.[54]
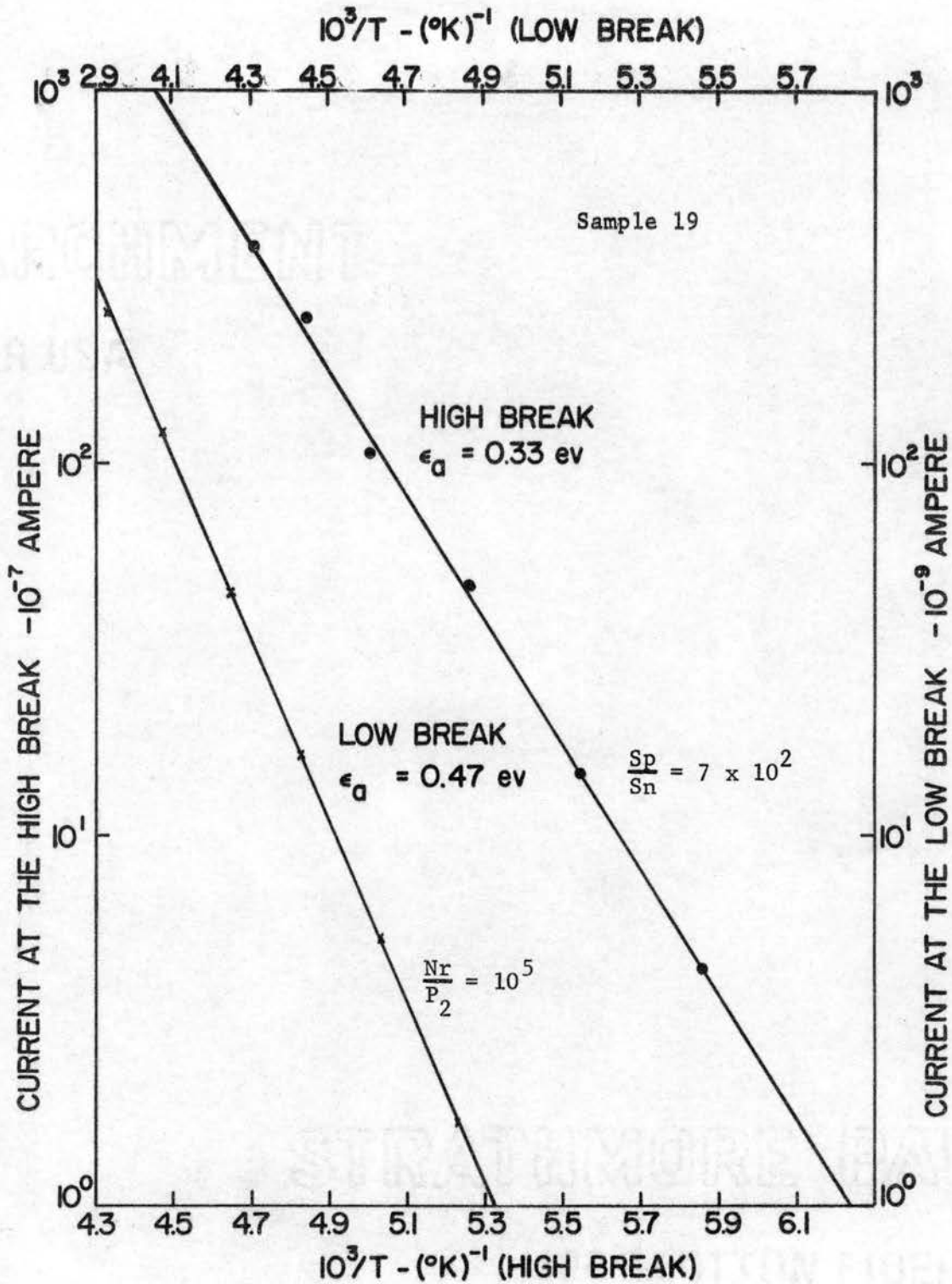
Figure 25. Logarithm of the photocurrent at the sensitivity
breaks versus $10^3/T$ at the breaks.
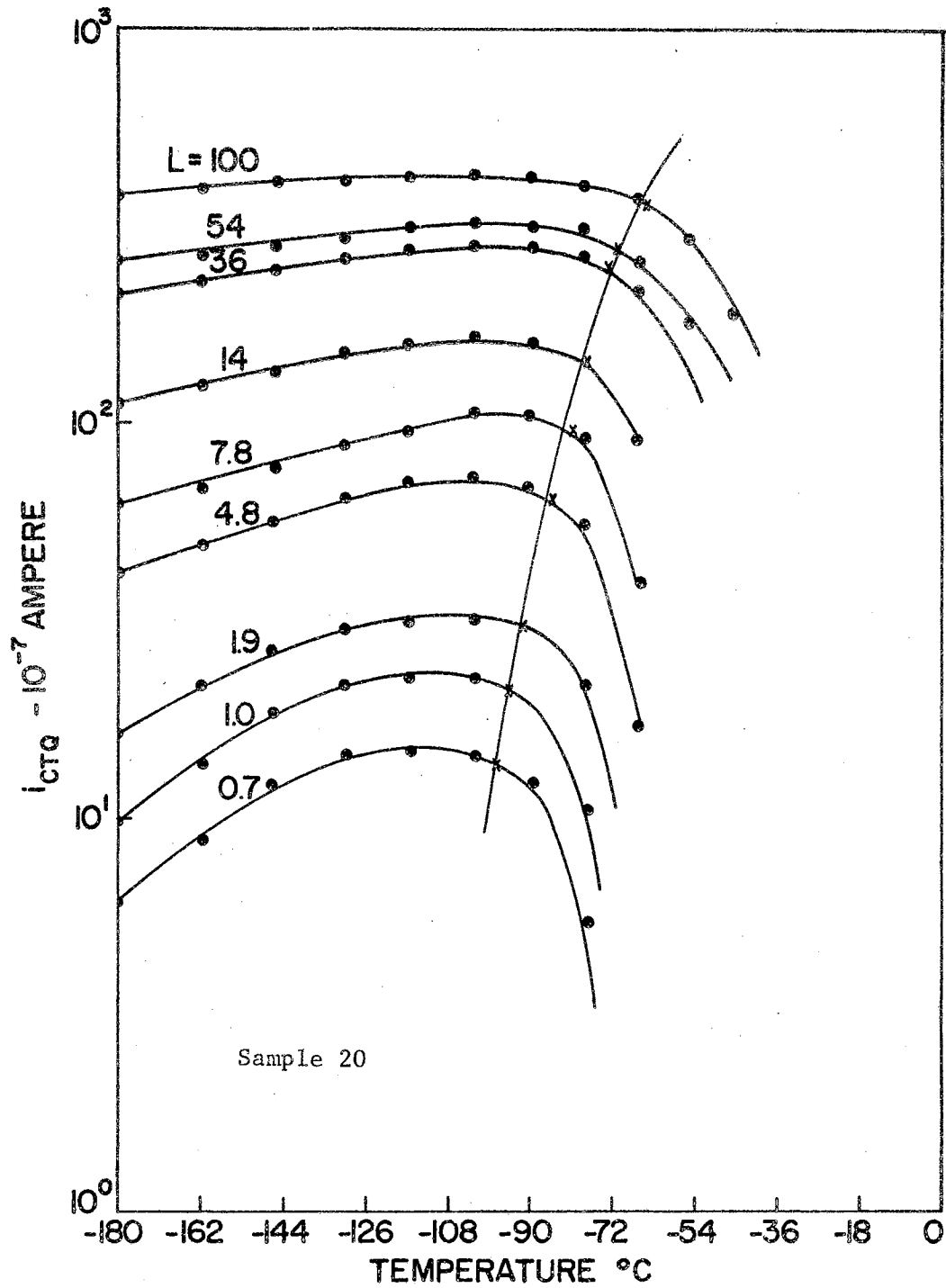
Figure 26. Continuous thermal quenching for the break from high sensitivity.
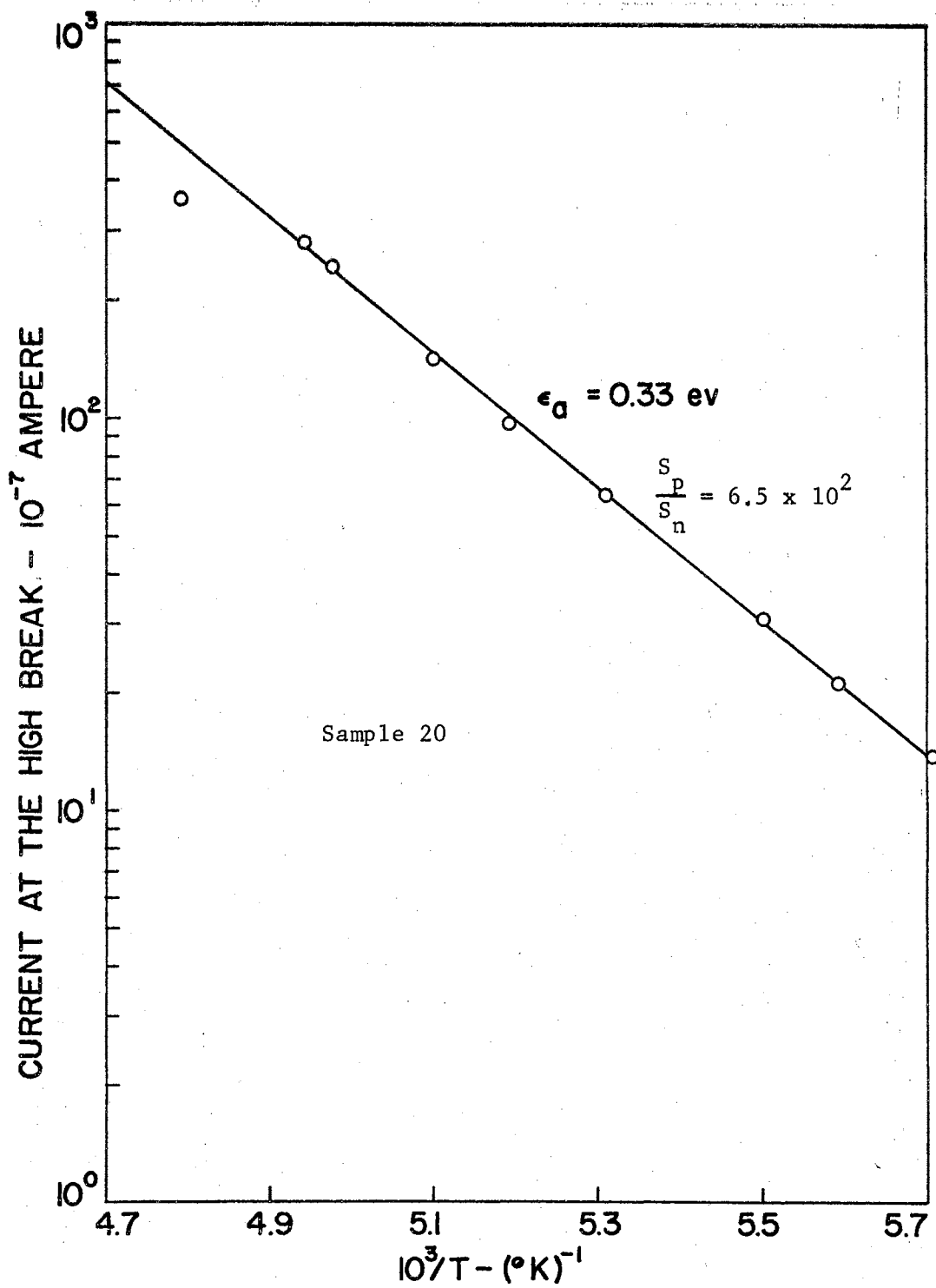
Figure 27. Logarithm of the photocurrent at the break from high sensitivity versus $10^3/T$ at the break.
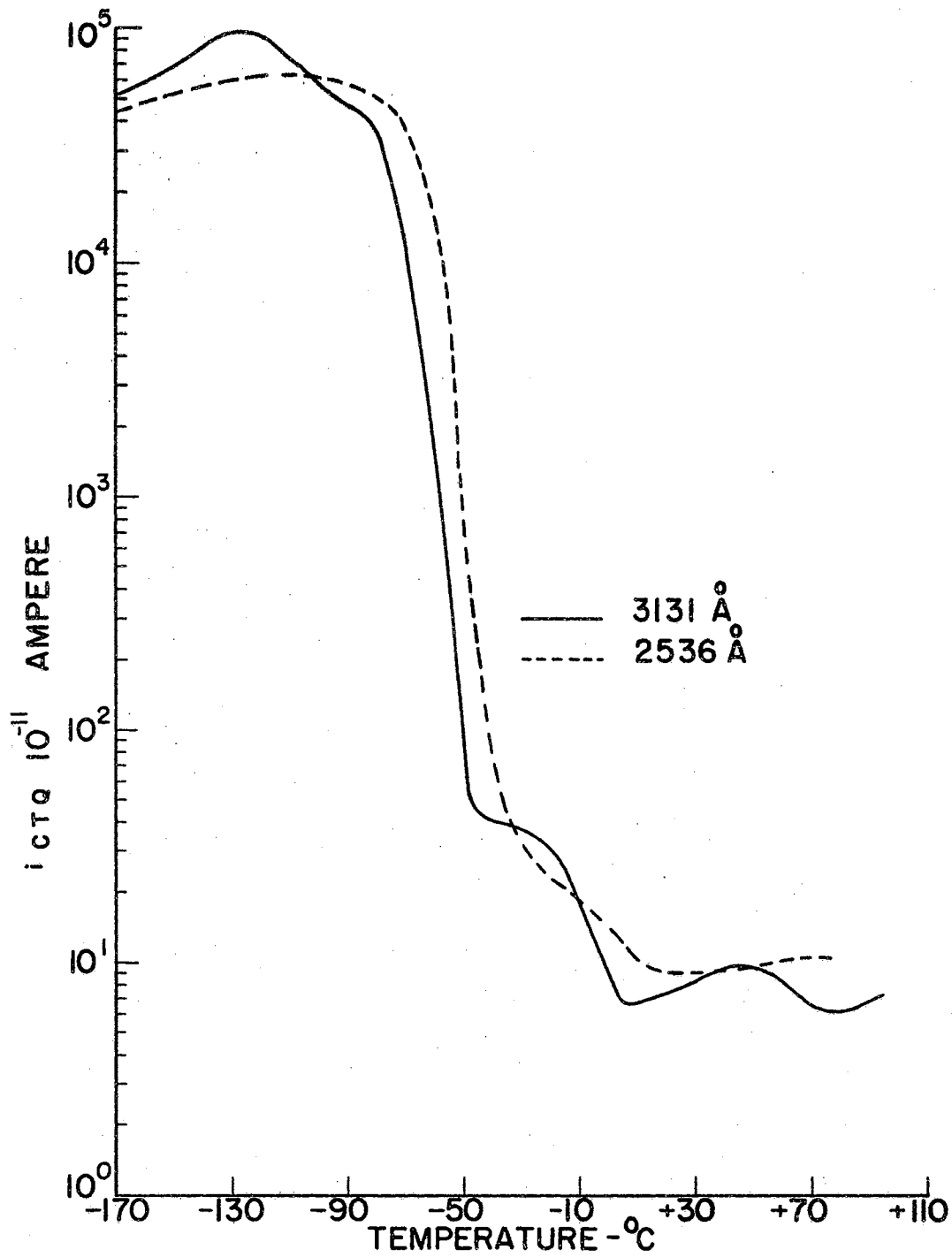
Figure 28. Continuous thermal quenching for two intrinsic wavelengths.
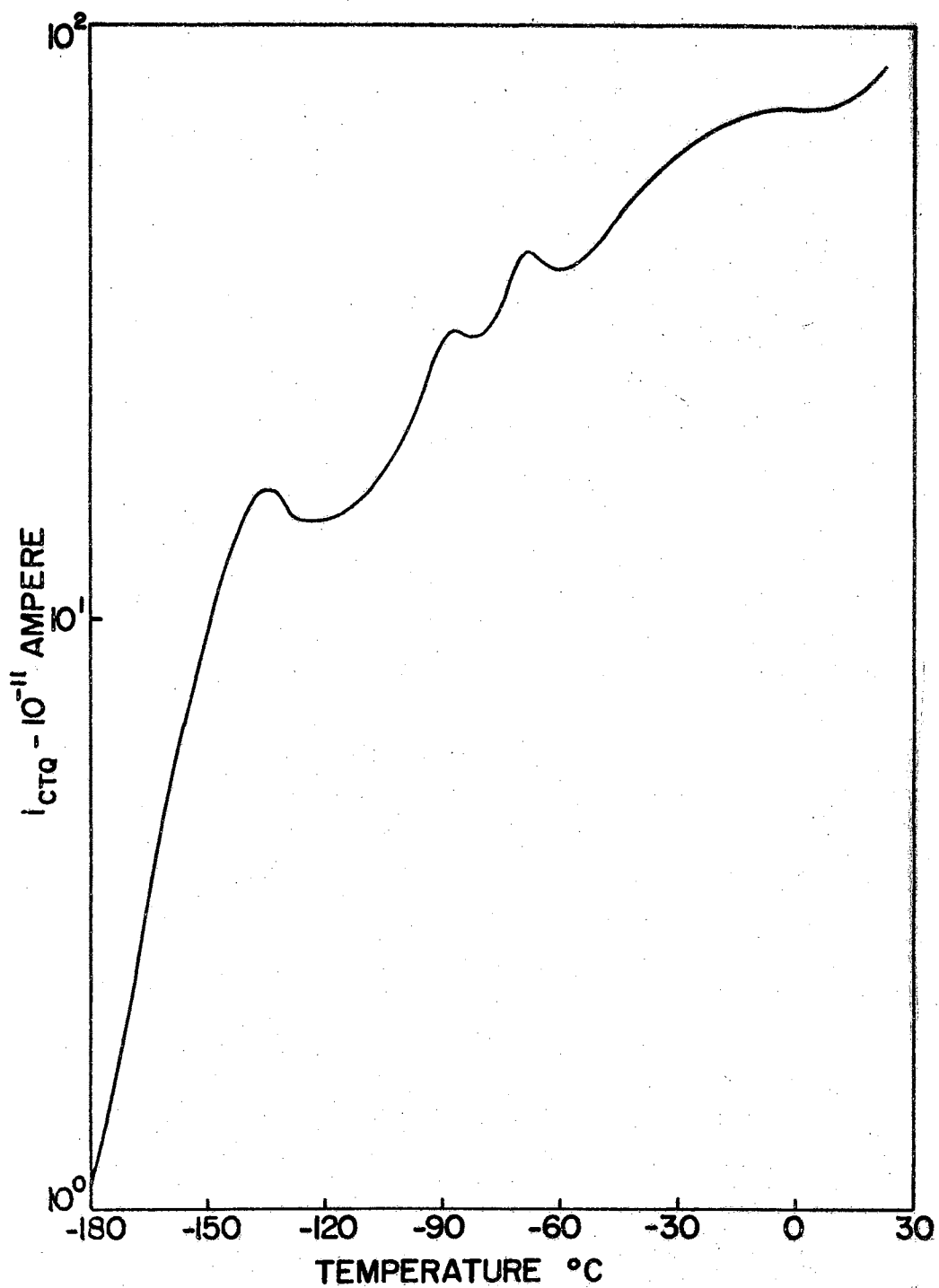
Figure 29. Continuous thermal quenching for a low light
intensity.

with the $i_S = 10^{-11}$ ampere curve of Figure 20. It is apparent from
this data that the large 0.21 ev TSC peak is associated with a sensiti-
zation at high light levels and as the sensitization disappears from
CTQ (with decreasing light intensity) this peak also diminishes.

Much has been written in recent years concerning the appearance of
a superlinear response in photoconductors. As explained earlier, this
behavior is virtually always present when a particular material shows
a region of impurity sensitization. It appears in stannic oxide in the
temperature region which represents the transition of the photoconductor
from its normal to sensitized state. This can be illustrated by plotting
the data of Figure 24 in a slightly different manner, i.e., photocurrent
versus relative light intensity (L-values) for constant temperatures.
Figure 30 shows such plots and, for clarity, uses only the -180, -60
and 0° C temperatures. As is normally the case, this graph shows
sublinearity for temperatures outside the transition region and a super-
linear behavior within it. The slopes of the three lines are also shown
on the figure indicating the exponent on the functional relation between
the two variables. This type data has actually been used by some investi-
gators in preference to CTQ. The sensitizor parameters are then calcu-
lated from the photocurrent and temperature at the break in slope.
Obviously these two methods differ only in the experimental techniques
used.

The final primary data to be presented is that of dark conductivity
as a function of temperature. This was taken continuously over a range
from -185 to 100° C by allowing the temperature to rise at a very slow
rate. Before each such measurement, care was taken to empty all trapping
levels by baking the sample at 100° C for several minutes. The data was
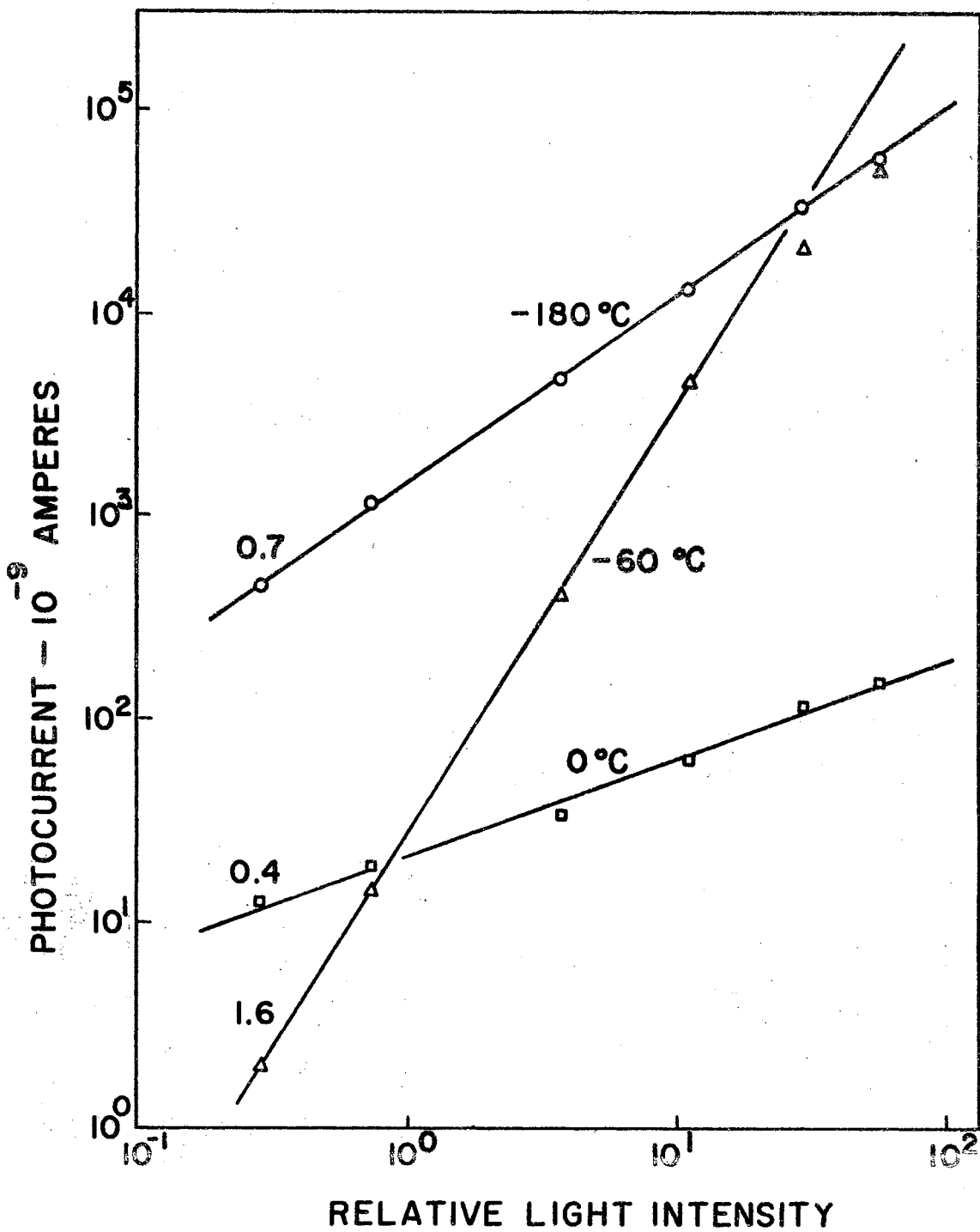
Figure 30. Saturation photocurrent as a function of light intensity.

taken with the older Keithley Model 621, which gave a maximum resistance capability of approximately 10^{14} ohms with a 90 volt series supply. A typical example of the current plotted against reciprocal temperature, is given in Figure 31 along with the activation energy as calculated from the slope. This energy value was obtained by using the expression,

$$E = kT\ln \sigma + constant. \tag{36}$$

Activation energies as obtained in this manner and room temperature resistance values for each crystal represented in the analysis are listed in Table I. Those samples for which values do not appear were found to have measurable resistivities over such a limited region of the high temperature range that significant data could not be taken.

Since the conductivity of stannic oxide single crystals is so drastically affected by past history, comparative data can only be valid if they are taken under similar conditions. Therefore in obtaining the data of Table I, care has been taken throughout to insure this similarity. The samples were all prepared and mounted in a standard way and the data obtained consecutively without disturbing the mounted sample.

Exploratory Results

Photo-carrier decay times were calculated from initial slope curves through the use of Equation 34. The electronics restricted data to saturation photocurrents at least 100 times greater than those used for any of the other techniques. Also, the light source provided the full mercury line spectrum so that the decay times are composite values as far as surface-bulk effects are concerned. Because of these restrictions, no attempt was made to take general data (as functions of temperature
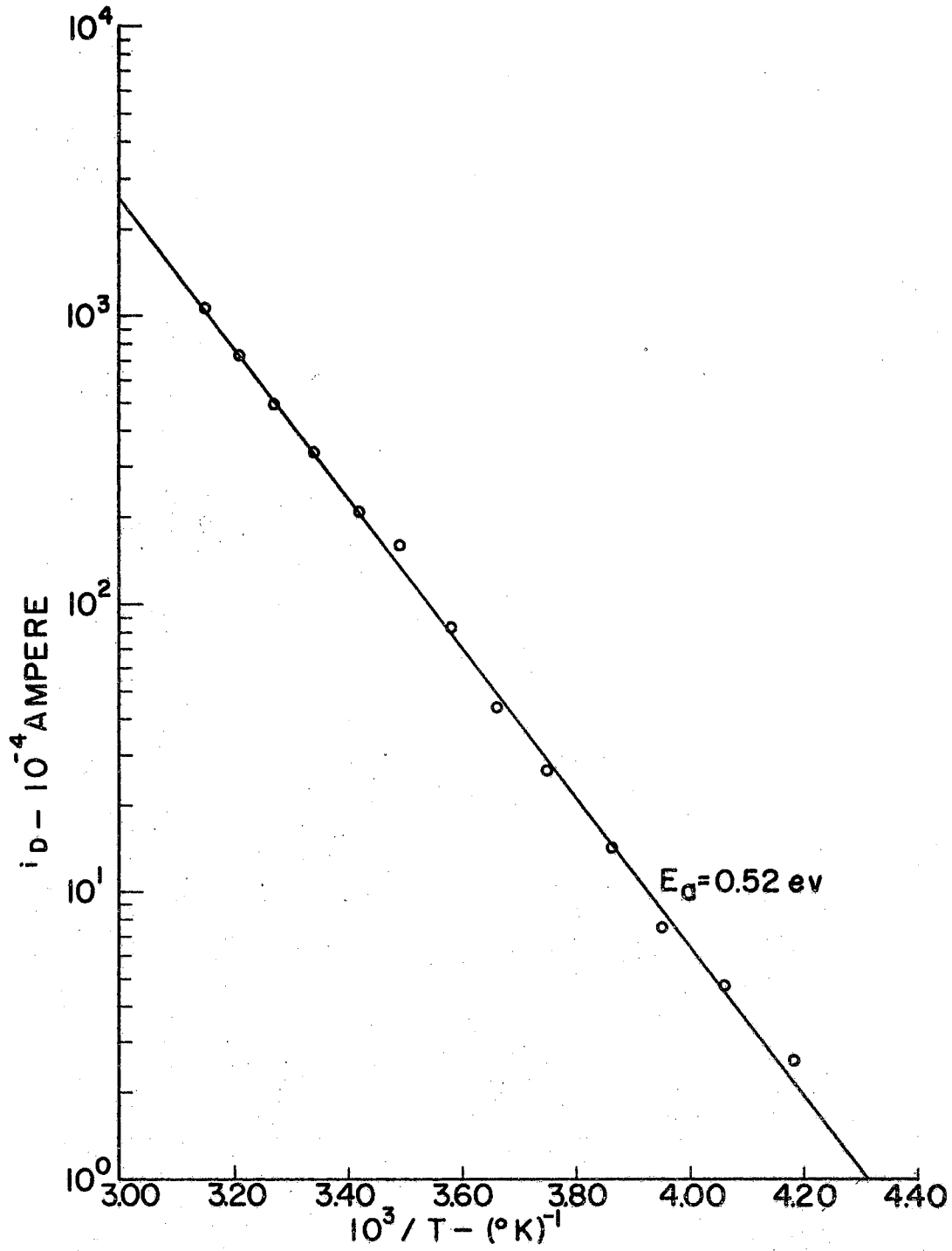
Figure 31. Dark conductivity as a function of reciprocal temperature.

TABLE I

RESULTS OF PRIMARY PHOTOELECTRONIC ANALYSIS

Sample #	Resistance (25° C) ohms	Activation Energy ($\sigma_D$vs 10^3/T) ev	Trapping Level Activation Energies Bube ev	DTSC ev
G-12	1.1×10^{12}	0.50	0.23	0.21
			0.55	0.41
			0.74	0.50
G-16	---	---	0.26	0.22
			0.57	0.60
			0.78	0.78
G-18	3.4×10^{12}	0.56	0.25	0.21
			0.53	0.52
			0.65	0.55
G-19	2.7×10^{12}	0.55	0.25	0.20
			0.61	0.39
			0.78	0.50
G-20	3.0×10^{13}	0.74	0.29	0.23
			0.74	0.67
			0.84	0.73

etc.) It has been taken only at room temperature over a limited range, controlled by the electronics on the low saturation photocurrent side (0.1 μa), and the lamp intensity on the high side (1.0 μa). The data is presented in Figure 32 as the value of the time contant τ versus saturation photocurrent. More will be said concerning these measurements in Chapters V and VI.

In previous chapters, it has been mentioned that the conductivity of oxide insulators is normally dependent on nonstoichiometry. It is suggested that in stannic oxide the conduction is due to thermal ionization of loosely bound electrons at oxygen deficiency sites. The equilibrium density of oxygen deficiencies is related to the ambient oxygen pressure and temperature, and variations in this density occur at very low rates for temperatures below 200° C. Therefore many of the properties of the samples at or near room temperature are determined by past history. The property which is found to be most directly affected is, of course, that of dark conductivity as a function of temperature.

The conductivity of some samples, however, is found to vary widely with ambient oxygen pressure even for temperatures as low as 100° C. It is suggested that this is due to a chemisorbed oxygen barrier modulating the ionization density of an inhomogeneous surface deficiency layer. As yet the processes responsible for such a layer have not been established. However, more or less homogeneous bulk reduction at convenient rates normally occurs above 500° C in a rough pump vacuum (10^{-3}mm Hg).

Photoelectronic measurements have been made as a function of pressure and excitation wavelength in an attempt to corroborate the surface layer assumption. Since the properties are essentially frozen in at temperatures below 100° C, the measurements were made as a function of
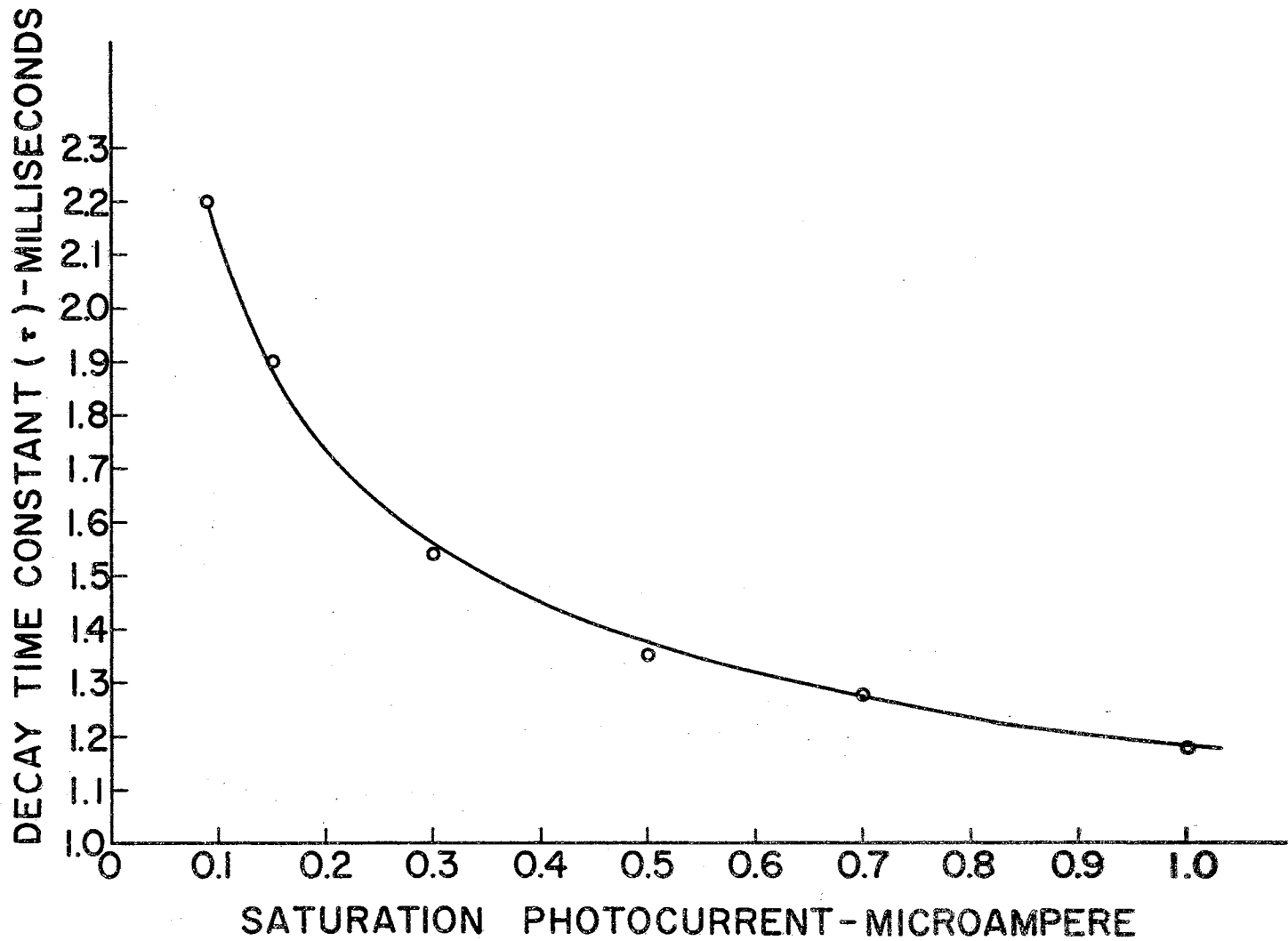
Figure 32. Carrier lifetime as a function of saturation photocurrent.

the "fixing" procedure. In other words, the samples were heated at 100° C and a certain ambient pressure for some time prior to the measurement. Later discussions will include the effects of heavy, high-temperature reduction on the analysis.

Vacuum fixing procedures seem to always produce two related effects: the displacement of the conductivity magnitude toward higher values and a decrease in the apparent activation energy. A typical example of these effects is shown in Figure 33 for several fixing pressures and periods. Note that there is a 70% change in apparent activation energy for an almost four-order-of-magnitude change in resistance. This relation between resistivity and activation energy has been noted in other materials and is sometimes referred to as Meyer's rule.*

The series of photoelectronic measurements made as a function of fixing procedure also included both TSC and CTQ. These were taken after having fixed the samples at 100° C for thirty minutes in either dry room air or a reduced pressure of 10^{-3} mm Hg. Each of the measurements was then repeated for two excitation wavelengths, 3131 and 2536 $\overset{o}{A}$. The results are typified by the plots shown in Figures 34, 35, 36 and 37.

The first two of these figures refer to TSC data as a function of fixing and wavelength. The important points to note here are the differences in the fixing effects on the peaks. One can see that the two higher energy peaks were affected to a greater extent by fixing than the lower one, and that these differences were even more pronounced at the shorter wavelength. Note should also be made of the fact that the lower temperature peak was decreased by vacuum fixing while the upper two were

----

*Refer to Chapter V of Mott and Gurney.[55]
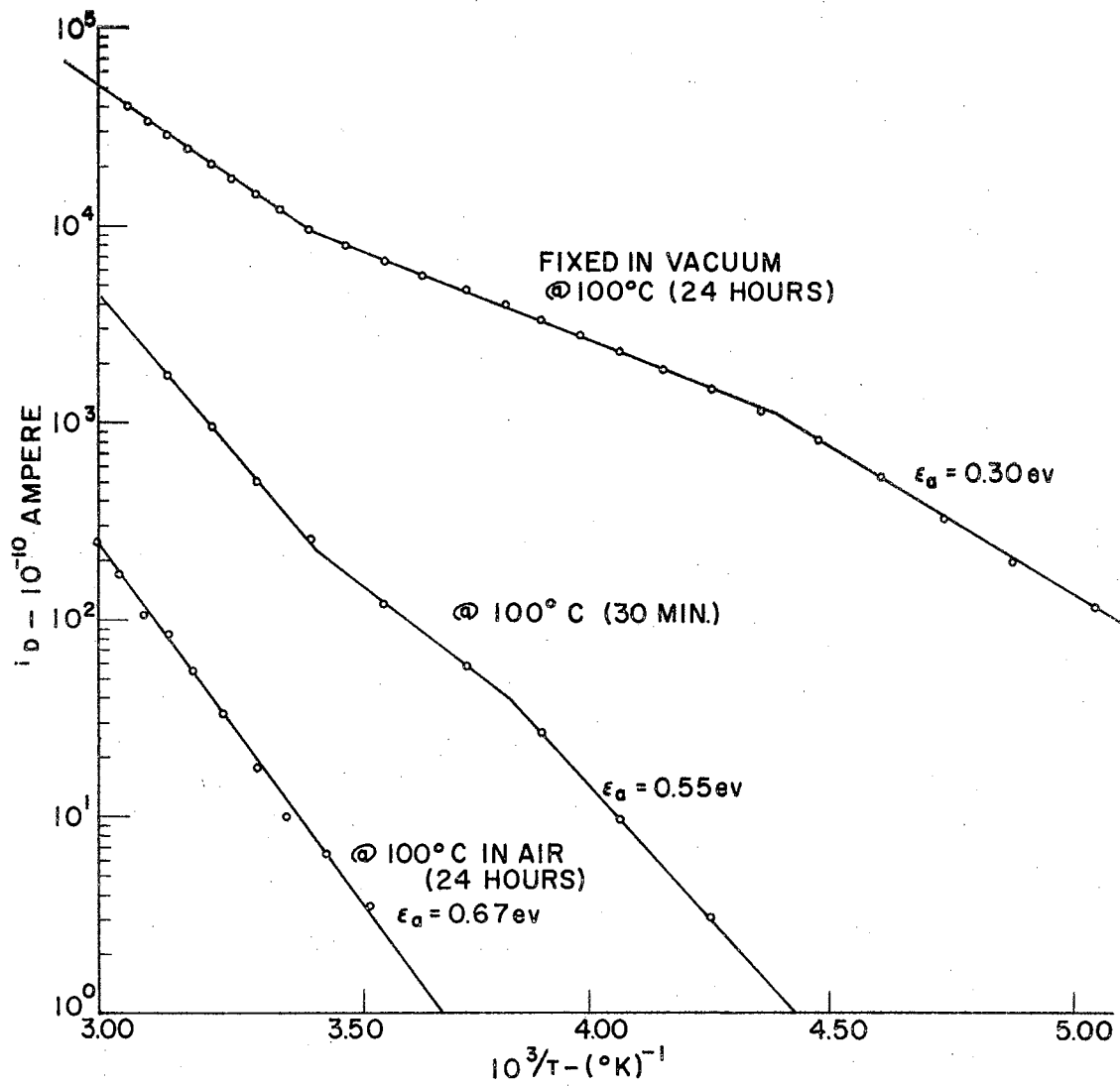
Figure 33. Dark conductivity as a function of reciprocal temperature for several fixing procedures.
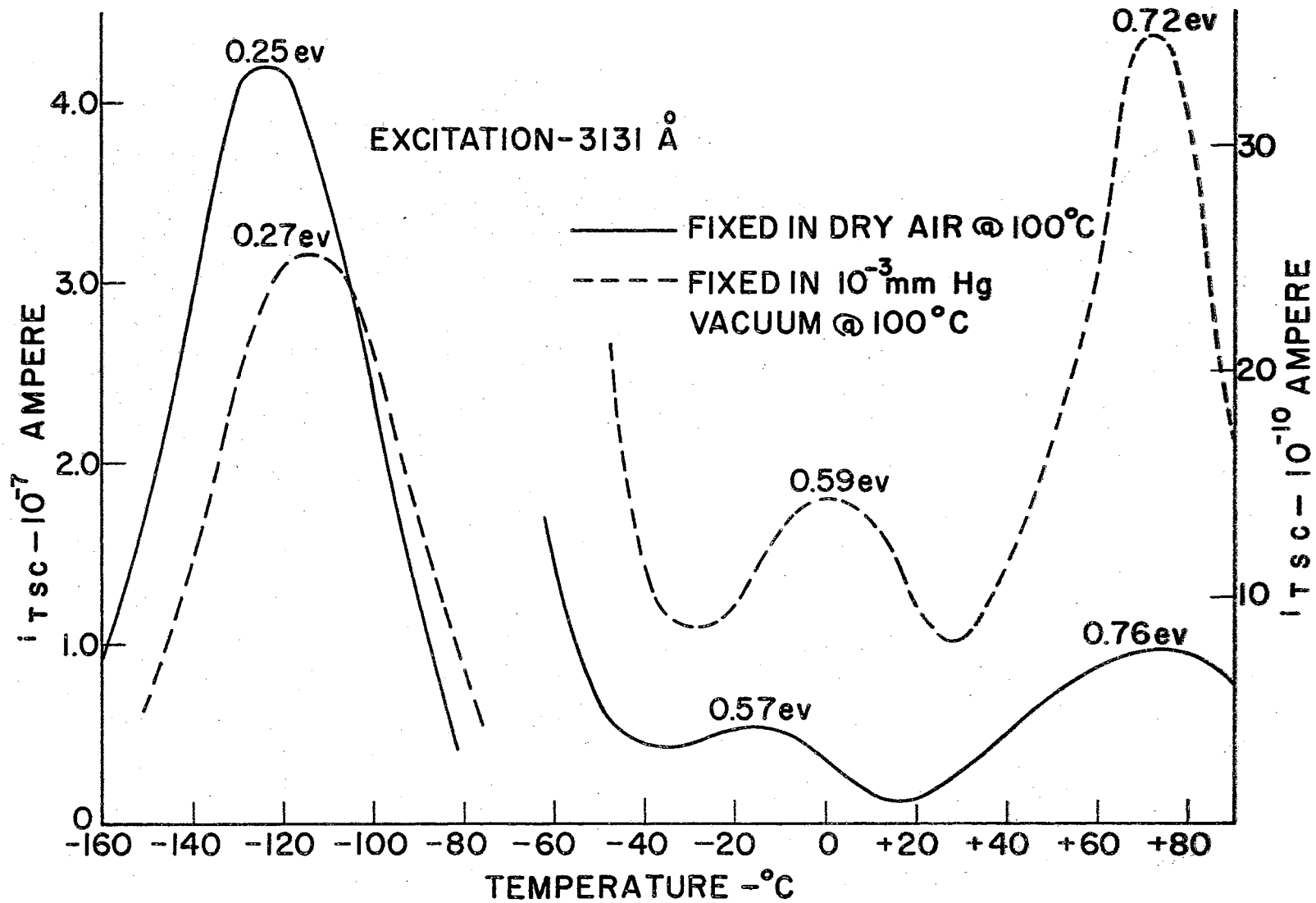
Figure 34. Thermally stimulated currents as a function of fixing procedure (3131 Å).
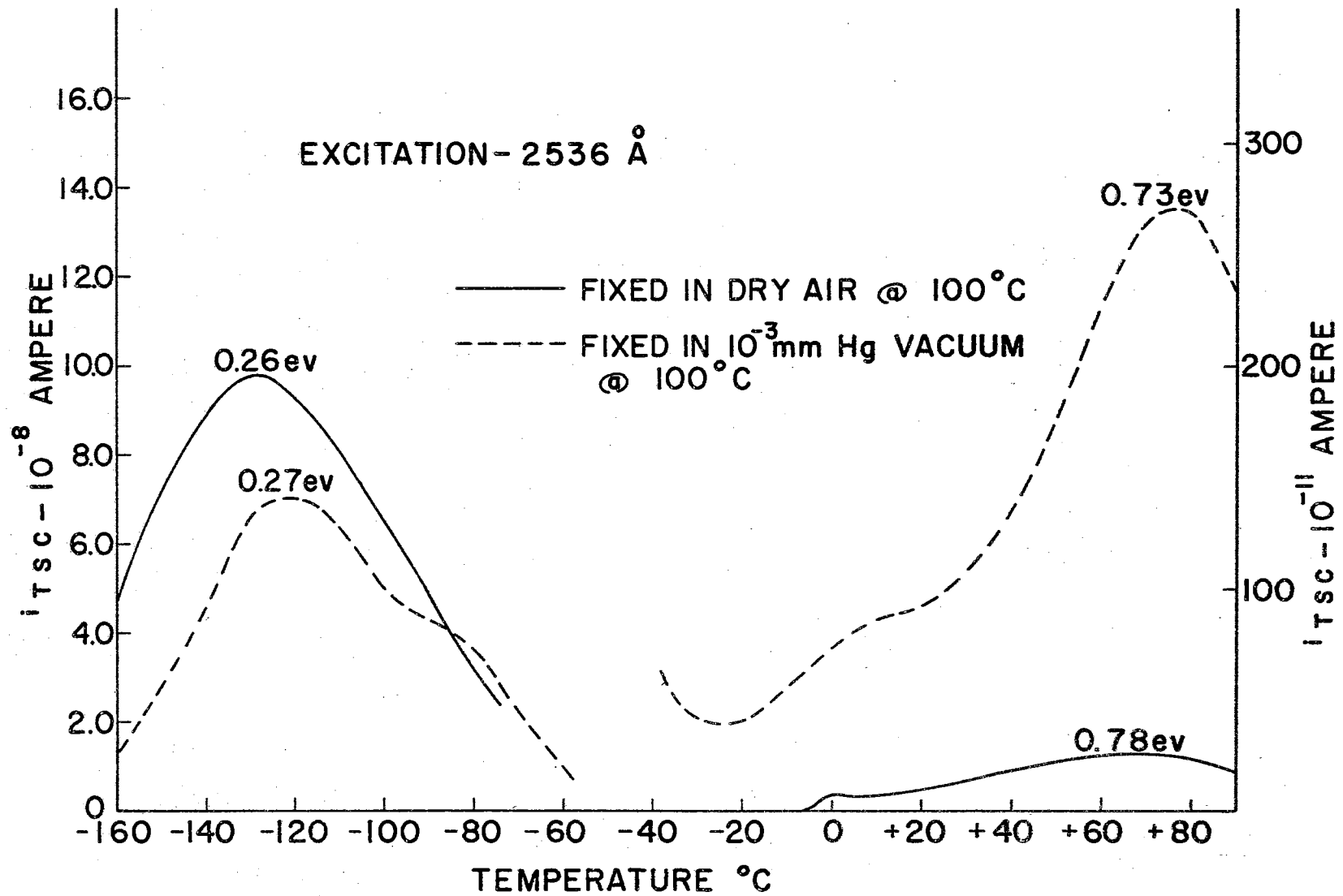
Figure 35. Thermally stimulated currents as a function of fixing procedure (2536 Å).
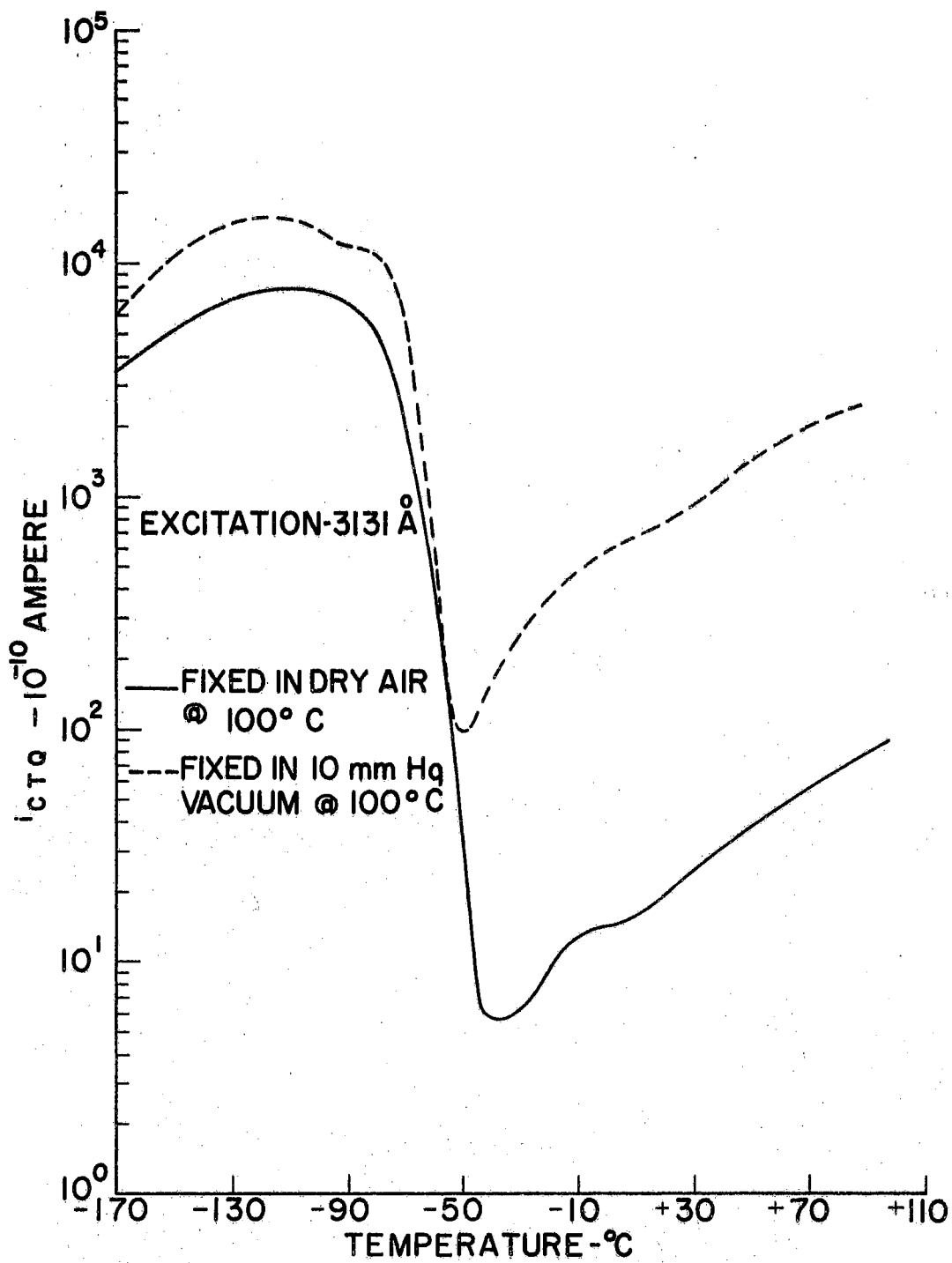
Figure 36. Continuous thermal quenching as a function of fixing procedure (3131 Å).
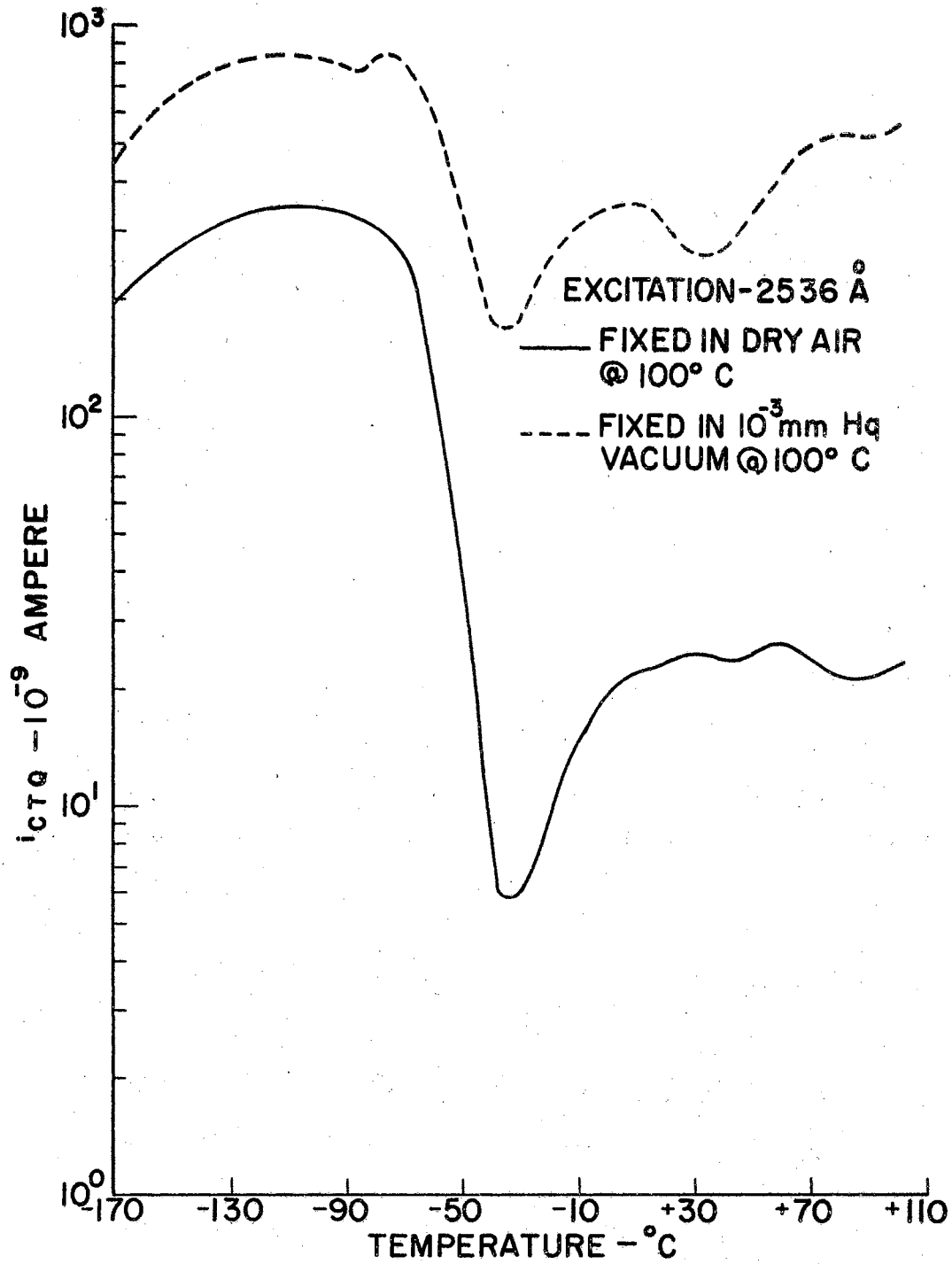
Figure 37. Continuous thermal quenching as a function of fixing procedure (2536 Å).

increased. Figures 36 and 37 concern the effects of these conditions of

fixing on the CTQ results. Note that the fixing procedures affected

the sensitive region to a lesser extent than the insensitive one

and that again what differences occurred were more evident for the

shorter wavelength excitation. As will be discussed in Chapter V,

these facts make it inviting to assume that the high temperature peaks

are associated with surface impurity concentrations.

If vacuum fixing was carried out at higher temperatures, the data

was even more drastically altered. It was particularly important as

far as TSC and CTQ were concerned that care be taken not to get the

dark resistivity so low that the desired data was masked. An example

of the effect of such a heavy reduction on TSC is shown in Figure 38.

Here the measurements were taken after one hour in rough vacuum at

520° C. Also shown on the figure for comparison is a TSC run taken

after a 700° C air fix. Note that not only did two new peaks appear in

the heavy reduction data, but also that the two high temperature ones

increased several orders in magnitude (refer to the TSC plot of Figure

19). These two upper peaks were obtained only after the subtraction

of a large dark current.

Again it was not clear whether the appearance of the new peaks and

the increased magnitude of the upper ones were the results of an increase

in trapping density or of an increase in carrier lifetime. In an effort

to clarify the situation, extrinsic spectral response data was taken

on this heavily reduced sample. Figure 39 illustrates these results

and indicates extrinsic response for wavelengths in excess of 1.4 mμ.

As one can see, definite plateaus appeared corresponding to optical

activation energies of approximately 1.0, 1.3 and 1.8 ev. Comparison
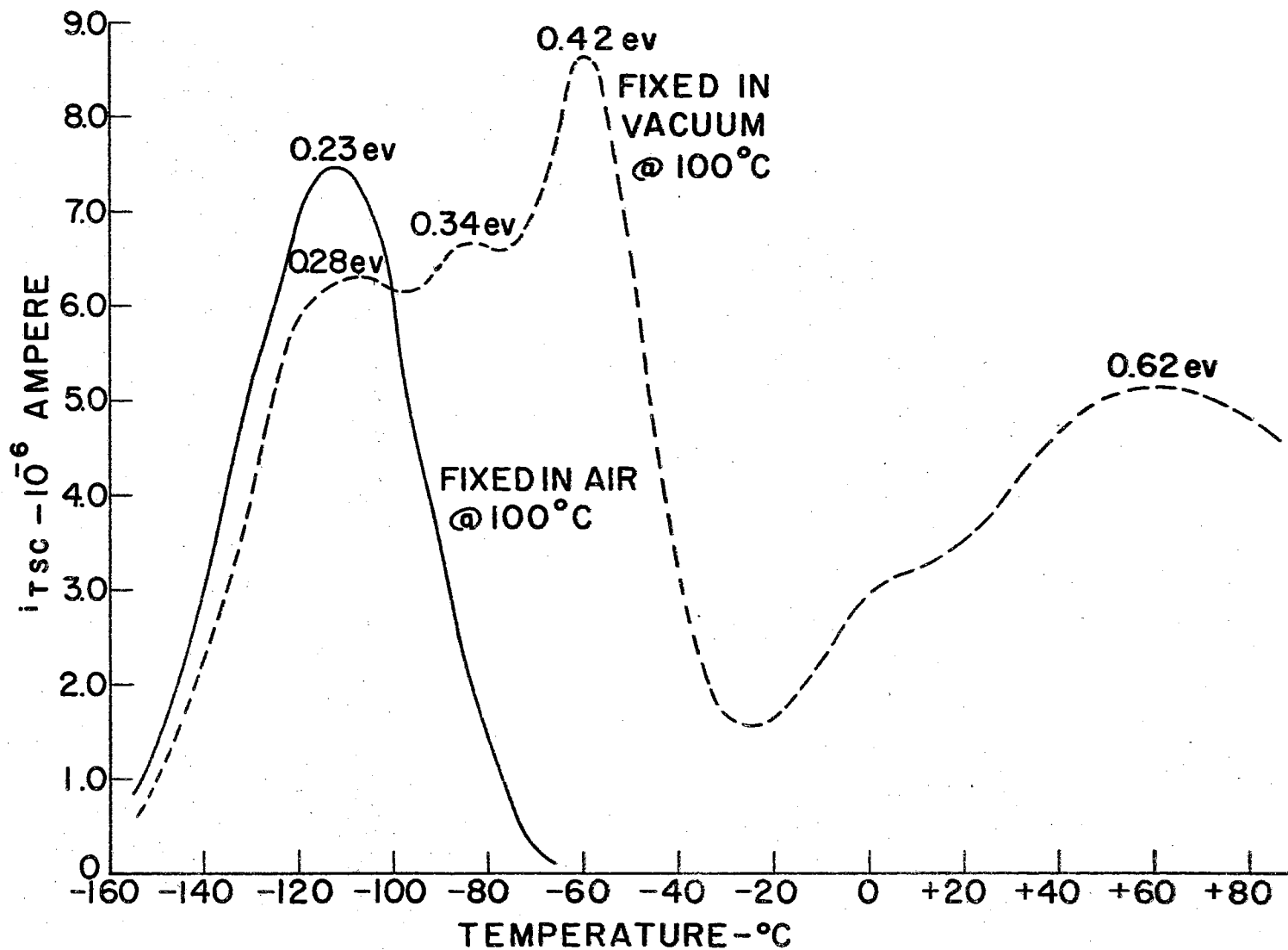
Figure 38. Thermally stimulated currents for a heavily reduced sample.

The figure is a semi-log plot. The vertical axis is labeled "RELATIVE PHOTORESPONSE – % PEAK PHOTOCURRENT" with values from 10^{-7} to 10^{2}. The horizontal axis is labeled "WAVELENGTH – MILLIMICRONS" with values from 250 to 1450.

Annotations on the plot:

FIXED IN 10^{-3} mm Hg
VACUUM at 528°C
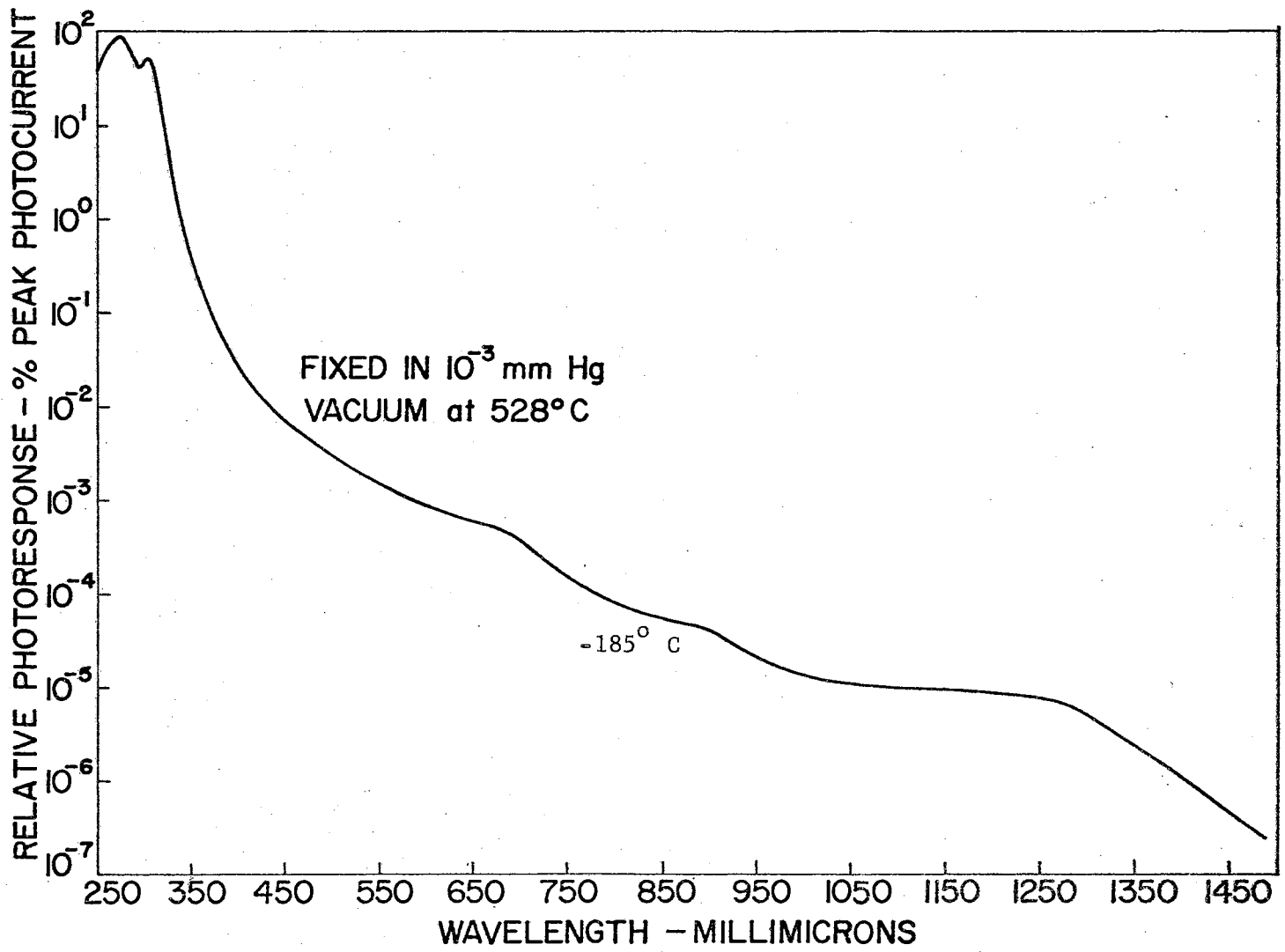
$-185°$ C

Figure 39. Extrinsic spectral response for a heavily reduced sample.

with the -185° C curve of Figure 18 also implied the existence of other
unresolved levels having energies between the 1.8 ev plateau and the
photoresponse peak at 4.0 ev. These latter states would of course
lie near the valence band in the region of very low energy resolution.

At first glance, this extrinsic response data seemed to indicate an
increase in the density of several impurity levels as a result of vacuum
fixing. However, it should again be emphasized that data of this type is
not capable of differentiating between increased density and increased
lifetime. In other words, it is entirely possible that heavy fixing
introduces some mechanism into the nonequilibrium kinetics which slows
photodecay.

Some of the most interesting exploratory results came from the
effects of combinations of intrinsic and extrinsic excitations on the
photoelectronic measurements. As far as the present work is concerned,
certain effects were discovered quite accidentally, although references
to them have since been found.[56,57] The sample was excited with intrin-
sic radiation prior to a normal measurement of extrinsic photoresponse.
It was subsequently found that large changes in the decay current
(which resulted from the 0.21 ev trap emptying) could be effected by
extrinsic radiation. An example of this extrinsic sensitization by
intrinsic pre-illumination as shown in Figure 40.

The time axis begins after an intrinsic decay of approximately five
minutes. The current level between abcissa values of zero and five
seconds is due again to the 0.21 ev trap emptying, and from five to
nine seconds it is due to the superimposed effect of exciting the
sample with 650 mμ light. Note that at first the extrinsic excitation
caused a rapid rise in current followed by a decay which was even steeper
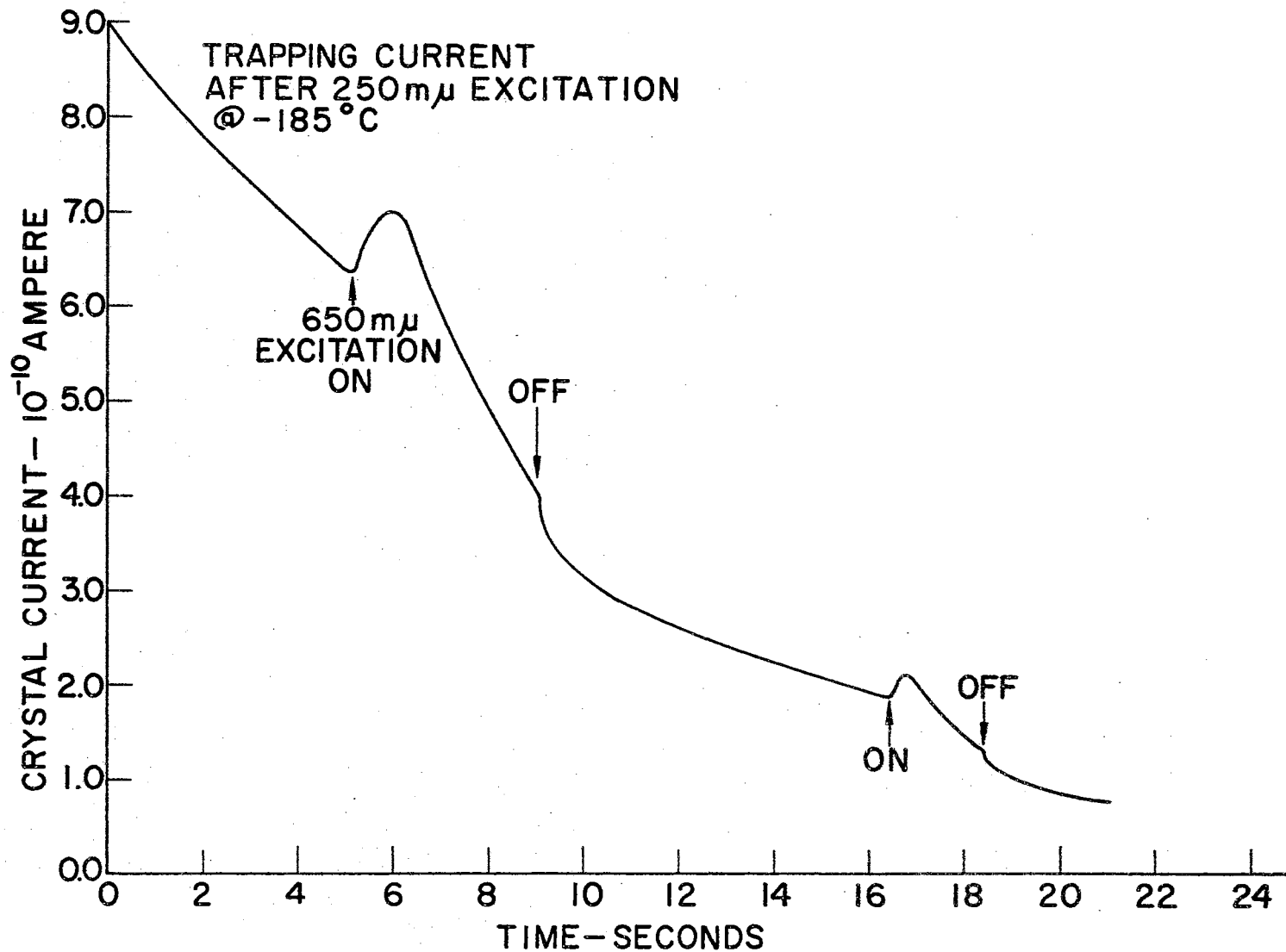
Figure 40. Extrinsic sensitization by intrinsic pre-illumination.

than before. The peak change in current as a result of the extrinsic illumination was about 6×10^{-11} ampere. This represented many orders of magnitude more response than ordinarily obtained at this wavelength (refer to the -185° C curves of Figure 18). It should also be noted that as the decay proceeded, less current change was effected by the extrinsic excitation, e.g., the peak change for the second irradiation was only about 2×10^{-11} ampere.

A very rough estimate of the wavelength dependence for this intrinsic sensitization was obtained by plotting peak-to-peak current change as a function of extrinsic wavelength. This was accomplished by illuminating the sample at several wavelengths for constant periods while recording current as a function of time. Figure 41 shows these results and indicates definite peaks at 0.48, 1.3 and 1.8 ev. Keep in mind, however, that as the trapping current decayed the sensitization decreased so that the curves became distorted depending on which end of the wavelength scale was taken first. This effect could have been eliminated by taking the data under constant intrinsic illumination. However, such a procedure proved difficult because the intrinsic photoresponse tended to mask that due to extrinsic excitation and a suggestion for further work in this area will be presented in Chapter VI.

It is proposed that this extrinsic sensitization is due to intrinsic filling of a shallow electron trapping level. The results shown in Figure 40 were then due to an extrinsic emptying of these states followed by recombination with trapped holes. A discussion is again deferred to the next chapter.

As a check on this general picture, a number of TSC and CTQ runs were taken as functions of combination excitations. The first of these
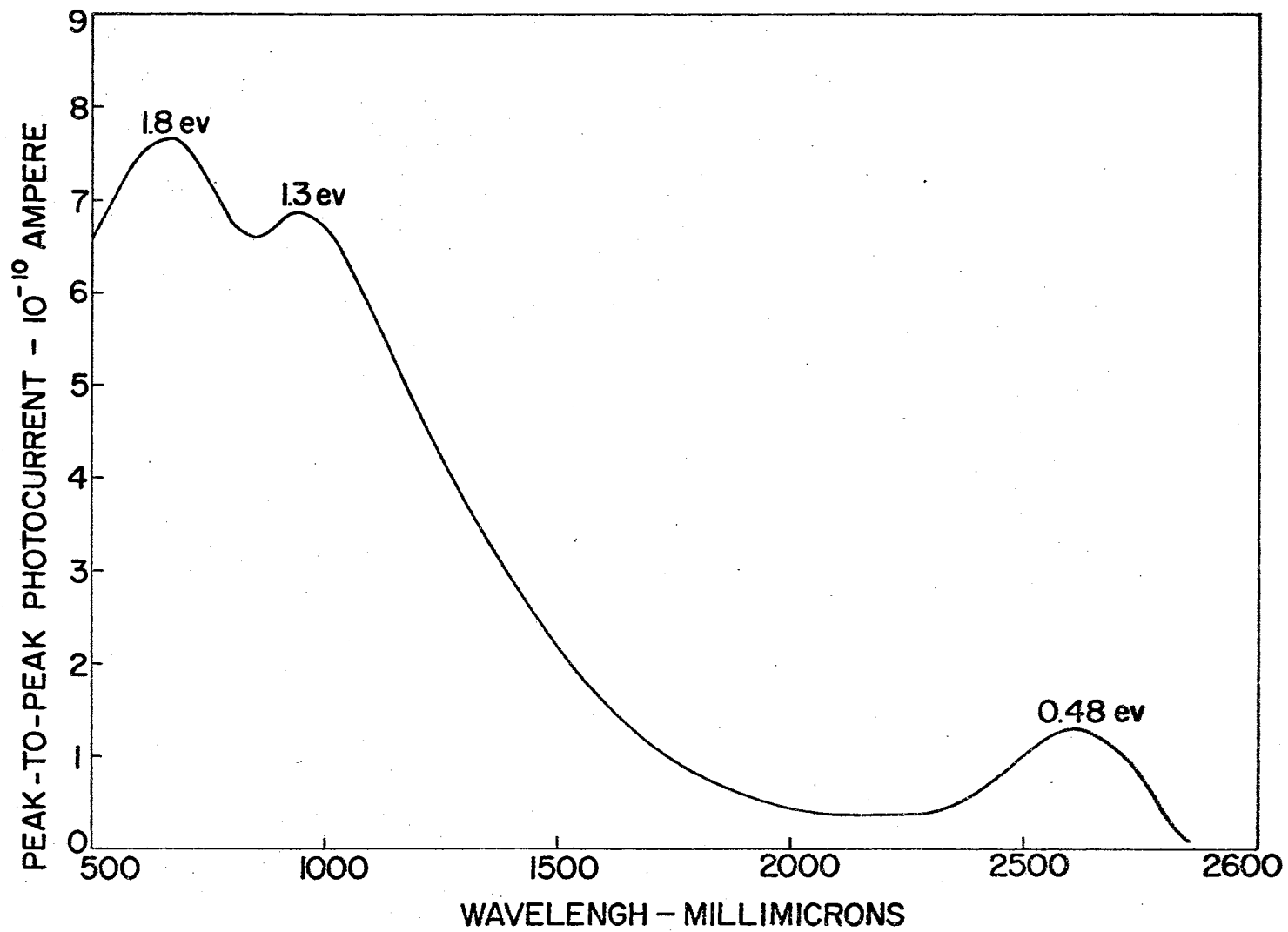
Figure 41. Spectral response of extrinsic sensitization by instrinsic pre-illumination.

sets is shown in Figure 42 where TSC has been taken following three different excitation procedures. The top curve shows a 250 mμ run taken at a low saturation photocurrent. In general it has a shape similar to those given in Figure 20 for low excitations. The middle curve shows TSC results when the sample was excited by 250 and then by 650 mμ light. The plot distinctly shows the absence of the low temperature peak. Presumably then, the data of Figure 40, along with that just described, indicates an emptying of the low temperature trapping states by the extrinsic light. Also shown on Figure 42 are the TSC results for just 650 mμ excitation, which shows only two large energy peaks.

The effects of this same set of conditions on CTQ are shown in Figure 43. Here the solid curve represents the low level 250 mμ CTQ. The dashed curve represents 650 mμ CTQ which was taken after a five minute period of 250 mμ pre-illumination. The over-all effect of the pre-illumination was a sensitization of the low temperature extrinsic photoresponse.

The trapping level responsible for the previously described sensitization by intrinsic pre-illumination was probably the same one which desensitized the extrinsic CTQ results shown as the dotted curve in Figure 43. In the prior situation the traps were being filled by intrinsic excitations and in the second case emptied by thermal ones. This explanation was checked by plotting the logarithm of extrinsic photocurrent versus reciprocal temperature, as illustrated in Figure 44 which shows graphically the low temperature effect of the 0.22 ev trapping level. It is interesting to recognize that the explanation for these extrinsic and the normal intrinsic CTQ behaviors parallel those for the
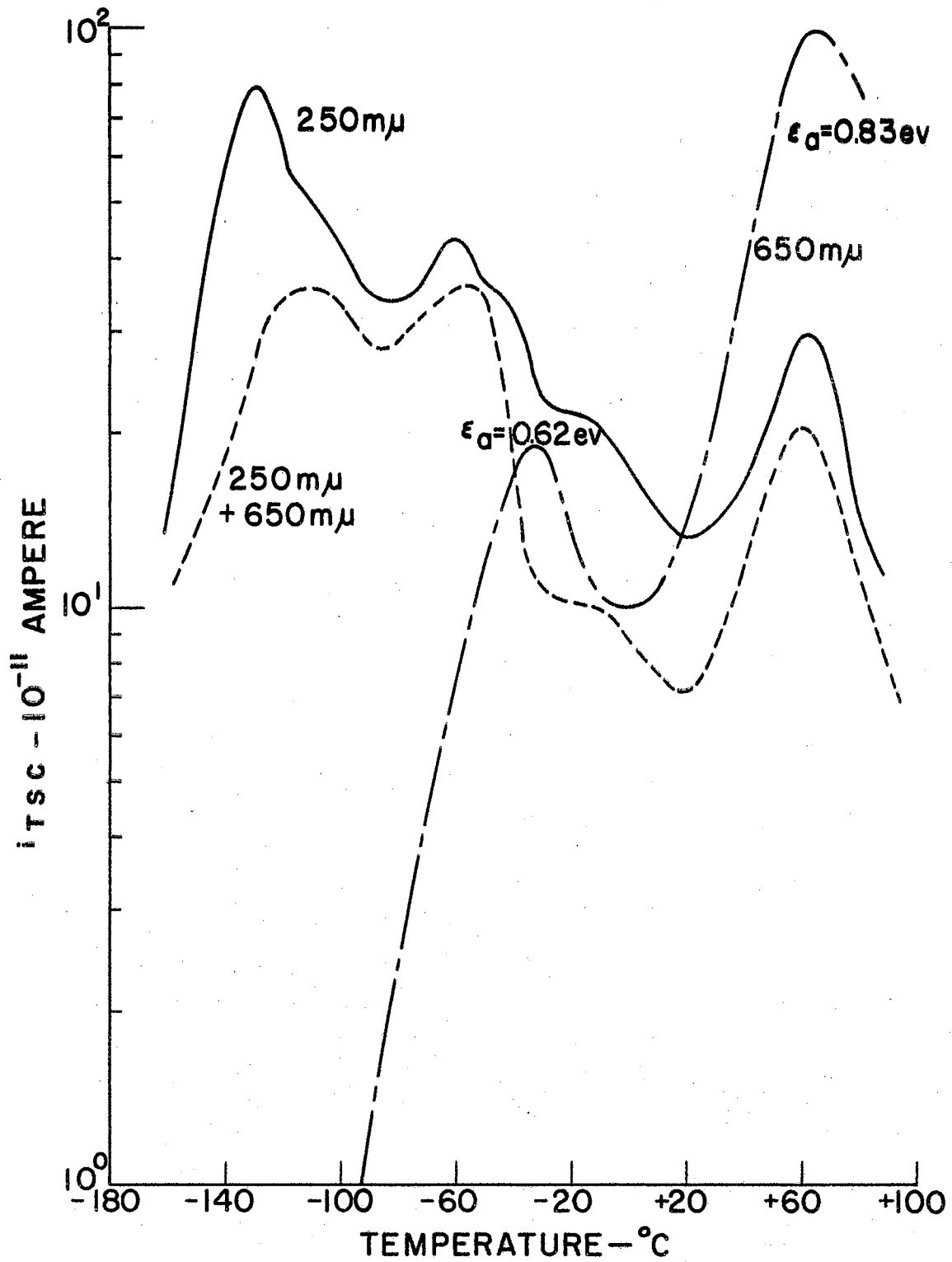
Figure 42. Thermally stimulated currents under combination excitation.
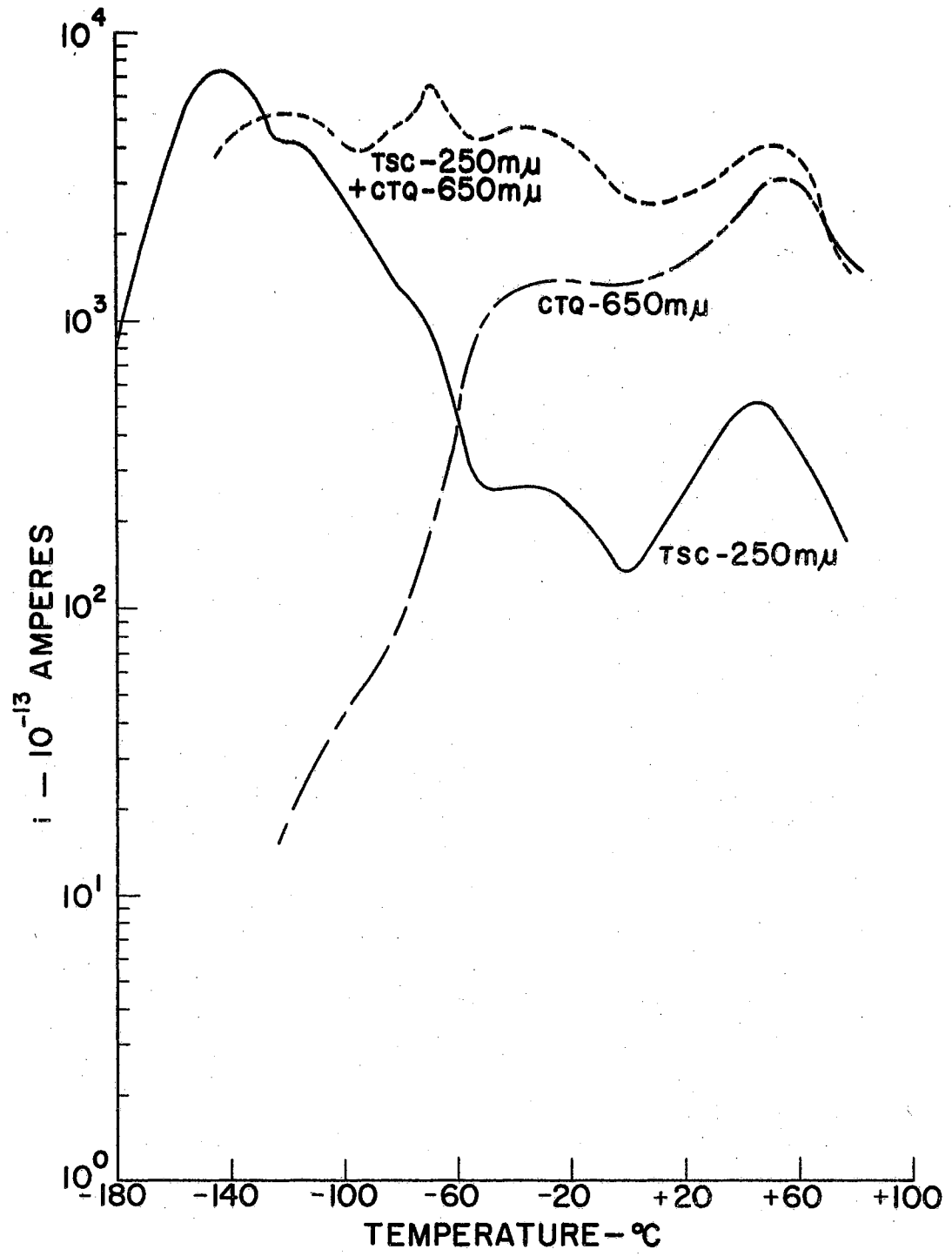
Figure 43. Continuous thermal quenching under combination excitation.
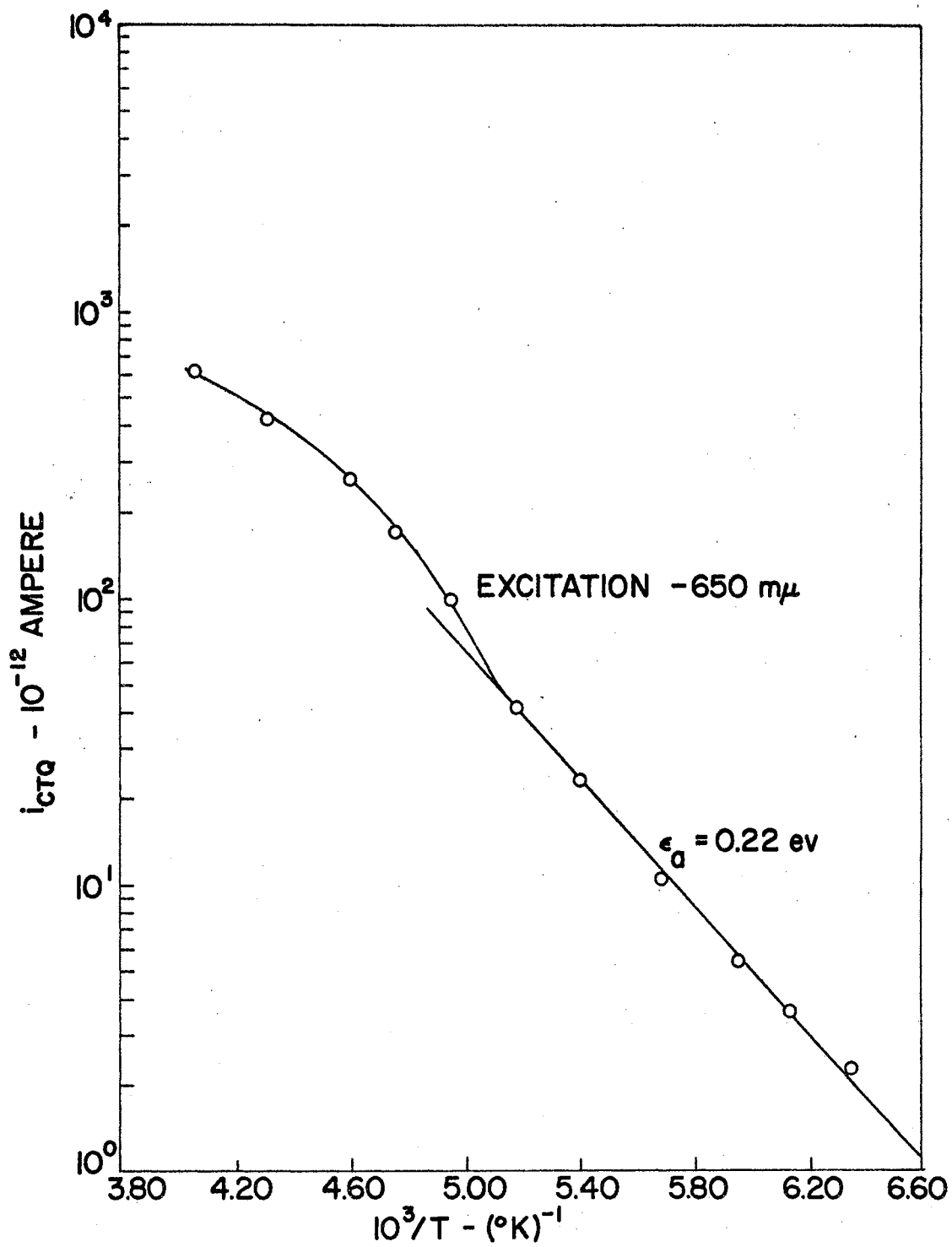
Figure 44. Logarithm of the extrinsic continuous thermal quenching as a function of reciprocal temperature.

temperature variations in the spectral response data of Figure 18. In other words, at low temperatures the intrinsic photoresponse was sensitized and the extrinsic desensitized, while for higher temperatures just the opposite effect took place.

The results of the exploratory photo-thermoelectric voltage measurements are given in Figures 45 and 46 and represent the voltage of the cold end of the crystal as its average temperature was raised. The temperature gradient itself was not measured and so these curves are plotted in terms of the temperature of the hot end. Data obtained in a TSC-type experiment is shown along with a characteristic TSC curve in Figure 45. Similarly in Figure 46, data is presented for CTQ procedures. In addition to these results, thermoelectric voltage measurements on crystals in the dark indicated n-type conductivity.

Although this investigation sought only qualitative information, a great deal of time was spent checking to determine that the results were directly attributable to the presence of the crystals rather than to extraneous effects. An interpretation of the data in terms of crystal properties under illuminated conditions is to be discussed in the next chapter.

This completes the collection of results that have been obtained in the present study. An attempt is made in Chapter V, to coordinate these to provide a unified energy level scheme for defects in stannic oxide crystals.
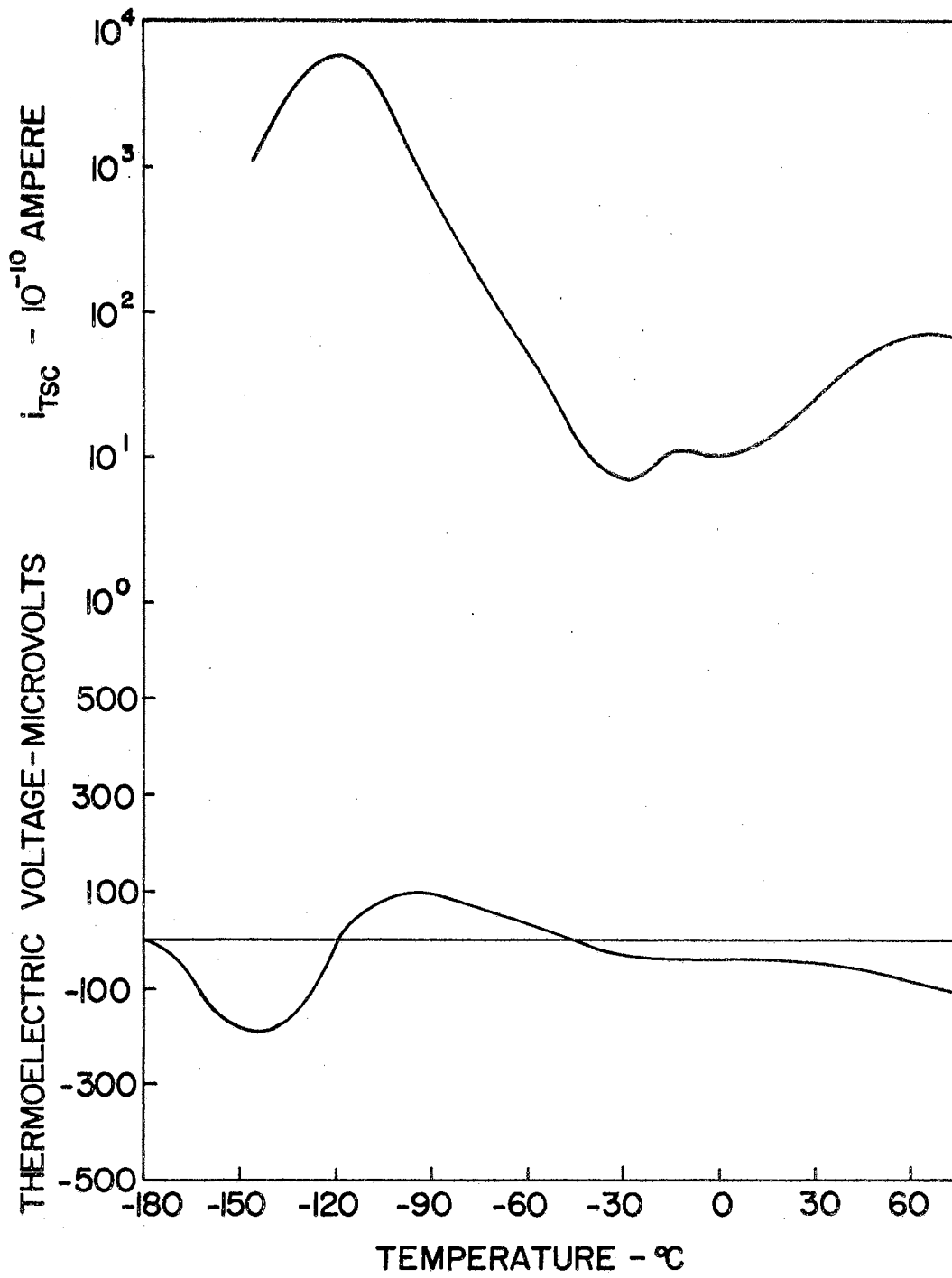
Figure 45. Photo-thermoelectric voltage for the
thermally stimulated current procedure.
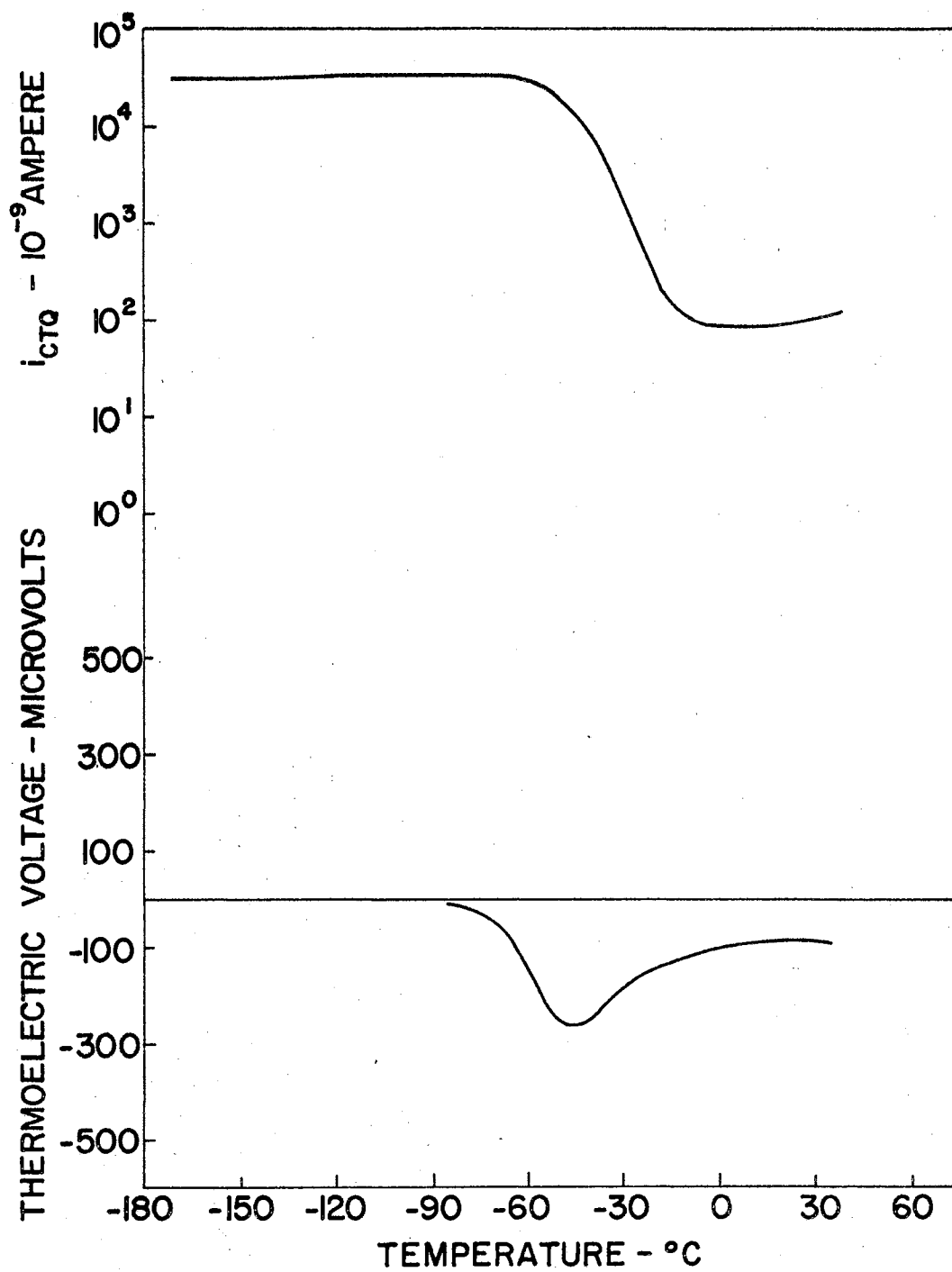
Figure 46. Photo-thermoelectric voltage for the
continuous thermal quenching procedure.

CHAPTER V

DISCUSSION AND CONCLUSIONS

Summary of Results

Before a comprehensive discussion of the data given in Chapter IV
is begun, it will be helpful to first outline the more important results.
The outline is arranged so that related results appear under a common
heading.

I. Spectral response data

    A. In every case, the photoresponse peak indicates a band gap of
       approximately 4.0 ev.

    B. The short wavelength intrinsic response exhibits a typical
       ambient effect.

    C. The temperature dependence of spectral response indicates a
       decrease in intrinsic, and an increase in extrinsic sensitivity
       with rising temperature.

II. Defect-sensitive results

    A. Extrinsic spectral response under heavy vacuum reduction shows
       plateaus giving calculated optical activation energies of
       1.0, 1.3 and 1.8 ev. It also implies the existence of levels
       lying closer to the valence band than 2 ev. The spectral
       response of extrinsic photoconductivity after intrinsic pre-
       illumination indicates levels having activation energies of
       0.48, 1.3 and 1.8 ev.

B. High intensity TSC data gives trapping levels having average
    activation energies of 0.21, 0.52 and 0.60 ev. The data
    indicates only small energy variations in the lower temperature
    peak, but a Meyer's rule behavior for the upper two. Low
    intensity TSC shows the existence of several new trapping
    peaks in the energy range between 0.21 and 0.52 ev. Also it
    is shown that the 0.21 ev peak is degraded by low level
    excitations.

C. CTQ data indicates a set of sensitizing centers having a
    0.33 ev activation energy, a ratio of catpure cross sections
    $S_p/S_n = 7.0 \times 10^2$ and a ratio of $N_r/N_t = 1.0 \times 10^5$.

D. Dark conductivity as a function of reciprocal temperature
    implies a donor level lying about 0.58 ev (on the average)
    below the conduction band and showing a Meyer's rule behavior.

III. Effects of combination intrinsic-extrinsic excitations

A. TSC data reveal that a decrease in the low temperature peak
    occurs if the sample is irradiated by both 250 and 650 mμ
    light.

B. From CTQ results it is found that the extrinsic photoresponse
    exhibits a low temperature sensitization as a result of
    intrinsic pre-illumination.

C. Transient decay of intrinsic photoconductivity at -185° C
    shows that extrinsic excitation first increases the decay
    current and then causes it to decrease at a greater rate.

IV. Low temperature fixing effects

A. TSC data shows that fixing has large effects on the upper two

peaks and only small effects on the lower one. In the first
case vacuum fixing increases the magnitudes while in the
second case the peak decreases. The changes are shown to be
more pronounced for shorter wavelength excitations.

B.   Similar CTQ results show very little effect on the sensitive
region and an increase in sensitivity of the high temperature
region after vacuum fixing. Again, any changes are favored
by shorter wavelength excitations.

V. Photo-thermoelectric voltage results suggest that the two main
trapping levels are both electronic states and give strong evidence
that in the sensitive region conduction is by electrons.

Spectral Response

Before discussing the results obtained from spectral response data,
the difficulties encountered in this technique should again be emphasized.
Recall first, that the measurement itself is defined as saturation photo-
current as a function of wavelength. The two principal obstacles to
obtaining results under this definition are (1) that for materials with
trapping, saturation times are unreasonably long and (2) that there may
be considerable interactions between the trapped carriers resulting
from one wavelength and the photocarriers produced by the next. There-
fore, in an exact measurement, the photocurrent would have to be saturated
at each particular wavelength and the trapping states thermally emptied
before proceeding to the next. Obviously, experimental time limitations
prohibit this procedure.

Many investigators, in an attempt to circumvent these difficulties,
have gone to A-C, chopped light techniques. However, some reflection

indicates that this alternative -- while possibly more convenient in some cases -- does not relieve the trapping problem. Another difficulty in encountered with light sources. These, without exception, have output intensities which vary widely with wavelength. This can lead to a distortion of the response curves since photocurrents seldom are directly proportional to light intensity. Accurate data of this type, in general then, can only be taken if the light intensities are high enough so that the density of current carriers is large compared with that of the trapped carriers, and if the spectral intensity of the light source is somehow flattened. As mentioned in Chapter III, it is because of these difficulties that the spectral response technique has been used in the present work only for qualitative results.

Although qualitative, the results that have been obtained from this measurement are nonetheless typical of those gotten on other materials. As outlined previously, these include (1) a peak in the photo-response on the short wavelength side of the fundamental absorption edge, (2) an ambient effect on the short wavelength intrinsic photo-response, (3) increased extrinsic response as the dark conductivity is increased (by increasing defect density), and (4) opposite temperature effects on the instrinsic and extrinsic photoconductivity.

Some investigators have actually used the wavelengths at the spectral response peak to calculate the band gap of their photoconductors.[58] Such a calculation for the response data given in Chapter IV, yields a value of approximately 4.0 ev; which is in fair agreement with results ranging from 3.3 to 4.1 ev reported by other authors.[10,14,59]

Figure 18 indicates characteristic ambient effects on photoresponse, similar to those reported on almost every material. An example of such

data on CdS is given by Bube.[60]

The fact that extrinsic photoresponse increases with dark conductivity is a common phenomenon and is used extensively as a probe of impurity properties. The data shown in Figure 39 for a heavily reduced sample has been taken as indicative of defect activation energies. Values were calculated from the wavelengths at the plateaus of photoresponse and found to about by 1.0, 1.3 and 1.8 ev. The results have particular importance in that they imply a set of more-or-less discrete levels lying at energies greater than approximately 0.80 ev from the conduction band and whose densities seem to be increased by vacuum reduction. Also, since this material is n-type, extrinsic transitions into the conduction band can take place only from states occupied by electrons. Valence band transitions are not allowed unless they involve electronic transitions into compensated donor states. A good review of such data on other photoconductors is given in Chapter 6 of Bube's book.[29]

The fact that intrinsic and extrinsic spectral response are oppositely affected by temperature is also noted on other materials* and it is felt that this result may have special significance in understanding the imperfection scheme in stannic oxide. However, a discussion of this significance, as well as the phenomenological reasoning behind it is to be postponed until intrinsic and extrinsic CTQ results are considered.

<p align="center">Defect-Sensitive Results</p>

Those results which have special bearing on the proposal for defect or

---

*This behavior is exemplified by data on ZnSe:Sb shown in Figure 6.4-11 of Bube's book.[29]

imperfection scheme will now be considered. First, the results of TSC indicate the presence of three main trapping levels. DTSC energy values for the low temperature peak fall within 15% of one another for the five samples tested. Note further that the Bube values for the same peak vary to a much larger extent and are found to be always greater than those obtained from DTSC. This last discrepancy is probably due to the fact that, since this data is taken with intrinsic excitation, the carriers are generated near the surface and become preferentially trapped there. Consequently, when a calculation is made based on Bube's assumption, an error results from an incorrect A/L ratio in the relation between measured conductance and the conductivity of Equation 25. Since this ratio appears in the denominator, surface conduction would result in erroneously large values of activation energy. It is expected, then, that more trust should be placed in the values obtained by the DTSC method.

Values for the mid-temperature peak are the most erratic and do not even show a general Meyer's rule behavior for either the Bube or the DTSC method. This may very well be due to the usual difficulty of getting data for this peak, arising from the fact that it is always overlapped by both the others. The high temperature peak is seen to be somewhat more consistent. Again, the Bube values are greater than the energies gotten from DTSC, but these latter values follow Meyer's rule rather well.

From what has just been said the following conclusions can be drawn concerning the values of trapping activation energy:

    1. The low temperature peak is indicative of a trapping level whose activation energy is, on the average, 0.21 ev. The

spread is an indication of the measuring accuracy.

2. Two other trapping levels exist and their activation energies depend rather sharply on dark conductivity. On the average their values are 0.52 and 0.60 ev.

3. The fact that the Bube calculation gives higher activation energy values than those obtained from DTSC implies that carriers are created at the surface and at least those of one sign are trapped before they have a chance to diffuse into the bulk.

Before leaving TSC, one other point should be recalled. This concerns the question of whether the three order of magnitude difference in maximum currents for the low and high temperature peaks represents a difference in trapping density or carrier lifetime. CTQ, which is so sensitive to carrier lifetime, should shed some light on this question.

Even though only a limited amount of CTQ data has been taken, it is found to yield consistently a value of 0.33 ev for the activation energy of those states responsible for the low temperature sensitivity. In other n-type materials that show similar sensitization, the responsible states have been found to be compensated acceptor levels.[51] Assuming this to be the case here, the centers would then lie 0.33 ev above the valence band and have a capture cross section ratio $S_p/S_n = 7.0 \times 10^2$. It is, of course, not inconceivable in an n-type material to have sensitization by compensated donor states having a large cross section ratio S_n/S_p. However, the balance of the data to be presented in this section points to the conventional pattern of sensitization by compensated acceptors.

It will be recalled from the discussion in Chapter II, that sensitizing centers increase the majority carrier lifetime in the low temperature region. As a matter of fact, the curves given in Figure 24 can be essentially considered as plots of majority carrier lifetime as a function of temperature for the particular carrier densities involved. Hence, it can be concluded that the magnitude of the thermally stimulated majority carrier density will basically have the same type temperature dependence as these CTQ curves. As an answer to the question posed earlier, a TSC peak for trapped majority carriers in the sensitive region will have about the same ratio to one in the high temperature region as the steady-state photocurrents have in these two regions if the trapping densities and capture cross sections are the same in the two situations. It can be inferred from this, then, that the 0.21 ev TSC peak is to be associated with trapping of the majority carriers. Conversely, the sensitizing centers must be trapping-recombination states for minority carriers. Of course, and TSC peaks due to thermal emptying of the minority carrier trapping states will be somewhat desensitized in the low temperature region.

It can be seen from Table I, that dark conductivity as a function of reciprocal temperature yields donor activation energies which are in agreement with DTSC values for the high temperature trapping peak. Further, it is noted that both values show Meyer's rule behavior. Therefor, a reasonable assumption is that the high temperature TSC peak is associated with electrons trapped in the compensated portion of those donor states responsible for the dark conductivity. These dark conductivity activation energies have been calculated using Equation 36 which, as pointed out in Chapter 2 of Bube's book,[29] is correct under compensated

conditions for which the density of conduction electrons is small compared with the density of acceptors. This relation takes the form

$$E = 2kT\ln\sigma + \text{constant} \tag{37}$$

if the material contains only a single donor level filled with electrons at low temperatures. The former expression is used here, then, for two reasons: (1) because TSC and CTQ data point to the fact that compensation exists and (2) because the activation energies calculated using it show excellent agreement with the high temperature peak DTSC data. As pointed out in Chapter V of Mott and Gurney,[55] the dilemma of which expression to use always exists for activation energy values calculated from this type data.

From what has already been said, it is concluded that these crystals contain a majority carrier trap having an activation energy of 0.21 ev and a minority carrier trap whose energy is 0.33 ev. The latter acts as a sensitizing center under conditions which force it to change from a trapping to a recombination level. However, the results discussed so far have not made it certain whether in the sensitized region electrons or holes are the majority carriers. Extrinsic CTQ results are of some help in this determination.

Consider again the dotted portion of Figure 42 which shows a large increase in extrinsic (650 mμ) response as the temperature is raised. In this procedure majority carriers are excited into the free band from states neighboring the center of the forbidden gap. It is felt that at low temperatures virtually all of these extrinsic carriers are trapped in shallow compensated states, and that as the temperature is raised the proportion of free to trapped carriers increases (see the last part

of Sensitization and Quenching of Chapter II). If this is true then the
rise of extrinsic CTQ with reciprocal temperature should indicate the
energy of the responsible trapping states. Figure 44 shows this data
and indicates that these trapping states have a calculated activation
energy of 0.22 ev, which implies that they are the same states responsible
for the low temperature TSC peak.

Since these crystals are n-type and dark conduction arises from
donor levels lying less than perhaps 1.0 ev below the conduction band,
donor levels with even smaller activation energies must be compensated.
Therefore, if extrinsic hole conductivity were present, it would have to
involve electron transitions into these compensated states or would
require exciting wavelengths shorter than 400 mμ (3.0 ev). Consequently
it seems evident that these extrinsic processes involve electrons and
that the 0.22 ev trap is an electron trap. Of course, this also implies
that the sensitization is due to a compensated acceptor level located
0.33 ev above the valence band.

This shallow electron trap can have a desensitizing effect on the
intrinsic photoconductivity, but in this case it must compete with the
acceptor state sensitization process. In the sensitive region of Figure
24 these trapping states are saturated (except possibly at the lower
intensities) and no temperature variation is seen. However, in the high
temperature region a variation is noted as the light intensities are
decreased. This interaction at the lower light levels is felt to be
responsible for the inconsistency noted in CTQ data taken on the break
to low sensitivity, i.e., the large difference in slope between the curves
of Figure 25. The low sensitivity break appears to occur at lower
temperatures as the light intensity is decreased (in the presence of

such an interaction). Consequently, data taken for the lower curve of the figure yields an erroneously high slope.

The extrinsic TSC data shown in Figure 42 also shows that the mid and high temperature TSC peaks are electron traps (the indicated Bube values again being high). The low temperature peak does not appear here because of the desensitization effect at these temperatures. The top two donor levels must be empty since a TSC peak shows up as due to the compensated portion of those states responsible for the dark conductivity, i.e., at an average of 0.60 ev below the conduction band.

The evidence of a shallow electron trap is further supported by the exploratory results of extrinsic sensitization by intrinsic pre-illumination. Figure 40 shows that if the 0.21 ev electron traps are first filled by intrinsic excitation, the extrinsic photoresponse is greatly increased. The increased decay rate which appears after extrinsic irradiation is due to the shortened lifetime resulting from extrinsic excitation of electrons from the main recombination centers and their subsequent decay into the trapped holes of the 0.33 ev acceptor states. All of the compensated donor levels tend to be filled by the intrinsic pre-illumination. Therefore, a subsequent extrinsic spectral response measurement (Figure 41) shows a long wavelength broadening which includes excitations from these levels. This broadened response extends to energies less than 0.48 ev.

As mentioned before, this type extrinsic spectral response data is taken during the transient trapping decay (Figure 40) and is at best only a guide to the actual response. Therefore, a great deal of reliability should not be placed on the specific values of activation energies taken from these results. The important conclusions are that

over-all extrinsic response is greatly enhanced and spectrally broadened by intrinsic pre-illumination. Both effects are due to the intrinsic filling of all available electronic states near the conduction band.

Supplementary data of TSC and CTQ utilizing this intrinsic sensitization are shown in Figures 42 and 43. The first of these is taken by pre-exciting the sample with both intrinsic and extrinsic radiation and running a normal TSC curve. The results, shown along with the normal low intensity intrinsic TSC, indicate an almost complete removal of the low temperature peak as a result of adding extrinsic pre-excitation. This is consistent with a decrease in lifetime caused by an extrinsic emptying of the main recombination centers. Figure 43 gives the results of CTQ taken by pre-illuminating intrinsically and allowing the temperature to rise under only extrinsic excitation. The results are those that might be expected of a material which has no compensation, i.e., CTQ which is virtually independent of temperature. Again this is due to the filling of shallow electron traps by the instrinsic pre-illumination.

The interaction behavior described above is even more pronounced at very low light levels. Such data are shown in Figures 20 and 29. In the second of these, low enough light intensities have been used so that the acceptor states have not become recombination centers; therefore sensitization is not present. The fact that the photoresponse increases with temperature is again the result of the shallow electron trap.

TSC at these low light levels (Figure 20) shows the low temperature peak diminishing, as expected, when sensitization does not occur. Notice also that in the absence of sensitization, the TSC data implies the existence of several unresolved trapping peaks between those normally obtained at 0.21 and 0.50 ev. These, of course, are completely

overshadowed in the high level measurement by the sensitized 0.21 ev peak. One of the trapping levels included in this region is undoubtedly the acceptor hole trap at 0.33 ev.

Two of these levels are also brought out in TSC data taken on highly reduced samples such as shown in Figure 38. Here, it seems, the over-all carrier lifetime has been increased, but the large difference in the hole and electron lifetime values no longer exists. Therefore, the data appears a great deal like that taken at low light values except for the magnitude of the photocurrents involved. The mechanism through which lifetime is changed by vacuum reduction is not understood at this time.

At this point, the data seems complete enough to establish an imperfection level model for these stannic oxide single crystals. But first, a summary of the salient features and the source of their justification will be given.

1. A stable, completely compensated electron trapping level lying 0.21 ev below the conduction band. (TSC, extrinsic TCQ)

2. A stable hole trapping level lying 0.33 ev above the valence band which can act as a sensitizing center at low temperatures. (CTQ)

3. Two prominent electron traps whose energies depend on dark conductivity. The shallow one is completely compensated and lies, on the average, 0.50 ev below the conduction band. The deeper one is partially compensated and is the same level responsible for the dark conductivity. It lies, on the average, 0.60 ev below the conduction band. (normal and extrinsic TSC, dark conductivity)

4. Other discrete levels appear to lie about 1.0, 1.3 and 1.8 ev
    below the conduction band. Indications are that levels exist
    between 2 ev and the valence band but resolution does not
    permit their separation. (spectral response, both intrinsic and
    extrinsic after intrinsic pre-illumination)

5. Intrinsic band gap of approximately 4.0 ev. (peak of intrin-
    sic photoconductivity)

Figure 47 shows the result summarized above in a normal energy band scheme.
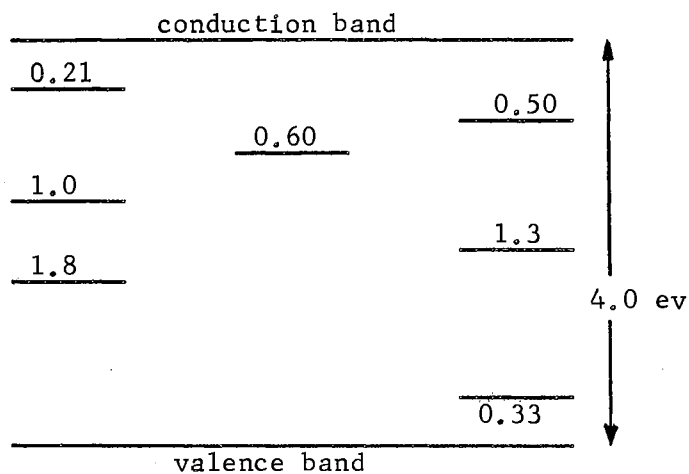
Figure 47. Proposed energy level scheme for grown
stannic oxide single crystals.

With the exception of the shallow electron and hole trapping levels,
the activation energies given in Figure 47 are to be taken as only crude
guides. The three energies which are determined from spectral response
data, of course, have the errors inherent in that procedure plus any
resulting from the lack of consideration of the Franck-Condon shift.*

On the other hand, the two deep electron trapping levels have a

---

*For a discussion of this effect refer to Chapter V of Mott and Gurney.[55]

Meyer's rule variation in their activation energies and the values given on the figure are averages. As yet the causes of this behavior have not been determined, but it appears certain that they are the same ones responsible for the similar behavior in the dark conductivity activation energies. It is presently suggested that in both instances the behavior may be simply the result of increasing the density of one or more of the donor levels shown in the figure. This has the effect of decreasing the over-all percentage compensation.

As mentioned earlier, the activation energies obtained from dark conductivity data actually represent the equilibrium Fermi level position. Therefore in a highly idealized model at low temperatures, the calculated activation energy tends to be that of the highest unfilled donor level. If the highest donor level is just filled at low temperatures, then the calculated value will correspond to the midway point between this level and the next higher empty one.

It seems possible that such a mechanism could explain the large variations in activation energies observed with vacuum reduction (refer to Figure 33). It might be assumed that the donor level whose density is increased by reduction, in this case, is the one associated with oxygen vacancies, but no data is available to establish which of the levels in Figure 47 it might be. This simple scheme could explain similar variations in trapping activation energies. This facet of the general oxide semiconductor problem is under investigation as another part of the project.

As yet no data is available on the defect responsible for the 0.33 ev sensitization center in these crystals. In analogy to results on CdS,[61] it is tempting to associate the sensitization with the presence

of copper. This is particularly appealing since the samples are grown in cuprous oxide flux and copper is found as a constituent in the spectrographic analysis. In addition, preliminary photoelectronic data on stannic oxide ceramics, pressed from high purity powder, shows an absence of sensitization.* It is hoped that cuprous oxide doping of the stannic oxide powder prior to firing may shed light on this question.

The energy scheme of Figure 47 represents the primary result of the present work and must be regarded in the light of the factors just mentioned. More than anything else, these somewhat qualitative results are intended to act as guides to additional studies which should now be undertaken to substantiate and complete the over-all picture. Several of these are to be discussed in Chapter VI.

<center>Low Temperature Fixing Effects</center>

Some samples were found to have large variations in dark conductivity with oxygen pressure for temperatures as low as 100° C (refer to Figure 33). In order to explain this behavior, a surface vacancy layer was assumed with electron occupancy controlled by the density of chemisorbed oxygen, i.e., each O_2 molecule taking up two electrons from the vacancy donors. A small amount of photoelectronic data has been taken in an attempt to corroborate this assumption and to determine if TSC and CTQ data might prove useful for studying surface properties.

TSC data taken as a function of fixing and wavelength are shown in Figures 34 and 35. The indications are that the vacuum fixing affects the peak association with dark conductivity to a much greater extent than

*Unpublished data by Matthews of the Oklahoma State University Physics Department.

either the 0.21 ev electron trapping level or the 0.33 ev sensitizing

centers (which are responsible for the enormous magnitude of the 0.21

ev TSC peak). It is also apparent that this effect is even more pro-

nounced for shorter wavelength excitation, i.e., for carriers generated

nearer the surface. Similar indications are obtained from the CTQ data

of Figures 36 and 37 which also show little fixing effect on the 0.33

ev sensitizing centers. The implication here is that those levels

responsible for most of the dark conductivity are located at or near the

surface of the crystal, whereas the shallow electron and hole traps

appear to be bulk states. Even though carrier lifetime data is necessary

to be certain, it would seem logical to assume that the high temperature

current magnitudes in both the TSC and CTQ procedures are larger after

such vacuum treatment as a result of an increase in carrier lifetime

rather than a density increase.

Photo-Thermoelectric Voltage

The results of the photo-thermoelectric voltage measurements should

logically appear in the section on defect-sensitive results since they

are indicative of the majority carrier sign (or type). However, it has

been decided to discuss them separately because of the interpretational

difficulties (refer to Chapter II), which hamper unique conclusions.

Recall that for these exploratory measurements, the difficulties arise

from a lack of knowledge as to the temperature dependence of the steady-

state Fermi level during the photoelectric procedures.

In the case of extrinsic dark conductivity, the function $E_{fq}(T)$ is

known, therefore unique carrier-type determinations are possible. In

the present work such measurements always indicate n-type conductivity

above room temperature, the crystal resistance being too high to conveniently take such data for lower temperatures. However, such a relation is not available for either the TSC or CTQ procedures and thus the results obtained must be compared with earlier conclusions to clarify their interpretation.

Figure 45 shows the results of thermoelectric voltage for the TSC procedure. Here the voltage rises negatively (cool end) along with the TSC, indicating the thermally stimulated carriers to be electrons. On the high temperature side of the peak, the voltage changes sign apparently indicating that in this region the integral term containing dE_{fn}/dT is larger than that for E_{fn}/T. In the high temperature region, the Fermi level again approaches the conduction band and the voltage sign is once again indicative of n-type TSC. The voltage in this case does not change signs but increases toward what is apparently a value associated with the dark conductivity. Note that, even though in the low temperature regions the results strongly support electronic conduction, the conclusions for the transition regions are chosen to explain earlier results.

Figure 46 shows the thermoelectric voltage results for the CTQ procedure. In the sensitive region the steady-state Fermi level is found near the conduction band (small E_{fn}) and is nearly independent of temperature with negligible experimental voltages being recorded. Actually, if larger heater currents are used in this region, detectable negative (cool end) voltages are noted. As the crystal enters the quenching region, The Fermi level falls rapidly away from the conduction band and apparently the rate of increase of the E_{fn}/T integral term far outweighs that due to E_{fn}/dT. Therefore, in this region the voltage of the cool end increases in negative magnitude.

CHAPTER VI

SUGGESTIONS FOR FUTURE STUDY

The results and conclusions just presented have emphasized several problems which need attention in order to round out the over-all imperfection analysis on these crystals. They have also pointed to extensions of the present work which can significantly contribute to the general understanding. In this chapter a few of the more important of these suggested studies have been selected for short discussions. Included are a group of measurements representing a broadened application of the present analysis along with measurements of carrier lifetime, photo-Hall effect and relative quantum efficiency.

Extensions of the Present Work

Suggestions concerning extensions to the present work are discussed first because (1) they involve familiar techniques and can be accomplished with the benefits of past experience and (2) they contain proposals for equipment modifications which can be used in two of the other suggested studies. These equipment modifications are based on the experience that has been gained in the present work and are felt to be necessary in improving the reliability and accuracy of the data.

Figures 48 and 49 show schematics of the proposed cryostat and sample holder. These schematics are drawn to scale but are not given as working plans for equipment construction. They represent only examples

Liquid
Nitrogen
Chamber

Housekeeper
Glass to Metal
Seal

Silvered
Inner
Surface

"O" Ring

Quartz
Window

Sample
and
Heater
Chamber

Vacuum
Feed
Throughs

Vacuum
Port

UG
Coaxial
Connector
for
Electrometer Lead

Cryostat
Flange

Figure 48. Suggested cryostat schematic.

Liquid Nitrogen
Chamber

Vacuum
Feed-through
(Heater lead)

Heater
Windings

Double
Capillary
Quartz Rod

Crystal

Teflon

Pressure
Spring
(Phosphor-Bronze)

Copper
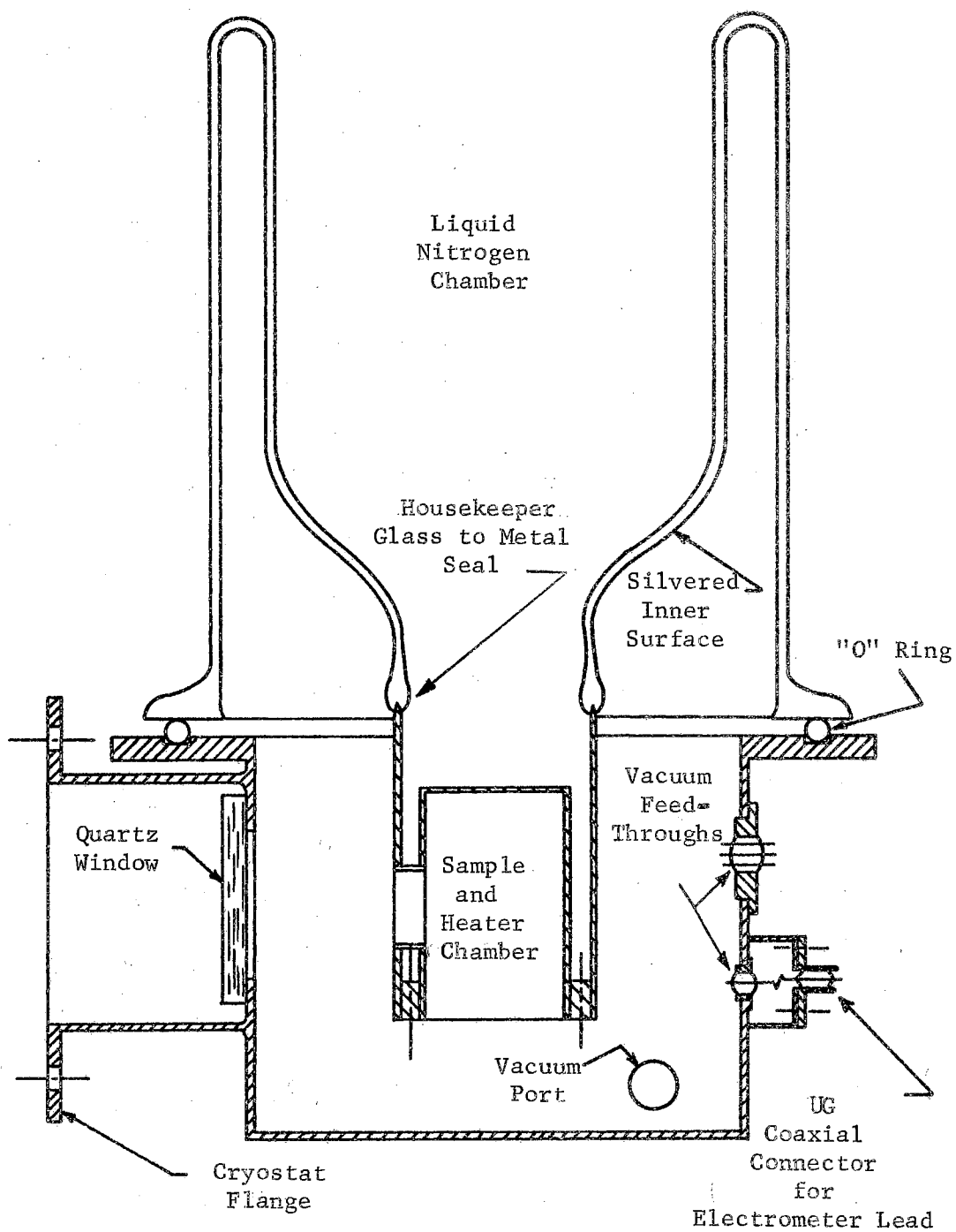Base Plate
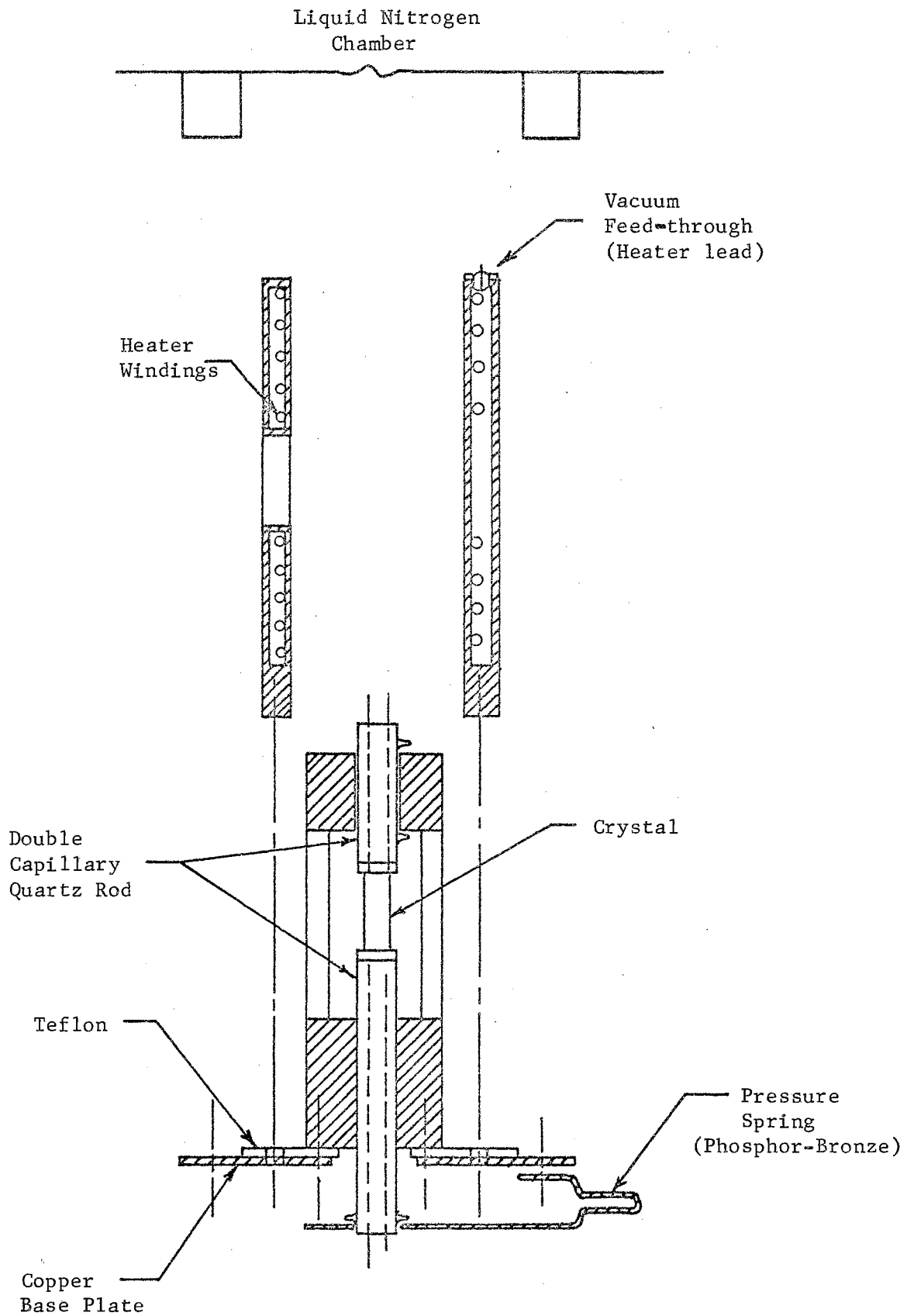
Figure 49. Suggestion sample holder schematic.

of design solutions for the following list of suggested improvements to existing equipment:

1. The sample should be surrounded by a chamber containing liquid nitrogen with only a small port for external radiation.

2. The sample temperature should be capable of being continuously controlled over the range from 77 to 400° K. This requires an isolated heating system which is also surrounded by the liquid nitrogen chamber.

3. The heater windings should be vacuum sealed to prevent out-gassing.

4. The electrometer lead from the crystal to the meter should be completely shielded.

5. Liquid nitrogen should be fed into a vertical chamber.

These requirements are felt to be adequately met by the designs given in the two figures, however, some improvements may still be necessary. One of these involves simplifying the connections between the sample holder and the cryostat base.

Two improvements are also felt to be necessary in the present data taking system. These involve the automatic control of both the sample temperature (for CTQ) and its time rate of rise (for TSC). No actual control system is to be suggested here since the problem is a common one and can, if necessary, be solved commercially.

The measurements suggested below are, of course, only a sample of the extensive work that is open to further study. However, these few are felt to be capable of giving the most useful information with the least experimental difficulty. For simplicity, the suggestions will be presented in outline form.

I. Thermal quenching

    A. Take the data point by point at as many temperatures as necessary to show clear results. Use as close to saturation photocurrent as practicable for each temperature. Take the data over a much broader range of light intensities.

    B. Repeat the above for several excitation wavelengths, both intrinsic and extrinsic.

II. Thermally stimulated currents

    A. Use a rate control system to take TSC as a function of temperature rise rate.

    B. Take the TSC data as a function of saturation photocurrent for fixed excitation periods.

    C. Take the TSC data at fixed saturation photocurrent as a function of the period of excitation.

III. Extrinsic sensitization by intrinsic pre-illumination (ESIP)

    A. Take ESIP data as a function of extrinsic wavelength (using extrinsic chopping system) for a broad range of intrinsic saturation photocurrents.

    B. Take ESIP data as a function of extrinsic intensity over the intrinsic wavelength range.

    C. Take the ESIP spectral response data as a function of intrinsic saturation photocurrent.

The extensions to thermal quenching data are designed to improve the quality of the results so that (1) reliable values of activation energy and capture cross section ratios can be calculated for the sensitizing centers and (2) a more detailed study of the effects of the shallow (0.21 ev) electron trapping states on the break to low

sensitivity data can be made. The additional TSC data should allow

both a corroboration of activation energy values by the method of

Haering and Adams[50] and an indication of the kinetics of trap filling.

It is felt that much more useful ESIP data can be obtained if it

is taken as a function of intrinsic saturation photocurrent. The

problem of separating the extrinsic response from the large intrinsic

background can be solved by chopping the former at some low frequency

value (say ten cycles per second), and recording the A-C output in

conjunction with a narrow band buffer amplifier having a high input

impedance. The data described in the above outline taken in this way

should not only lead to a better understanding of the general mechanism,

but should also more definitely establish the energy of the particular

defect levels responsible for the behavior.

Carrier Lifetime

Throughout the present work repeated mention has been made of the

importance of distinguishing between processes which cause increased

excitation and those which cause a decrease in recombination rate.

Therefore measurements of carrier lifetimes are considered to be of

prime importance in extending the present photoelectronic analysis.

Specifically, lifetime data are essential in establishing (1) the

density of trapped carriers from TSC data, (2) the effect of the environ-

ment and past history on trapping density and extrinsic quantum efficien-

cies, (3) the mechanism of the sensitization process and (4) the mechanism

which causes the extreme temperature dependence of the extrinsic CTQ data.

One scheme for measuring carrier lifetimes has been mentioned in

Chapter II along with a few of the experimental problems to be expected.

The most difficult of these problems is the design and construction of an electronic buffer amplifier which has both a high input resistance ($\approx 10^{10}$ ohms) and a fast rise time (< 0.1 msec). Such characteristics require guarded electrometer techniques, examples of which are contained in articles by Krakauer[62] and MacDonald.[63] This method of measuring lifetimes also requires a monochromator shutter with a closure time of less than 0.1 msec.

The actual carrier lifetime data obtained from this procedure would appear as a family of curves describing the function $\tau(\sigma, T)$ of Equation 34 over the desired ranges of conductivity and temperature. As an example of the application of this type data consider the problem of finding the density of trapped carriers from TSC data. In theory the TSC results follow the relation described by Equation 24. Therefore, the trapping density is gotten by integrating the expression

$$(n_t)_o = \int_{(n_t)_o}^{o} dn_t = -\frac{1}{b} \int_{T_o}^{T_1} \frac{n(T)}{\tau(n,T)} \, dT \qquad (38)$$

where majority carrier conduction has been assumed such that $\sigma \propto n$, $(n_t)_o$ is the density of trapped electrons, b is the heating rate and T_o, T_1 are chosen so that they completely encompass the TSC peak. Solution of Equation 38 will probably take the form of machine integrations with the constants b, T_o, T_1 and the point-by-point mappings of the functions $n(T)$, $\tau(n, T)$ acting as the program data.

Relative Quantum Efficiency

The technique for measuring carrier lifetime also suggests a method of obtaining relative quantum efficiencies. To illustrate this method,

consider Equation 33 and assume that it is possible to exapnd the function $\sigma/\tau(\sigma, T)$ in a power series in σ (the coefficiencts being temperature dependent). Then, if initial rise rate data is taken over small enough changes in σ, such that $\sigma/\tau(\sigma, T) \approx 0$, the quantum efficiency can be calculated from the expression

$$\alpha(\lambda) = \frac{(d\sigma/dt)_{t\approx 0}}{AL(\lambda)} \tag{39}$$

where $(d\sigma/dt)_{t\approx 0}$ represents the initial rise rate. One simple test for the initial rise condition is that $\sigma(t)$ be a linear function of time. Therefore, $(d\sigma/dt)_{t\approx 0}$ is measured as the initial linear slope of the transient rise data.

This technique could utilize the same equipment as that used in the lifetime experiments and would require in addition a source of high intensity short duration excitation. From this information one could determine how the quantum efficiency behaves in the short wavelength region beyond the optical cutoff, and whether it is dependent upon temperature or free carrier density. Such data is not readily available at this time and would add significantly to the general understanding of optical properties of solids.

Photo-Hall Effect

A knowledge of the carrier type and mobility is fundamental to a study of material properties. The classical method for determining these parameters is the Hall effect measurement. As mentioned earlier, such data is available for the natural stannic oxide crystals. However, these measurements on the grown samples are hindered by both their size and their high resistance.

Recall that the Hall voltage is given by the expression

$$V_h = \mu B V_L (w/L) \cdot 10^{-4} \qquad (40)$$

where V_h is the transverse Hall voltage, μ the carrier mobility in $cm^2/volt\text{-}sec$, B the magnetic field in Webers/m^2, V_L the longitudinal crystal voltage and w/L is the width to length ratio of the sample. For the present samples w/L ordinarily ranges from ½ to ¼ and does not degrade the Hall voltage to a great extent. However, the small sample sizes create the greatest difficulty in obtaining good potential probe contacts.

Equation 40 is an expression for the open circuit Hall voltage which means that the measuring system would have to have an input impedance greatly in excess of the crystal impedance. This fact makes it virtually impossible to take Hall data in the dark on the grown samples. However, measurements made under photoconductive conditions seem quite feasible using sensitive electrometers to measure the probe voltages. According to Equation 40, the Hall voltage would be about 5 millivolts for μ = 1 $cm^2/volt\text{-}sec$, B = 1 Weber/m^2, V_L = 100 volts and w/L = ½. It is felt that such measurements are possible for photoconductivities greater than about 10^{-10} (ohm-cm)$^{-1}$.

The problem of making probe contacts can probably be solved by using tungsten point probes* in contact with small abraded areas on the crystal surfaces. The abraded areas are formed by using a very fine cylindrical rod in an ultrasonic drill. This method has been used in preliminary four probe conductivity measurements on the grown samples.**

*These probes are commercially used in 1N21A diodes and are available from Sylvania Electric Products, Inc.
**Unpublished data Kunkle.

Photo-Hall data would be helpful not only as an indication of
carrier mobility but also in corroborating the conclusions drawn in the
present work concerning the trapped carrier type. Along with these are
the possibilities of obtaining the dependence of mobility on temperature,
its relation to free carrier density and possibly a qualitative look
at its spatial dependence -- by taking photo-Hall data as a function of
wavelength.

BIBLIOGRAPHY

1. Verwey, E. J. W., _Semiconducting Materials_, ed. H. K. Henisch, Butterworths Scientific Publications Ltd., London (1951).

2. Gray, T. J., _Semiconducting Materials_, ed. H. K. Henisch, Butterworths Scientific Publications Ltd., London (1951).

3. Gray, T. J., _Chemistry of the Solids State_, ed. W. E. Garner, Butterworths Scientific Publications Ltd., London (1955).

4. Grant, F. A., Revs. Mod. Phys., $\underline{31}$, 646 (1959).

5. Coffeen, W. W., J. Am. Ceram. Soc., $\underline{36}$, 207 (1953).

6. U. S. Pat. 2,617,745 (Nov. 11, 1952) Pittsburgh Plate Glass Co.

7. Berkman, S., Morrell, J. C. and Egloff, G., _Catalysis_, Reinhold Publishing Corp., New York (1940).

8. Bauer, G., Ann. Physik., $\underline{30}$, 433 (1937).

9. Fisher, A., Z. Naturforsch, $\underline{9a}$, 508 (1954).

10. Ishiguro, K., Sasaki, T., Arai, T. and Imai, I., J. Phys. Soc. Japan, $\underline{13}$, 296 (1958).

11. LeBlanc, M. and Sache, H., Physik Z., $\underline{32}$, 887 (1931).

12. Guillery, P., Ann. Physik., $\underline{14}$, 216 (1932).

13. Miloslavskii, V. K. and Lyashenko, S. P., Optics and Spectrosc., tr., $\underline{7}$, 154 (1959).

14. Foex, M., Bull. Soc. Chim. France, $\underline{11}$, 6 (1944).

15. Northrip, J. W., Unpublished Master's Thesis, Oklahoma State University (1959).

16. Belski, A. J., Unpublished Master's Thesis, Oklahoma State University (1960).

17. Hurt, J. E., Unpublished Ph.D. dissertation, Oklahoma State University (1959).

18. Marley, J. A. and MacAvoy, T. C., _Investigation of the Mechanism of Single Crystal Growth in High Temperature System_. Final Report, June 1961 - June 1962, Contract No. AF 19(604)-8447.

19. Marley, T. A. and MacAvoy, T. C., J. Appl. Phys. <u>32</u>, 2504 (1961).

20. Read, T. B., Roddy, J. T. and Maricano, A. N., J. Appl. Phys.,
    <u>33</u>, 1014 (1962).

21. Kunkle, H. F., J. Appl. Phys., (to be published, 1965).

22. Smith, W., Nature, <u>7</u>, 303 (1873).

23. Adams W. G. and Day, R. E., Proc. Roy. Soc., Series A, <u>25</u>, 113
    (1876).

24. Gudden, B. and Pohl, R., Physik. Z., <u>23</u> 417 (1922); <u>3</u>, 98 (1920);
    <u>4</u>, 206 (1921); <u>5</u>, 176 (1921); <u>1</u>, 365 (1920).

25. Pohl, R., Ber. Physik. Ges., 961 (1911).

26. Weimer, P. K., Forque, S. V. and Goodrich, R. R., R.C.A. Rev.,
    <u>12</u>, 306 (1951).

26. Kazan, B. and Nicoll, F. H., Proc. I.R.E., <u>43</u>, 1888 (1955).

28. Rose, A., Paper in <u>Photoconductivity Conference</u>, John Wiley and
    Sons, New York (1956).

29. Bube, R. H., <u>Photoconductivity of Solids</u>, John Wiley and Sons,
    New York (1960).

30. Bube, R. H. Proc. I.R.E., <u>43</u>, 1836 (1955).

31. Bube, R. H., J. Chem. Phys., <u>23</u>, 18 (1955).

32. Bube, R. H., Lind, E. L. and Dreeben, A. B., Phys. Rev., <u>128</u>,
    532 (1962).

33. Bube, R. H. and Lind, E. L., Phys. Rev., <u>110</u>, 1040 (1958).

34. Bube, R. H. and Lind, E. L., Phys. Rev., <u>105</u>, 1711 (1957).

35. Blanc, J., Bube, R. H. and MacDonald, H. E., J. Appl. Phys., <u>32</u>,
    1666 (1960).

36. Bube, R. H. and Lind, E. L., Phys. Rev. <u>115</u>, 1159 (1959).

37. Newman, R., Woodbury, H. H. and Tyler, W. W., Phys. Rev., <u>102</u>,
    613 (1956).

38. Bube, R. H. and Barton, L. A., J. Chem. Phys., <u>29</u>, 128 (1958).

39. Broser, I. and Warminsky, R., Ann. der Physik., <u>7</u>, 288 (1950).

40. Rittner, E. S., Paper in <u>Photoconductivity Conference</u>, John Wiley
    and Sons, New York (1956).

41. DeVore, H. B., Phys. Rev., 102, 86 (1956).

42. Subashiev, V. K., et al., Sov. Phys. Solid State., 2, 925 (1960).

43. Fortin, E., et al., Can. J. Phys., 40, 1703 (1962).

44. Petrusevich, V. A., et al., Sov. Phys. Solid State, 3, 109 (1961).

45. Porozhnikova, G., et al., Sov. Phys. Solid State, 3, 2657 (1962).

46. Randall, J. T. and Wilkins, M. H. F., Proc. Roy. Soc. (London)
    A184, 366, 390 (1940).

47. Garlick, G. F. J. and Gibson, A. F., Proc. Roy Soc. (London) A60,
    574 (1948).

48. Haake, C. H., J. Opt. Soc. Am., 47, 649 (1957).

49. Bube, R. H., J. Appl. Phys., 35, 586 (1964).

50. Haering, R. R. and Adams, E. N., Phys. Rev., 117, 451 (1960).

51. Bube, R. H., J. Phys. Chem. Solids, 1, 234 (1957).

52. Rose, A., R.C.A. Rev., 12, 362 (1951).

53. Houston, J. E., Unpublished Master's Thesis, Oklahoma State University
    (1962).

54. Tolley, E. E., Unpublished Master's Thesis, Oklahoma State University
    (1959).

55. Mott, N. F. and Gurney, R. W., Electronic Processes in Ionic Crystals,
    Dover Publications, New York (1964).

56. Mirtskhulava, I. A., et al., Sov. Phys. Solid State, 5, 1289 (1964).

57. Arkad'eve, E. N., et al., Sov. Phys. Solid State, 2, 1051 (1960).

58. Bube, R. H., Phys. Rev., 98, 431 (1954).

59. Ecklebe, F., Neues Jahrbuch Mineral. Geol., Beil. Bd., 66A, 47 (1933).

60. Bube, R. H., J. Chem. Phys., 21, 1409 (1953).

61. Goercke, P., Ann. Telecommun., 6, 325 (1951).

62. Krakauer, S., Rev. Sci. Inst., 24, 7 (1953).

63. MacDonald, J. R., Rev. Sci. Inst., 25, 2 (1954).

64. Seitz, F., Modern Theory of Solids, McGraw Hill, Inc., New York and
    London (1940).

APPENDIX

Seitz (62) gives an expression for the electrical current that passes
through a unit area in the x-direction in a material. In general terms
for single-type carriers of charge q,

$$I_x = \int q v_x f_q \, d\sigma \qquad\qquad A(1)$$

where v_x is the x-velocity component of the carriers, f_q is the velocity
distribution function and $d\sigma = dv_x dv_y dv_z$. In the case of a material over
which both a thermal gradient and an electric field exist, Equation A(1)
changes to

$$I_x = -q \int \frac{v_x^2 L}{v} \left(\frac{\partial f_q^o}{\partial x} + q E_x \frac{\partial f_q^o}{\partial \epsilon} \right) d\sigma \qquad\qquad A(2)$$

where L is the mean free path of the carriers, f_q^o is the field-free
velocity distribution and E_x is the electric field in the x-direction.
Also, the function f_q^o is related to the Fermi function by

$$f_q^o = \frac{2m^3}{h^3} \, f(\epsilon) \qquad\qquad A(3)$$

Therefore, by the chain rule, one can see that

$$\frac{\partial f_q^o}{\partial x} = \frac{\partial f_q^o}{\partial T} \frac{dT}{dx} = KT \frac{\partial f_q^o}{\partial \epsilon} \frac{d\alpha}{dT} \frac{dT}{dx} \qquad\qquad A(4)$$

where $\alpha = E_{fq}/kT$. Substituting this relation into A(2) yields

$$I_x = -q \int \frac{v_x^2 L}{v} \left(kT \frac{d\alpha}{dT} \frac{dT}{dx} + q E_x \right) \frac{\partial f_q^o}{\partial \epsilon} \, d\sigma \qquad\qquad A(5)$$

137

which, for $I_x = 0$, implies the relation

$$E_x = \frac{-kT}{q} \frac{d\alpha}{dT} \frac{dT}{dx} \ .$$

A(6)

The thermoelectric voltage is then

$$V_{\Delta T} = - \int E_x \cdot dx = \frac{k}{q} \int_{T_1}^{T_2} T \frac{d\alpha}{dT} \ dT.$$

A(7)

But α is a function of temperature, i.e., $\alpha(T) = E_{fq}(T)/kT$ therefore

$$V_{\Delta T} = - \frac{1}{q} \int_{T_1}^{T_2} (\frac{E_{fq}}{T} - \frac{dE_{fq}}{dT}) \ dT$$

A(8)

which is the desired result when q is given the sign and magnitude of

the charge carrier. The treatment should be valid for _either_ electrons

of holes when E_{fq} is taken as the appropriate steady-state Fermi level.

VITA

Jack Edward Houston

Candidate for the Degree of

Doctor of Philosophy

Thesis: PHOTOELECTRONIC ANALYSIS OF IMPERFECTIONS IN GROWN STANNIC OXIDE SINGLE CRYSTALS

Major Field: Physics

Biographical:

Personal Data: Born in Arkansas City, Kansas, March 11, 1933, the son of Earnest and Ruth Houston.

Education: Graduated from Cushing High School in Cushing, Oklahoma, in 1951; received Bachelor of Science degree from the Oklahoma State University, with a major in Physics, in May, 1956; received the Master of Science degree from the Oklahoma State University, with a major in Physics, in August, 1962.

Professional Experience: After receiving the Bachelor of Science degree, worked as a staff engineer for Sandia Corporation in Albuquerque, New Mexico; during this time served six months active duty with the United States Army Signal Corp; before returning to graduate school worked one year as a research engineer at the Jet Propulsion Laboratory in Pasadena, California.